Self-Scheduling Operations of a Compressed Air Energy Storage Facility Under Uncertainties

by

Matheus Zambroni

A thesis
presented to the University of Waterloo
in fulfillment of the
thesis requirement for the degree of
Doctor of Philosophy
in
Electrical and Computing Engineering

Waterloo, Ontario, Canada, 2022

Examining Committee Membership

The following served on the Examining Committee for this thesis. The decision of the Examining Committee is by majority vote.

Supervisor:	Claudio A. Cañizares University Professor, Department of Electrical and Computing Engineering University of Waterloo
Supervisor:	Kankar Bhattacharya Professor, Department of Electrical and Computing Engineering University of Waterloo
Internal Member:	Mehrdad Kazerani Professor, Department of Electrical and Computing Engineering University of Waterloo
Internal Member:	Sahar Pirooz Azad Assistant Professor, Department of Electrical and Computing Engineering University of Waterloo
Internal-External Member:	Mehrdad Pirnia Lecturer, Department of Management Sciences University of Waterloo
External Examiner:	João A. Peças Lopes Full Professor, Department of Electrical and Computer Engineering Porto University, Portugal

Author's Declaration

I hereby declare that I am the sole author of this thesis. This is a true copy of the thesis, including any required final revisions, as accepted by my examiners.

I understand that my thesis may be made electronically available to the public.

Abstract

High penetration of Renewable Energy Sources (RES) such as solar and wind in power systems reduce carbon emissions and decentralize the energy generation. However, the intermittency of these sources introduces new challenges, since solar power is only available during sunlight hours and wind power is difficult to forecast and may present a high variability. Thus, since RES generation is not dispatchable, a power system with large RES penetration may not meet the demand at peak hours and experience voltage flickers and frequency fluctuations. To tackle these challenges, various Energy Storage Systems (ESS) technologies have been developed and deployed at different scales throughout the grid, providing either energy arbitrage or frequency regulation services to the power system. For the former, there are two mature large-scale ESS: pumped hydro storage and Compressed Air Energy Storage (CAES), with the latter being less restrictive in terms of location. Despite being a mature technology, there are only two large-scale CAES facilities worldwide. However, with the challenges modern power systems face nowadays, the bulk capacity, fast response, and efficiency of CAES facilities makes them an attractive ESS alternative.

Electricity prices vary throughout the day depending on the system demand. At low demand, low-cost generators operate, resulting in cheaper electricity; at peak demand, more expensive units operate, hence increasing electricity prices. These electricity price variations opens opportunities for profitable businesses. In this context, an ESS facility owned by a private investor, depending on its capacity compared to the overall system, may participate as a price-taker or as a price-maker in electricity markets. Due to its bulk capacity, CAES can provide energy arbitrage to the grid and participate in the energy and reserve markets. Also, CAES newer designs decouple the charging and discharging processes using two synchronous machines, providing enhanced frequency regulation services.

Since a CAES facility presents physical limitations, its optimum daily schedule must be determined *a priori*. Given the day-ahead electricity price forecast, an optimum schedule can be determined through self-scheduling models, where the daily profit of the facility is maximized, which requires that the facility be properly modeled. Furthermore, with the high penetration of RES new and large sources of uncertainty have been introduced, particularly in generation and real-time market prices. Therefore, these uncertainties must be properly considered in CAES modeling and operation.

In this thesis self-scheduling models for a price-taker CAES facility, that partakes in energy and reserve markets under electricity price uncertainties, are proposed. Using an existing non-linear model for a CAES facility, Robust Optimization (RO) is employed to

represent price uncertainties, yielding an optimum schedule that protects against the worst-case scenario for a given level of conservatism. The model is benchmarked with Monte Carlo Simulations (MCS), presenting a lower computational burden while computing scenarios that the MCS fails to obtain. Thereafter, a novel linear thermodynamic model for the CAES is proposed, using mathematical tools for linearization such as McCormick Envelopes and linear-piecewise approximation, which compared with an existing non-linear model, it yields similar results at significantly lower computational costs. The novel model is further expanded considering uncertainties in electricity prices using RO and Affine Arithmetic (AA) approaches. The AA method keeps track of correlated uncertainties, yielding an optimum range of schedule with adjustable power dispatch for given real-time mismatches in price forecasts. Both methods are compared and benchmarked with the MCS approach, presenting significantly lower computational costs, with profit intervals obtained from AA being more conservative than MCS and RO, i.e., the former method envelops the intervals obtained from the latter techniques. The CAES profit and schedules for different levels of initial and final State of Charge (SOC) of the facility are then assessed in order to estimate an ideal SOC level where the facility may maximize its participation and profit.

Finally, a Principal Components Analysis (PCA)-Affine Policy (AP)-based self scheduling model for the CAES facility is proposed. PCA is a knowledge extraction based mathematical tool to reduce the dimension of a mathematical model by removing the less relevant variables, which may decrease the accuracy of the model. The method of AP, similar to AA, keeps track of correlated uncertainties and provides an optimum range of schedule with adjustable power dispatch for real-time mismatches in price forecast. The PCA-AP model is compared with AA and MCS, which is computational more expensive compared with AA, provides a tighter interval of profit, hence ensuring a safer margin of operation in pessimistic scenarios. Compared with the MCS, similar results were obtained at a lower computational cost. The operation of a CAES facility charging and discharging concurrently is then examined, which offers the facility with a larger set of combinations for its operational states, and hence greater profit, but at increased computational costs.

Acknowledgements

First, I want to thank God for giving me strength in the moments I felt weak and alone, and for all the wonderful people I met during these years.

I would like to express my profound gratitude to my supervisors, Professor Claudio Canizares and Professor Kankar Bhattacharya for their great guidance during my graduate studies in the University of Waterloo. It was through their supervision and support that I was able to complete this thesis, especially at the moments when I felt insecure on which direction things were going. During these past years, I had the opportunity to learn a lot from such amazing researchers and human beings.

I want to thank my Ph.D. Committee for their valuable comments and observations: Professor Mehrdad Kazerani and Sahar Pirooz Azad from the Department of Electrical and Computer Engineering at the University of Waterloo; Professor Mehrdad Pirnia from the Department of Management Sciences at the University of Waterloo, and Professor João A. Peças Lopes from the Department of Electrical and Computer Engineering at the Faculty of Engineering of Porto University.

My sincere thanks to my amazing friends and colleagues from the EMSOL lab: Bharat, Carlos, Chioma, Dario, Diego, Emin, Enrique, Fabian, Hisham, Ivan, Jean-Michell, Mauricio, Mariano, Nitin, Samuel, Sofia, Talal, Walter and William. It was great sharing time with them.

A special thanks to Ricardo and Eliana Von Staa for all the times they invited me to their home, and their kids Martina, Olivia and Klaus that adopted me as their Uncle Matheus. I lack words to express my gratitude for all the family moments they provided during this time.

I want to thank my family and friends for all the good and reinvigorating conversations, even being distant from one another, especially: Gabriel Alvarenga, Giovanni Antonaccio, Rosineide Xavier, Thomas Seixas and Yuri Reis.

Finally, I want to thank the two most important people in my world, my parents Antonio and Marli. Thank you for always being there for me, I am what I am today because of your unconditional love and support. You will always be my inspiration and example.

Dedication

This is dedicated to my parents, Antonio and Marli.

Table of Contents

List of Figures

List of Tables

List of Acronyms

AA Affine Arithmetic.

AFR Air Flow Rate.

AGC Automatic Generation Control.

AP Affine Policy.

BESS Battery Energy Storage Systems.

CAES Compressed Air Energy Storage.

CI Confidence Interval.

DoD Depth of Discharge.

EMS Energy Management System.

ESS Energy Storage System.

HOEP Hourly Ontario Electricity Price.

HR Heat Rate.

MCS Monte Carlo Simulations.

MILP Mixed Integer Linear Programming.

MPE Mean Percentage Error.

NPC Number of Principal Components.

OPF Optimal Power Flow.

PC Principal Component.

PCA Principal Components Analysis.

PDF Probability Density Function.

PF Power Flow.

PHS Pumped Hydro Storage.

RES Renewable Energy Sources.

RO Robust Optimization.

SMES Superconducting Magnetic Energy Storage.

SO Stochastic Optimization.

SOC State of Charge.

UC Unit Commitment.

UPS Uninterrupted Power Supply.

VOM Variable Operational and Maintenance.

Nomenclature

Indices

0	Center value.
h	Noise terms.
n	Principal Components from 1 to NPC.
s, s'	Segment of operation.
t	Operation time intervals from 1 to T.
X	Power dispatch type (discharging D, charging C, spinning reserve discharging SRD, spinning reserve charging SRC or idle ID).
Y	Electricity price for appropriate day-ahead market product (energy E, spinning reserve SR and idle reserve ID).

Parameters

$AFR_{s/s'}^{C/D}$	Charging/Discharging air flow rate corresponding to step s/s' (kg/(s.MW)).
$ang_{s/s'}^{D}$	Slope of Discharged Power function in segment s/s' (kg/(s.MW)).
$\overline{b}^{C/D}$	Length of each segment (MW).
$\overline{CA}$	Max. mass of air the cavern can store (kg).
$\overline{\Delta\pi}_t$	Max. price mismatch at t (%).
$\overline{\Delta PC}_n$	Max. uncertainty associated with Principal Component n.

$\underline{D}_{s/s'}$	Min. air discharged in segment s/s' (kg/s).
$\mathbf{\Lambda^Y}$	Eigenvalue matrices for electricity prices for Y.
$\mathbf{V^Y}$	Eigenvector matrix for electricity prices of Y.
Γ	Budget of uncertainty.
$HR_{s'}$	Heat rate corresponding to step s' (GJ/MWh).
$\mathbf{L^Y}$	Matrix used to determine π_t^Y as a function of Principal Components.
M	Large number used for Big M method.
$\underline{NG}$,$\overline{NG}$	Min. and max. heat rate of CAES facility (MBTU/h).
NPC	Number of Principal Components.
PC_n	Principal Component n.
π_t^Y	Price of Y at time t ($/MWh).
$\mathbf{\Pi^Y}$	Matrices of electricity prices for Y ($/MWh).
π^{NG}	Price of natural gas ($/MBTU).
$\underline{P}^X, \overline{P}^X$	Limits on X mode dispatch of CAES facility (MW).
$\underline{q}_{s,s'}$	Min. power discharged in segment s/s' (MW).
QSC	Quick start capability of CAES facility (MW).
$\underline{S}_s^C$	Min. state of charge in segment s (%).
$\underline{SOC}, \overline{SOC}$	Limits on State Of Charge (%).
SOC^f	Final State of Charge (%).
$VOM^{c/e}$	Variable operation and maintenance cost of compressor c or expander e ($/MWh).
Variables	
A	Revenue from energy arbitrage ($/h).

$air^{C/D}$	Amount of air charged/discharged (kg/s).
$\underline{air}_t^D, \overline{air}_t^D$	Min. and max. air discharged at t (kg/s).
α^Y	Dual variables.
B	Revenue from spinning reserve service ($/h).
$b_{s/s'}^{C/D}$	Fractional value of segment s/s' (MW).
CO^{NG}	Cost of natural gas ($/h).
$\Delta air^{C/D}$	Deviation of air charged/discharged (kg/s).
ΔCO^{NG}	Deviation of cost of natural gas ($/h).
ΔP^X	Deviation of P^X (MW).
ΔPC_n	Deviation of PC_n.
$\Delta\pi^Y$	Price deviation of Y (%).
$\Delta\pi^{Y+/-}$	Upward/Downward price deviation of Y (%).
ΔSOC	Deviation of State of Charge (%).
Δw	Deviation of w.
ε^Y	Noise term of Y.
OC	Operation cost ($/h).
P^X	Power dispatched in X mode (MW).
$p_{n,t}^{X,Y}$	Adjustment in power dispatch X, for price Y, at hour t, for principal component n (MW).
SOC	State Of Charge (%).
$u_{s/s'}^{C/D}$	Binary variable to identify the operating segment s/s'.
w	Variable used to linearize bi-linear terms.
$x^{C/D/ID}$	Binary variable indicating Charging/Discharging/Idle mode.

$xp_{n,t}^{X,Y}$	Binary variable to calculate the modulus of $p_{n,t}^{X,Y}$.
$\hat{\cdot}$	Affine representation of an uncertain variable.

Functions

$AFR^{C}(SOC)$	Charging air flow rate as a function of the SOC ($kg.MW^{-1}.s^{-1}$).
$AFR^{D}(P^{D})$	Discharging air flow rate as a function of P^{D} ($kg.MW^{-1}.s^{-1}$).
$f(P^{X})$	Revenue equation as a function of the power dispatch ($/h).
$HR(P^{D})$	Heat rate as a function of P^{D} (GJ/MWh).
$\mathcal{F}$	Objective function.

Chapter 1

Introduction

1.1 Motivation

Power systems are faced with the challenge of maintaining the demand-supply balance on a continuous basis while operating in a secure and reliable manner [1]. Global climate change considerations have motivated governments to implement policies to phase out fossil fuel-based generation sources and integrate Renewable Energy Sources (RES) into the electricity grid [2]. This has led to large-scale development and integration of wind turbines and solar photovoltaic (PV) panels to reduce greenhouse gas emissions, decentralizing the generation portfolio. Simultaneously, several changes are taking place in the demand side, such as improving the efficiency and reliability of equipment, replacing fossil fuel-based heating systems for electrical appliances, and large-scale adoption of electric vehicles [3]. However, these changes have introduced new and significant challenges for power systems operation.

RES are highly intermittent, since solar generation is only available during sunlight and wind is quite variable, making its resulting power difficult to predict. These characteristics may lead to frequency fluctuations and voltage flickers as studied in, for example, [4] and [5], which is highly undesirable. Therefore, even though there may be enough capacity to supply the loads, there is a possibility that the generation may not meet the demand, specially at peak hours. To this effect, Energy Storage System (ESS) are being integrated into power systems to provide the necessary balancing and flexibility in operations, storing energy when there is generation surplus and discharging when the load increases, thus improving grid stability, power quality and supply reliability [6, 7].

Over the years, various ESS technologies have been developed, with sizes ranging from small to large-scale. Storage can be used for energy arbitrage, capacity reserve, Uninterrupted Power Supply (UPS) and other services, based on their characteristics such as energy and power density, charge/discharge rates, energy and power capacity, and charge/discharge efficiency [8–10]. For bulk power applications, Pumped Hydro Storage (PHS) and Compressed Air Energy Storage (CAES) are the two economically and technologically feasible ESS existing technologies [11]. In terms of location, PHS requires different elevation levels for its reservoirs, whereas CAES requires a geological formation suitable for underground air storage; hence, CAES is less restrictive in terms of location as compared to PHS.

Despite CAES not being a recent technology, there are only two large-scale existing facilities; the first of 290 MW was built in Huntorf, Germany, in 1978, [12], and the second of 110 MW was constructed in McIntosh, Alabama, USA, in 1991 [13]. Several CAES pilot projects are now being commissioned worldwide, ranging from small- to large-scale, proposing different means for air storage and thermodynamic models [14–17]. With the aforementioned challenges to power system operations nowadays, the bulk capacity, efficiency, and fast response of CAES facilities render them attractive for grid operation. Furthermore, given that electricity prices vary significantly over a day, with low off-peak and high peak prices, investment in ESS can be a cost-saving option as a system asset or a profit-making decision if owned by a private investor. For the latter, and depending on the facility's capacity as compared to the overall system capacity, the facility may partake in electricity markets as a price-taker or price-maker [18]. However, to influence electricity market prices as a price-maker, the ESS capacity must be quite large, which is not yet feasible. Thus, a price-taker facility is most likely and realistic for ESS participating in electricity markets.

Several studies focusing on the operation of CAES systems in power systems, have been reported in the literature. Due to their bulk storage capacity, CAES systems can participate in energy and reserve markets, and given that these can charge/discharge simultaneously, they can also be used to provide ancillary services, thus enhancing their investment value. Therefore, static and dynamic models of CAES systems have been proposed (e.g. [19, 20]). However, most of the works reported in the literature either do not consider the thermodynamic characteristics of the CAES facility or are based on detailed nonlinear models with a high computational burden, specially in the presence of uncertainties, that are not suitable for electricity market operations.

Uncertainties have always been an issue for power systems operation. For power grids, the main source of uncertainty has been traditionally load forecast and generation dispatch in the context of competitive electricity markets, where uncertainty in electricity prices has

presented significant challenge. With the integration of large-scale RES, new uncertainties have been introduced due to their intermittent nature, such as in RES generation and real-time market prices [21]. Thus, to ensure secure operations within reasonable cost, these uncertainties must be considered in Unit Commitment (UC) and self-scheduling models. Some classical approaches to handle uncertainties in these models are Stochastic Optimization (SO) and Monte Carlo Simulations (MCS); however, these methods face several challenges. In both cases, uncertainties are represented using Probability Density Functions (PDFs), which require large quantities of data to yield a robust representation and their nonlinear shape may increase the model computational burden significantly [22]. The MCS approach involves simulating the model multiple times with different combinations of input data [23], which yields robust results, but at high computational costs. There are several SO algorithms in the literature used to solve single and multi-stage problems, such as Sample Average Approximation, Stochastic Approximation, Markov Decision Processes, etc. Despite yielding robust results, these methods require a careful selection of scenarios, which may be complex and/or result in large sets to achieve an accurate representation of the model [24].

Due to the challenges with MCS and SO, methods based on range arithmetic such as Robust Optimization (RO), Affine Arithmetic (AA) and Affine Policy (AP) have been proposed in the literature. At the core of these approaches is the representation of uncertain parameters using an established range of uncertainty based on historical data. Thus, the uncertainties are modeled using linear equations, avoiding the nonlinearities introduced by PDFs and the repetitive characteristic of the MCS and SO approaches. Hence, these methods present a lower computational burden.

Based on the aforementioned discussions, the main objective of the research presented in this thesis is to develop new self-scheduling models for a price-taker CAES facility operating under uncertainties. For this purpose, a novel linear model is proposed based on the thermodynamic characteristics of a CAES facility. Thereafter, uncertainties are introduced in the model using RO, AA and AP approaches, resulting in new models for uncertain dispatch of an investor-own CAES facility, presenting a comparative assessment of the performance of the proposed uncertainty models benchmarked against MCS results.

1.2 Literature Review

The literature review presented in this section concentrates on the participation of CAES facilities in electricity markets, discussing their thermodynamic models and participation

strategy, and applications of RO, AA, and AP to represent uncertainties in power systems operation modeling and applications.

1.2.1 Participation of Compressed Air Energy Storage Facilities in Electricity Markets

This section discusses research works focused on CAES models and their participation in electricity markets. Thus, a risk constrained bid/offer strategy for a CAES facility using information gap decision theory is proposed in [25]. The facility is assumed to operate in either charging, discharging, simple-cycle gas discharge (discharge using purely gas), and idle modes. Taking electricity price uncertainty into account, the bid/offer strategy ensures a minimal profit for the most critical scenario. However, the CAES model does not take into account the thermodynamic characteristics of the facility or the minimum charge/discharge limits, and does not participate in services other than energy.

In reference [26], an RO approach to obtain the offer/bid curves for a CAES facility is proposed considering electricity market price uncertainties. The facility is assumed to operate in charging, discharging, simple-cycle gas discharge or idle modes. The proposed method yields better results in optimistic and pessimistic scenarios as compared to the deterministic model. Despite the uncertainty immunized solution, thermodynamic characteristics and minimum charge/discharge limits are not considered. Furthermore, the facility participates only in the energy market, not offering reserve services to the system.

An adaptive self-scheduling model for a wind producer paired with a CAES facility is presented in [27]. The model considers uncertainties in electricity prices and wind power production using RO, and its robustness level is controlled through a parameter known as "budget of uncertainty". The objective function presents a max-min-max structure and is solved in an iterative approach using bi-level decomposition. In the first level, the profit of the facility is maximized in terms of the dispatch decisions, while in the second level, the worst-case realization of uncertainties is determined, sending primal cuts to the first level. The optimum dispatch for the CAES facility maximizes the daily profit by storing the energy from wind power during low-price periods, and selling during periods of high prices. However, the facility only participates in the energy market, not providing reserve services to the grid; also, the thermodynamic characteristics and minimum charge/discharge limits are not taken into account.

In [28], a self-scheduling model of a CAES facility participating in day-ahead and real-time markets is proposed. The facility is assumed to be a price-taker and participates in the energy and reserve markets. To achieve a more realistic representation of the facility,

the physical characteristics of the compressor and expander are considered using linear piece-wise functions. While higher profits are achieved as compared to other methods, the model did not consider uncertainties. Also, the complete thermodynamic characteristics of the CAES facility is not considered, particularly the pressure inside the cavern and the efficiency of the high pressure turbine.

A self-scheduling model to maximize the daily profit of a CAES facility, considering its thermodynamic characteristics is proposed in [19]. The facility is assumed to be a price-taker participating in energy, spinning and idle reserve markets. The thermodynamic characteristics are modeled using step-functions, based on data from an operating CAES facility, taking into account the pressure inside the cavern used for storage and efficiency of the high pressure turbine. Despite providing a more realistic representation, the model presents solutions without protection against uncertainties, which are not considered. Furthermore, the representation of thermodynamic characteristics using step-functions introduces new binary and auxiliary variables, which increase the complexity of the model, specially for implementation of range arithmetic methods to represent uncertainties. Finally, in the proposed model, the compressor is assumed to operate within 15%-100% of its rated capacity, which is an issue, since operation below 40% severely compromises its efficiency [29], with the thermodynamic representation becoming inaccurate.

Reference [20] proposes a detailed mathematical model of a diabatic CAES system in steady-state and dynamic studies. The facility is assumed to be capable to charge/discharge simultaneously, thus providing frequency regulation services. The studies presented reveal that the CAES facility contributes significantly to reduce the cumulative frequency deviation of the system. However, even though the proposed model provide an accurate representation of CAES systems considering their thermodynamic characteristics, it is not a suitable representation for electricity market participation, since the model is rather complex and nonlinear.

An adiabatic CAES facility integrated into a distribution network to minimize operating cost and provide continuous reactive power support is proposed in [30]. A detailed mathematical model for the CAES facility is presented, taking into consideration the thermodynamic characteristics and components' efficiency. The model is tested using a bi-objective Optimal Power Flow (OPF), where the first objective is system cost minimization and the second is system voltage quality improvement. A Nash Bargaining approach is used to select a unique solution from the Pareto optimum set. The results demonstrate that participation of the CAES facility to provide reactive power to the system, improved the voltage quality and voltage regulation, and reduced losses. However, uncertainties are not considered in this work.

1.2.2 Modeling Uncertainties in Power Systems Operation

This section focuses on a review of the modeling and representation of uncertain parameters in power system operational models. Discussions on operational models have been excluded.

In [31], an Energy Management System (EMS) model for isolated microgrids, which features RES, ESS and interruptible loads, is presented. The paper considers the application of RO to model the RES generation uncertainties, which are represented using a linear function given by the forecast value and range of uncertainty. The representation of RES uncertainties in this work can be extended to represent electricity price uncertainties for CAES self-scheduling models.

An RO approach to integrate electric vehicles in Ontario's grid is proposed in [32]. The mathematical formulation takes into account the electricity grid and transport sector constraints. A sensitivity analysis using MCS is carried out to determine the most relevant parameters the model is sensitive to, which are found to be the Hourly Ontario Electricity Price (HOEP) and price of export/import power. Accordingly, their uncertainties are integrated into the model using RO, assuming a maximum mismatch of 10%. Simulations are carried out for different levels of conservatism, i.e., varying the budget of uncertainty from a deterministic case to the most conservative scenario. It is noted that a high budget of uncertainty is not required to achieve an optimal solution while ensuring a low probability of violation of the constraints. Hence, implementing RO to self-scheduling models of a CAES facility may provide optimum schedules that ensures a reasonable profit, without having to resort to conservative scenarios, since low levels of conservatism may present low probability of violation of the system constraints.

A hybrid stochastic RO approach is proposed in [33], with the objective of obtaining an optimal bid strategy for a microgrid in a day-ahead market. Uncertainties in distributed generation output and day-ahead market prices are modeled as an SO problem using a forecast data base. The RO approach is used to model the uncertainty in real-time market price, in order to limit the power unbalance in real-time. The approach is divided into three stages: first, the microgrid submits bids based on which prices and distributed generation outputs are obtained; second, the day-ahead market is cleared; and third, the real-time market is cleared. It is noted that microgrids can benefit significantly from bidding in the day-ahead market, and the budget of uncertainty can be used to set different risk levels. However, the ESS devices present in the system are generic and do not capture the specific characteristic of ESS technologies such as CAES.

The scheduling of a set of ESS is proposed in [34] using RO to represent the uncertainties in RES, load, and real-time thermal ratings of transmission lines. The deterministic

problem objective is to minimize the operational cost of the ESSs. The RO problem is solved for the worst-case scenario considering a specific value of budget of uncertainty. The RO method is compared with the deterministic model using two sets of input data, namely, no uncertainties, and the most conservative scenario, i.e., the largest range of uncertainty. The scenario without uncertainties yields the lowest cost as expected; however, the lack of protection against uncertainties is not desirable, since it may increase costs and accelerate battery degradation if real-time data deviates from the forecast. As the budget of uncertainty increases, so does the probability of the RO model not violating any constraints, and the operational cost increases as well. However, a high probability of not violating any constraints may be achieved for lower budgets of uncertainty. Thus, the proposed method ensure a safe operation of ESSs without having to resort to the most conservative scenario. However, ESS are considered as system assets that do not provide reserve services to the grid.

An AA method is applied to represent the RES uncertainties in an OPF problem in [35]. The model does not rely on PDFs, since uncertainties are represented within a numeric interval. RES generation, and real and imaginary components of voltages and currents are represented in their affine forms to keep track of correlated uncertainties. The algorithm executes the OPF for the expected demand, i.e., their center values, obtaining these values for the voltages and currents. Thereafter, a sensitivity analysis is carried out by perturbing the demand at each bus, and executing the OPF to compute the variations in the voltages and currents of each bus. Furthermore, executing the Power Flow (PF) equations, the upper and lower bounds of active and reactive power injections at each bus are determined. The model yields slightly more conservative results than the MCS at a significantly lower computational burden. The affine representation of uncertain quantities can be used to represent electricity price uncertainties and power dispatch for self-scheduling CAES models. Accordingly, the optimum solution would provide the center and radius of the profit and power dispatch, allowing the CAES facility to adjust its dispatch, given the mismatch in real-time electricity prices from the forecast price; hence, this approach is used in this thesis to model uncertainties for CAES optimal dispatch.

An AA-based framework for PF and OPF studies is presented in [36]. Considering uncertainties in RES generation and representing the uncertain quantities and variables in their affine forms, the paper proposes to separate the center and noise terms, thus, turning the model into a multi-objective optimization problem. The proposed method yields precise results at a lower computational costs compared with MCS. To further improve the model's performance, the use of Principal Components Analysis (PCA) to determine the optimum number of independent uncertainties is reported, while improving significantly convergence time. Thus, for self-scheduling models with a large set of noise variables, the PCA is shown

to be a useful tool to reduce the dimension of the problem and improving the computational burden. This approach of solving the center and radius of the original problem separately is only valid because all variables present in the model are continuous.

Reference [37] proposes an EMS for isolated microgrids wherein the UC model includes uncertainties in RES generation and load that are represented using AA. An ESS is integrated in the microgrid, which introduces binary and inter-temporal variables, associated with the operational state of the ESS and its State of Charge (SOC), respectively. Consequently, the approach presented in [36] to determine the center and radius in a decoupled manner, cannot be applied in this case. To this effect, the center and radius terms of the AA-based UC model are optimized simultaneously, where the conservativeness of the model is controlled by multiplying these terms with complementary weights. To ensure no operational limits are violated, inter-temporal constraints are decomposed into two constraints, the first takes into account only the central variables, and the second only the noise variables. The results obtained are benchmarked with an SO solution, achieving a high degree of accuracy at lower computational burden, without having to use PDFs. While the ESS facility is assumed to be a system asset, the proposed AA formulation can be adapted to take the point of view of the owner for self-scheduling models of a CAES facility, as done in this thesis.

A comparison between RO and AA to represent uncertainties in microgrids integrated with ESS, is proposed in [38]. A UC model considering uncertainties in RES generation and loads is proposed. The RO problem is optimized for the worst-case scenario using a min-max objective, i.e., minimizing the cost in terms of the dispatch decisions and maximizing it in terms of the uncertainties for a given budget of uncertainty, which is transformed into a tractable Mixed Integer Linear Programming (MILP) problem. As for the AA model, the uncertain parameters and variables are represented in their affine forms to keep track of correlated uncertainties. Since there is an ESS in the model, the center and radius of the objective function are minimized simultaneously. Comparing their results, RO incurs the largest operational cost since its objective is to achieve a conservative solution against the worst-case realization, while the AA model resulted in a slightly lower cost compared with the deterministic model. While in this work, the ESS is assumed to be a system asset, the model may be adapted from the perspective of a price-taker CAES facility and the performance of AA and RO in self-scheduling models can be assessed, as done in this thesis.

While AA is focused on optimizing the center and radius of the objective function, RO focuses on optimizing for the worst-case scenario. However, classical RO methods provide non-adjustable solutions; hence, to address this shortcoming, AP has been proposed to make RO computationally tractable. Thus, [39] proposes an adjustable AP-based robust

OPF considering uncertainties in load and RES generation. From the forecast data, i.e., the center value of uncertain parameters, the OPF is executed to obtain the base-point schedule of the Automatic Generation Control (AGC) units. Each unit is associated with a participation factor, which helps with adjusting their output according to the variations of the forecast parameters. This approach presents a large computational burden; therefore, an iterative process using successive constraint enforcement is reported. Although the proposed approach yields robust results for a nonlinear problem, all variables in the model are continuous, since ESSs are not integrated with the system and all AGC units are assumed to be operating.

Reference [40] proposes a multistage adaptive RO for the UC problem, which can assume significant dimensions for a large-scale power system. Applying a basic AP to the model is not computationally viable in this case; hence, a simplified AP is proposed by aggregating the uncertain parameters and thus reducing the problem dimension. To further reduce the computational burden, the model is solved using a constraint generation approach. Therefore, the model is first executed without considering any limit constraints; thereafter, if limits are violated their constraints are integrated in the model and executed again, with the process being repeated until no limits are violated. In this case, the main source of uncertainties are the loads, and the optimization problem presented is of a min-max-min structure, in which, the costs are first minimized in terms of dispatch decisions, then maximized in terms of load uncertainty, and finally minimized with recourse actions to adapt with the final outcome. The model provides robust results against significant uncertainty within a reasonable computational burden. However, the model does not consider the participation of ESS.

A multistage robust UC model with dynamic uncertainty sets and ESS is presented in [41] for high penetration of RES, and applied to a large practical system. Due to the high dimensionality of the uncertainty sets, PCA is used to capture the joint temporal and spatial correlation of RES, thus reducing the dimension of the problem. As in [40], uncertain parameters and variables are represented in their affine forms, with the objective function presenting a min-max-min structure. To reduce the computational burden, the problem is solved using constraint generation approach. It is noted that the proposed method leads to more utilization of ESS and less curtailment of RES. Adapting the AP for self-scheduling models, the PCA method may be used to capture correlations from historic data of electricity prices, thus reducing the model computational burden, as done in this thesis.

1.2.3 Discussions

From the aforementioned literature review, it is noted that several works have proposed the participation of CAES facilities in electricity markets. However, some of the proposed models do not consider the full potential of CAES in the market environment, considering only their participation in energy markets, while neglecting reserve markets, where the CAES systems can contribute to grid reliability and increase their revenue. It is also important to emphasize that some works do not consider the thermodynamic characteristics and minimum charging and discharging limits of the CAES facility, which is an inaccurate representation of CAES. On the other hand, works that consider CAES thermodynamic characteristics, these are modeled using nonlinear representations and thus are not the most suitable for day-ahead market modeling, especially when uncertainties are considered.

One of the main challenges to execute an SO model is to obtain an accurate representation of the PDFs, in a way that uncertainties are represented with high precision and the model yields robust results. However, lack of data may lead to weak PDF representations, which may compromise the results. Therefore, techniques based on range arithmetic, such as RO, AA, and AP have been proposed for power system studies. Representing uncertainties using linear relations help avoid the nonlinearities introduced by PDFs, hence reducing the computational burden. These techniques presented good performances, achieving robust results, i.e., conservative solutions against worst-case realization, and results with real-time adjustment, where the dispatch can be updated in real-time with uncertainty realization. However, these studies are mostly focused on UC, PF, and OPF, where ESS facilities are considered a system asset rather than owned by private investors, without taking their perspective into account.

Only a few works have proposed self-scheduling models of CAES systems participating in energy and reserve markets. Due to the complexity of representing the thermodynamic characteristics, several papers neglect them, yielding inaccurate models. Others propose detailed nonlinear models, which may be highly complex for day-ahead market simulation studies. To represent uncertainties in power systems studies, the aforementioned techniques based on range arithmetic present a good performance, but only a few have focused on self-scheduling models. Therefore, this thesis focuses on proposing a novel linear thermodynamic model based on a real-world facility, for a price-taker CAES system that participates in energy and reserve markets, while considering price uncertainties using range arithmetic techniques such as RO, AA, and AP.

1.3 Research Objectives

Based on the aforementioned review of the state-of-the art in CAES self-scheduling models and uncertainty representation through range arithmetic techniques, the main objectives of this thesis are the following:

- Develop a novel thermodynamic model for a CAES system based on a real-world CAES operating facility, taking into consideration the pressure inside the cavern and the efficiency of the high pressure turbine. Using linearization techniques, such as McCormick Envelopes and linear-piecewise approximation, the nonlinear constraints are linearized for the application of the proposed model electricity markets.

- Develop a self-scheduling model for a price-taker CAES facility, including detailed thermodynamic modeling, for its participation in the day-ahead electricity market to provide energy and reserve services to the power system. The model is validated and compared with a nonlinear model of the CAES facility proposed in the literature, carrying out simulations for deterministic scenarios of electricity market prices.

- Considering electricity market price uncertainties, develop a RO model for the CAES facility participating in day-ahead electricity market, maximizing its profit in terms of power dispatch and minimizing it in terms of the price mismatch, using a budget of uncertainty to control the level of conservativeness.

- Model the electricity price uncertainties using AA, representing the uncertain parameters and all decision variables in their affine forms, keeping track of correlated uncertainties. Maximizing the center and radius of the profit simultaneously, an AA solution is obtained that provides the range of optimal schedules for given electricity price forecasts.

- Develop a PCA-AP self-scheduling model of the CAES facility wherein the uncertain parameters and all variables are represented in their affine forms, using APs to keeping track of correlated uncertainties, and applying PCA to extract information from the electricity prices to reduce the problem dimension. Thus, for a given information level established by the PCA, a range of optimal adjustable power dispatch solutions for given electricity price forecasts.

- Benchmark the proposed RO, AA, and PCA-AP models against MCS studies carried out on the CAES facility to compare their performances and suitability for the proposed application under price uncertainties.

1.4 Thesis Outline

The rest of the thesis is organized as follows:

- Chapter 2 discusses the relevant background on ESS technologies and the services they may provide when integrated into power systems, providing details of CAES facilities. A general overview on optimization using range arithmetic techniques to represent uncertainties using RO, AA and AP is also presented. Finally, a brief background of the PCA and Box Cox Transformation tools used in the thesis is also presented.
- Chapter 3 presents a deterministic self-scheduling model for a price-taker CAES participating in energy and reserve markets. First, an existing nonlinear formulation to represent the thermodynamic characteristics is presented. Thereafter, a linear thermodynamic model is developed applying linearization techniques.
- Chapter 4 presents the mathematical models where uncertainties in electricity prices are represented using range arithmetic techniques, namely RO, AA, and PCA-AP.
- Chapter 5 presents the results and comparisons of the simulation studies based on an existing CAES facility. The novel linear thermodynamic model is benchmarked with the existing nonlinear model, comparing optimum profits, dispatch and computational burden. Thereafter, results obtained when uncertainties are modeled, using range arithmetic representations, are presented, compared and benchmarked against MCS results.
- Chapter 6 summarizes the thesis, and the main conclusions and contributions of the presented work. The scope for future work is also discussed.

Chapter 2

Background

In this Chapter, an overview of ESS and the services they may provide when integrated into the power system are presented. A general representation for a CAES facility is also discussed, followed by the thermodynamic configurations associated with the facility, i.e., diabatic, adiabatic, and isothermal. Finally, a general representation of optimization techniques based on range arithmetic and the mathematical tools employed in this research are presented.

2.1 Energy Storage Systems (ESS)

The high penetration of RES in power systems introduces new challenges for reliable operation of the grid. Thus, there are a limited number of hours of available solar power, since it only occurs during the day, and although wind generation may be available at all hours of the day, the stochastic behavior of these RES can lead to frequency fluctuations and voltage flickers [5]. Furthermore, the output of RES is not controllable, which may result in excess generation at low demand hours and shortfall at peak hours. Thus, ESS technologies plays a very important role in modern power systems, storing energy when there is a surplus and releasing it when the system needs it.

Different ESS technologies exist, which can be classified as follows [11]:

- Mechanical energy storage: Can be divided into the following subcategories:
  - Potential energy based: PHS and CAES.

  - Kinetic energy based: High and Low-Speed Flywheels.

- Electromagnetic energy storage: Conventional Capacitors, Superconducting Magnetic Energy Storage (SMES), and Super Capacitors.
- Chemical energy storage: Battery Energy Storage Systems (BESS), Flow Batteries, and fuel cells.
- Biological-based energy storage.
- Thermal energy storage: Cryogenic, Ground Source Heat Pump (GSHP), and Electrical Thermal Storage (ETS).

PHS, along with CAES, is a large-scale ESS technology. It consists of two reservoirs located at different elevations. During off-peak hours, the water is pumped to the upper reservoir while during peak hours, power generation takes place and water is discharged to be stored in the lower reservoir, with potential energy being converted into electricity by going through a turbine [42]. It is a mature technology, with high energy and power capacity; ratings can be between 100 - 3,000 MW, and may have long storage periods, high efficiency, and low capital cost per unit of energy. Thus, PHS is suitable for energy arbitrage applications, although it requires particular geographic settings with significant elevation differentials, and it presents high construction costs and long gestation lags.

Flywheels are made of material that have either high or low inertia, which results in low or high speed flywheels, respectively [43]. The energy is stored in the angular momentum of the spinning mass, which operates as a motor during charging and as a generator during discharging, with the kinetic energy of the spinning mass being converted into electricity. Several advantages are its high power density, fast response time, very high efficiency, and long life with hundreds of thousands cycles. The main drawbacks are the high self-discharge, low energy density, and high capital cost because of the need for expensive equipment. Therefore, flywheels are used to provide UPS services to the grid.

Conventional capacitors consists of two metallic plates separated by a dielectric. They can be charged much faster than BESS, presenting high efficiency and long life cycle. However, the low energy density and inability to achieve higher values of capacitance do not make the technology attractive for energy storage applications in power systems. With the introduction of super capacitors, made of two electrodes submerged in an electrolyte solution, very large capacitances and high energy density have been achieved [44], making them viable for power system applications. The drawbacks of super capacitors are the high self-discharge losses, short duration operation, and low voltage breakdown limit. Thus, super capacitors are also used to provide UPS services.

SMES systems store energy in the form of electric current. DC current flows through a superconducting coil immersed in liquid helium, which maintains the temperature below 5 °K in a vacuum sealed vessel, so that the material of which the inductor is made, is kept in its superconducting state [45]. The main advantages of SMES are the very fast response time and high energy storage efficiency, which makes it suitable as a UPS. The disadvantages are its high cost and the strong magnetic field, which can be harmful for the environment and human health.

Conventional BESS is the oldest form of energy storage, which consists of electrochemical cells with an electrolyte, an anode, and a cathode. The reactions that take place are reversible, so the battery operates in cycles, i.e., can be fully charged and discharged many times. However, as the number of cycles increases, the state of health of the battery deteriorates, reducing drastically the amount of energy that it can deliver back to the system. The scale of BESS may range from small to large, thus, depending on its characteristics may provide energy arbitrage or UPS services to the grid. An overview of some BESS technologies and their respective advantages and disadvantages are presented in Table 2.1 [8].

Table 2.1: BESS Technologies [8].

Technology	**Advantages**	**Disadvantages**
Lead Acid	Low cost, high reliability and efficiency	Short life as low as 1,000 cycles; and low energy density
Nickel Cadmium	High energy density, high reliability and life between 2,000-2,500 cycles	High cost and toxicity of cadmium
Sodium Sulphur	Life of 2,500 cycles, high power and energy density and high efficiency	High cost and self-discharge
Lithium Ion	Very high energy density and life cycle (up to 10,000 cycles), and efficiency close to 100%	High cost makes it unsuitable for large-scale applications

Flow batteries consist of reservoirs containing electrolyte solutions and two electrodes separated by a cell, through which the solutions flow. In order to avoid mixing the electrolytes, an ion exchanging membrane is placed in the middle of the cell, which is impermeable to electrons. Ions migrate from one electrode to the other through the membrane,

and electrons flow through an external circuit, hence generating electricity [46]. The reaction is reversible, which allows charging and discharging cycles. The main advantage of flow batteries is its storage capacity, since high storage levels can be achieved with larger tanks, providing energy for many hours at a high discharge ratio with no self-discharge, thus being suitable for energy arbitrage applications. The disadvantages are its low power and energy densities compared to other technologies, and the presence of shunt currents in the electrolytes, which affect its efficiency.

In cryogenic energy storage, air is stored in its liquid state, i.e., at a very low temperature, during off-peak hours. At peak hours, the ambient air temperature heats the liquid air that goes through a cryogenic heat engine, generating electricity [47]. It is benign to the environment, while presenting a high energy density and low capital cost per unit of energy, thus being suitable for energy arbitrage. However, its low efficiency is a major drawback [8].

Biological-based storage is in its early development stage and requires several advancements for it to be suitable for practical applications. Through photosynthesis it is possible to store solar energy in large scale. However, photosynthesis is not a high efficiency technology currently, and the process to store the energy released from it, named rewired carbon fixation, requires some technological breakthroughs [48].

In summary, ESS have a wide range of applications, from large-scale at the transmission level to small-scale at the customer end. Traditionally, CAES and PHS have been the only technologies delivering very large quantities of power, above 100 MW, but in recent years, some large-scale BESS projects have been commissioned. In most storage technologies, there is a trade-off between the energy and power density, and another important aspect to be considered is their response time. Depending on these parameters, ESS are typically used to provide the appropriate services to the power system. For a robust operation of the power system with significant variable RES generation, ESS with different range of applications must be employed. Thus, ESS can provide UPS services to mitigate transient flickers, maintaining an acceptable power quality, as well as energy arbitrage to provide load following and balancing services, helping to provide energy when the grid sources, particularly RES, are not able to meet the demand.

2.2 Compressed Air Energy Storage (CAES)

A CAES plant mainly consists of the following components, as illustrated in Figure 2.1 [8], assuming that charging (Motor) and discharging (Generator) are decoupled, which is the approach being used in new CAES installations:

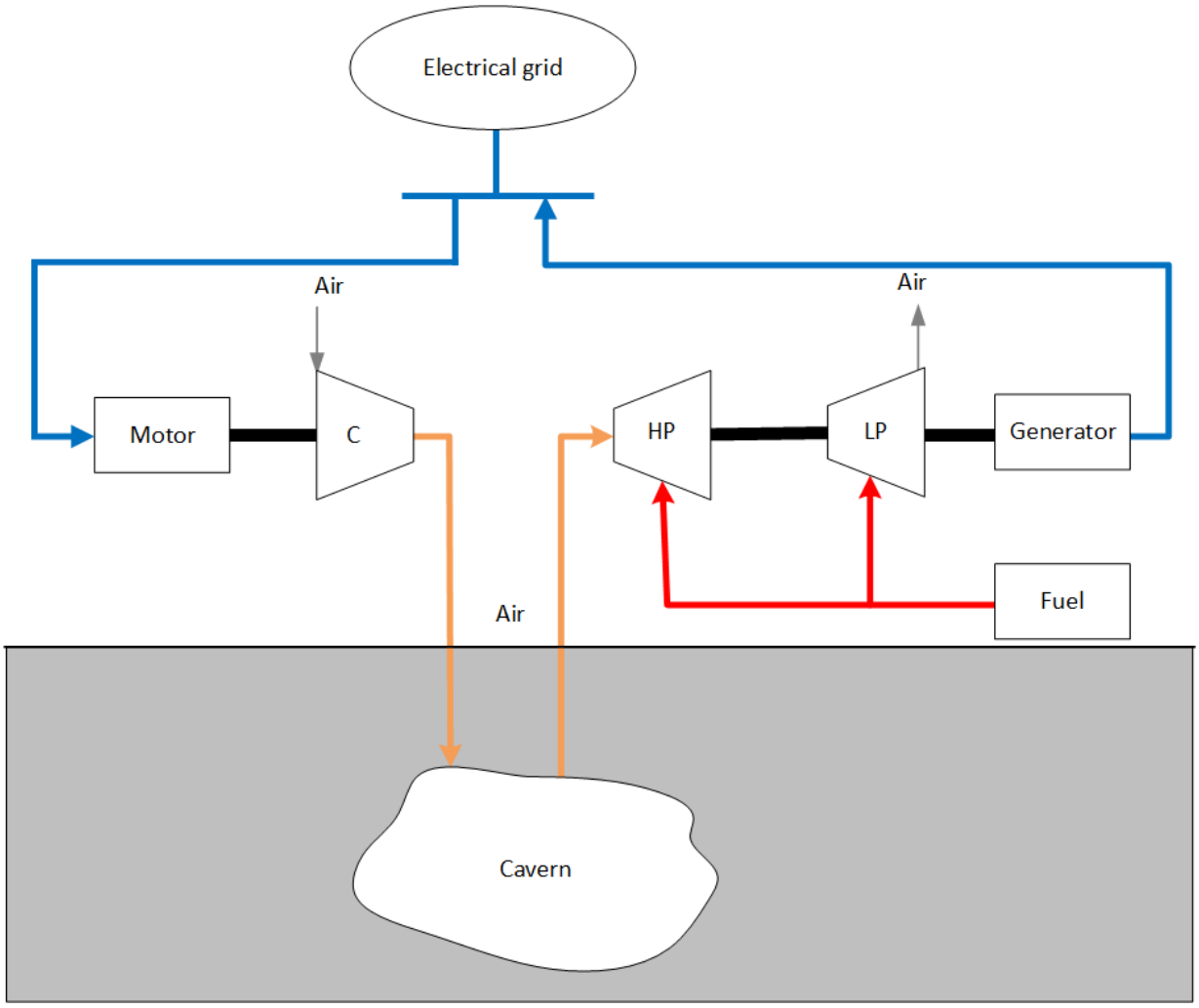

Figure 2.1: Typical configuration of a CAES components and its components.

1. A motor connected to the power system, clutched to one or more compressors.
2. Compressors coupled with intercoolers and aftercoolers, removing the humidity in the air and improving the compression efficiency.
3. Container to store air, such as salt cavern or rock mines.
4. Turbine train: a turbine at high pressure, and another at low pressure.
5. Generator clutched to the turbine train.

6. Auxiliary equipment to control the fuel and heat exchanging units.

A CAES facility may operate in the following modes:

- Charging: The air is pressurized by a compressor, which is powered by a motor supplied by the electrical grid. Through pipes, the compressed air is conducted to a reservoir where it remains stored. In order to improve the compression efficiency, intercoolers and aftercoolers are used to reduce the air temperature and remove humidity [49]. As the mass of air stored in the reservoir increases, so does the pressure inside and the charging air flow rate decrease, and it becomes increasingly difficult to store more air. When charging, the CAES facility pays for the energy drawn from the grid, but it may offer load balancing services to the grid.

- Discharging: The compressed air from the reservoir is extracted through pipes, preheated and expanded in a turbine train. The air is released with high temperature from this process, thus a recuperator can be used to capture the residual heat and use it in the preheating stage [50]. When discharging, the CAES facility is paid for the energy supplied, and may also provide spinning reserve service if not operating at full power.

- Idle: In this mode, the CAES facility is neither charging nor discharging, but remains connected to the grid, thus being able to provide non-spinning reserve services.

There are two large-scale CAES facilities operating in the world. The first is located in Huntorf, Germany, built in 1978, which consists of two salt caverns, each with a volume of 150,000 m^3 and approximately 700 meters in depth, and can generate up to 290 MW for 2 hours [12]. The second is located in McIntosh, Alabama, USA, built in 1991. It consists of only one cavern, but with the much greater volume than Huntorf of 500,000 m^3; its maximum generation capacity is 110 MW for 26 hours [13]. The McInthosh CAES plant also uses a recuperator to capture the waste heat and preheat the air, hence saving 25% of fuel as compared to the Huntorf plant.

Both Huntorf and McIntosh facilities have a single machine for charging and discharging. Thus, during the charging process the machine is clutched with the compressor, while during discharging the machine is clutched with the turbine train [51]. Therefore, these facilities can only operate either in charging, discharging, or idle mode, at a given time. New CAES projects have used novel configurations using two synchronous machines, one clutched with the compressor and the other with the turbine train, as in the CAES facilities

in Goderich, Ontario, Canada [16], and in Bethel, Texas, USA [52]. In these systems, the charging and discharging modes are independent and the CAES facility can charge and discharge concurrently. This enables participation of the facility in frequency regulation markets, hence expanding its opportunities to increase revenue earnings.

The CAES facilities of Huntorf, McIntosh, and Bethel store the air inside underground salt caverns and presents a diabatic thermodynamic configuration, where natural gas is burned to increase the temperature of the air before being expanded in the turbine [12, 13, 52]. The round-trip efficiencies of the Huntorf and McIntosh facilities are 46% and 54%, respectively [53]. However, new thermodynamic models and man-made vessels to store air have been proposed [54], such as:

- Adiabatic: Captures the heat produced in the compression stage, stores it in thermal systems and uses it to reheat the air before reaching the expansion stage. The objective is to create a closed-loop process, but heat losses are inevitable, thus limiting the efficiency of the plant to 70%. The Goderich facility presents an adiabatic thermodynamic configuration [16].

- Near-isothermal: Compression and expansion processes take place at a slow rate, avoiding significant temperature changes. Since the processes does not burn any fuel, the efficiency is increased significantly. This technology is still under research and not much data is available.

- Adsorption Enhanced: Adsorbent chemicals are used to adsorb the molecules from the compressed air into a solid layer. From that, greater storage capacities can be achieved in smaller spaces. However, it is a very recent idea and not much data is available to confirm if it is feasible in economic and engineering terms.

- Underwater: Air is stored inside underwater man-made vessels, as in case of [55]. When the facility is charging, the compressor sends the air inside the vessels, and when discharging, the water pressure forces the air out to the turbines.

Several other examples can also be mentioned, such as [54]: diabatic solar-assisted CAES, hydrokinetic energy, transportable CAES, and vehicle compression. There are a few small-scale projects with these technologies around the world, but they are still in the research and development stage.

2.3 Optimization in the Presence of Uncertainties

Electrical power systems offer several decision-making problems where optimization methods and models are employed to arrive at the best possible decisions, such as UC and self-scheduling problems. In UC problems, the optimum commitment and dispatch of generation units are obtained, while satisfying the load demand and reserve requirements, at minimum cost [56]. With integration of large-scale ESS and their possibility of being owned by a private investor, self-scheduling models have gained importance where the investor seeks to maximize its profits based on the day-ahead market price forecast [19, 27, 28].

Although the optimization models may have an accurate mathematical representation, the solutions obtained may not necessarily be the optimum in practice. This is because models are subject to uncertainties in their parameters, and depending on the degree of uncertainty, the solution can lead to economic losses, which is highly undesirable. Load uncertainty have always been a challenge for power system operation, with the high penetration of RES uncertainties in wind and solar generation, and electricity prices being more recently considered [57]. Thus, in order to ensure reliable operational decisions, these uncertainties must be taken into account.

A classical approach to deal with uncertainties is through SO [58]. There are several SO techniques depending on the problem formulation, with uncertainties in parameters or constraints [59, 60]. In these models, uncertainties are represented by PDFs, which are nonlinear, hence making the problem more complex. Despite presenting robust results, adequate PDF representations for the uncertainties considered are only possible if there is a considerable amount of data; hence, the lack of data may lead to assumptions regarding the PDFs, which may yield poor representations with significant errors [31]. Due to these challenges, alternative methods based on range arithmetic have been proposed, such as RO, AA, and AP, which are discussed next.

2.3.1 Robust Optimization (RO)

Initially proposed in [61], RO presents an attractive approach to represent random variables through uncertainty sets, rather than probabilistic models, i.e., this method does not use PDFs, and thus no assumptions are made regarding the characteristics of the uncertainties. The method was originally employed in a linear optimization problem, seeking to optimize the objective in the worst-case uncertainty; however, the method has been criticized because of its highly conservative strategy. A less conservative model has been reported in [62] which solves the robust counterparts of the problem, representing the uncertainties

in elliptical sets. Despite the reasonable approximations provided by this method, a major drawback was the introduction of nonlinearities, thus increasing the computational cost.

A method to make the level of conservatism more flexible while maintaining the advantages of the linear model in the original framework is proposed in [22]. A parameter known as the budget of uncertainty Γ is introduced, which can take any value in $[0,\ J]$, where J represents the set of parameters that are subject to uncertainties. Varying Γ from 0 to J allows a trade-off between the level of conservatism and robustness. Thus, for $\Gamma = 0$ the model is deterministic, i.e., no uncertainties are considered, while for $\Gamma = J$, the most conservative scenario is considered, yielding the model proposed in [61].

RO problems seeks to optimize an objective function for the worst-case scenario, as follows:

$$\min_{x} \sum_{n=1}^{N} c_n x_n \tag{2.1}$$

$$\text{s.t. } Ax \leq b \tag{2.2}$$

where c, A and b are parameters, x is a variable, and n is an index. Observe that the objective is to minimize the function in terms of the decision variables x_n. By considering uncertainties in the parameters c_n, it is assumed that there is a mismatch of up to $\overline{\Delta c}$ in its value. Hence, the values that c_n may assume are in the following interval:

$$c_n \in [c_{n,0}(1 - \overline{\Delta c}), c_{n,0}(1 + \overline{\Delta c})] \tag{2.3}$$

where $c_{n,0}$ represents the forecast and most likely value of the parameter c_n. Thus, c_n can be expressed as:

$$c_n = c_{n,0}(1 + \Delta c_n) \tag{2.4}$$

where Δc_n is a variable that represents the mismatch of the parameter c_n. Substituting

(2.4) in (2.1) and adding several constraints reflecting c_n uncertainty, one has:

$$\min_{x} \max_{\Delta c_n} \sum_{n=1}^{N} \left(c_{n,0} x_n + c_{n,0} \underbrace{\Delta c_n x_n}_{\text{Bi-linear term}} \right) \tag{2.5}$$

$$\text{s.t. } \Delta c_n = \Delta c_n^+ - \Delta c_n^- \qquad \forall n \tag{2.6}$$

$$\Delta c_n^+ \leq \overline{\Delta c} \qquad \forall n \tag{2.7}$$

$$\Delta c_n^- \leq \overline{\Delta c} \qquad \forall n \tag{2.8}$$

$$\sum_{n=1}^{N} \frac{\Delta c_n^+ + \Delta c_n^-}{\overline{\Delta c}} - \Gamma \leq 0 \tag{2.9}$$

$$\Delta c_n^+, \Delta c_n^- \geq 0 \qquad \forall n \tag{2.10}$$

Observe in (2.5) that the problem seeks to minimize the function in terms of x, and maximize it in terms of Δc_n. In (2.6), the variable Δc_n is broken into two positive variables Δc_n^+ and Δc_n^- which represents the uppward and downward deviations, respectively, and are limited by $\overline{\Delta c}$ in (2.7) and (2.8). Finally, the level of conservatism is controlled using (2.9), where the budget of uncertainty Γ limits the number of times the value of c_n deviates from the forecast. For this problem, the range of values for the budget of uncertainty is, $\Gamma \in [0, N]$, where $\Gamma = 0$ corresponds to the deterministic model, i.e., no uncertainties considered, and $\Gamma = N$ corresponds to the most conservative scenario, where all values of c_n deviate from the forecast. Hence by choosing different combinations of ($\overline{\Delta c}$, Γ), a set of possible optimum decisions can be obtained, with different degrees of uncertainty.

Note that a bi-linear term is introduced in the objective function (2.5), which makes the problem nonlinear. Another issue is that, a min-max structure is a saddle-point mathematical problem, which may be non-convex. However, the internal maximization problem in (2.5) is linear, and hence it can be replaced by its dual problem using the concept of Strong Duality, as discussed in Section 4.1.

2.3.2 Affine Arithmetic (AA)

AA is a range analysis technique that keeps track of correlated uncertainties between the variables [63]. It handles both external and internal sources of uncertainty, with imprecise data and uncertainty in the mathematical model being external sources, while truncation and round-off errors are internal sources. Each uncertain variable χ is represented in its

affine form as follows:

$$\hat{\chi} = \chi_0 + \chi_1\varepsilon_1 + \chi_2\varepsilon_2 + \cdots + \chi_p\varepsilon_p = \chi_0 + \sum_{h=1}^{p} \chi_h\varepsilon_h \tag{2.11}$$

where χ_0 denotes the center value of χ and ε_h and χ_h are the noise variables and magnitudes of the corresponding uncertainty components, respectively; the noise variables are within the interval $[-1, 1]$. Hence, when all variables are represented in their affine forms, they share the same noise variables, thus tracking correlated uncertainties. If the interval of χ is within $\left[\underline{\chi}, \overline{\chi}\right]$, its affine representation $\hat{\chi}$ is given as follows:

$$\chi_0 = \frac{\overline{\chi} + \underline{\chi}}{2} \tag{2.12}$$

$$\chi_1 = \frac{\overline{\chi} - \underline{\chi}}{2} \tag{2.13}$$

$$\hat{\chi} = \chi_0 + \chi_1\varepsilon_1 \tag{2.14}$$

In AA, there are affine and non-affine operations. Thus, considering the affine quantities $\hat{a} = a_0 + \sum_{h=1}^{p} a_h\varepsilon_h$ and $\hat{b} = b_0 + \sum_{h=1}^{p} b_h\varepsilon_h$ and the parameter λ, affine operations are the following:

$$\hat{z} = \hat{a} \pm \hat{b} = (a_0 \pm b_0) + \sum_{h=1}^{p} (a_h \pm b_h)\varepsilon_h \tag{2.15}$$

$$\hat{z} = \lambda\hat{a} = \lambda a_0 + \lambda \sum_{h=1}^{p} a_h\varepsilon_h \tag{2.16}$$

$$\hat{z} = \hat{a} \pm \lambda = (a_0 \pm \lambda) + \sum_{h=1}^{p} a_h\varepsilon_h \tag{2.17}$$

and a non-affine operation is:

$$\hat{z} = \hat{a}\hat{b} = a_0b_0 + \sum_{h=1}^{p} (a_0b_h + b_0a_h)\varepsilon_h + z_k\varepsilon_k \tag{2.18}$$

where the resulting variables contains the information provided by $\hat{a}$ and $\hat{b}$, and the approximation error is denoted as $z_k\varepsilon_k$. Despite being a conservative approach, to avoid

information loss ε_k is usually assumed to be 1, and $z_k = \sum_{h=1}^{p} |a_h| \sum_{h=1}^{p} |b_h|$. Thus, (2.18) can be rewritten as:

$$\hat{z} = a_0 b_0 + \sum_{h=1}^{p} (a_0 b_h + b_0 a_h)\varepsilon_h + \sum_{h=1}^{p} |a_h| \sum_{h=1}^{p} |b_h| \tag{2.19}$$

The general representation for AA in an optimization problem is given by [36]:

$$\min_{\hat{z}} \hat{\mathcal{F}}(\hat{z}) \tag{2.20}$$

$$\text{s.t. } \hat{g}_l(\hat{z}) \overset{A}{\approx} 0 \quad \forall l \in L \tag{2.21}$$

$$\hat{h}_m(\hat{z}) \overset{A}{\leq} 0 \quad \forall m \in M \tag{2.22}$$

where the equality $\overset{A}{\approx}$ and inequality $\overset{A}{\leq}$ constraints are defined in the AA domain for the aforementioned AA quantities $\hat{a}$ and $\hat{b}$ as follows:

$$\overset{A}{\approx}\text{: } a_0 = b_0 \wedge a_h = b_h \qquad \forall h \tag{2.23}$$

$$\overset{A}{\leq}\text{: } a_0 + \sum_{h=1}^{p} |a_h| \leq b_0 - \sum_{h=1}^{p} |b_h| \tag{2.24}$$

Thus, (2.23) implies that one affine variable is equal to the other if all their terms are equal, and (2.24) states that one affine variable is less than the other if the upper boundary of the left-hand side is lower than the lower boundary of the right-hand side. Therefore, objective function $\hat{\mathcal{F}}$ in (2.20) can be expressed as:

$$\min_{\hat{z}} \hat{\mathcal{F}}(\hat{z}) = \underbrace{\mathcal{F}_0(\hat{z})}_{\text{Center terms}} + \underbrace{\sum_{h=1}^{p} \mathcal{F}_h(\hat{z})\varepsilon_h}_{\text{Affine terms}} + \underbrace{\sum_{h=p+1}^{p+p_{na}} \mathcal{F}_h(\hat{z})\varepsilon_h}_{\text{Non-affine terms}} \tag{2.25}$$

In [36], a decoupled solution approach is proposed considering a multi-objective function as follows:

$$\min_{\hat{z}} \left\{ \mathcal{F}_0(\hat{z}), \sum_{h=1}^{p+p_{na}} |\mathcal{F}_h(\hat{z})| \right\} \tag{2.26}$$

where the first term minimizes the center value, without taking into account the uncertainties represented by the noise symbols. The second term minimizes the radius, thus

resulting in a lower tolerance of data uncertainty. Based on a trade-off between the two objectives, the risk level can be flexibly adjusted.

The approach proposed in (2.26) is only valid if all variables in the model are continuous and no inter-temporal variables are taken into account, since the solution for one problem may turn out to be infeasible for the other. An AA-based UC model is proposed in [37], where the center and radius are minimized concurrently, and the protection against uncertainty is flexibly controlled by using a multi-objective function, as follows:

$$\min_{\hat{z}} \left(\mu \mathcal{F}_0(\hat{z}) + (1-\mu) \sum_{h=1}^{p+p_{na}} |\mathcal{F}_h(\hat{z})| \right) \tag{2.27}$$

where $\mu \in [0,1]$, and $\mu = 1$ denotes a deterministic representation, i.e., no protection against uncertainties, while $\mu = 0$ is the most conservative scenario. An alternative model is presented in [38], as follows:

$$\min_{\hat{z}} \left(\mathcal{F}_0(\hat{z}) + \sum_{h=1}^{p+p_{na}} |\mathcal{F}_h(\hat{z})| \right) \tag{2.28}$$

where the center and radius are minimized simultaneously, without any mechanism to control the level of conservatism of the model, thus providing a single conservative solution against the range of uncertainty.

The solution obtained when AA is used to represent uncertainties provides the center and adjustment terms of the variables in the model. Hence, in real-time, as the parameters of the model deviates from their expected values, their noise terms ε_h are determined and the output variables of the model are adjusted according to this variation.

2.3.3 Affine Policies (APs)

One of the main differences between traditional RO techniques and AA, is that RO solutions fail to adjust to real-time uncertainties. APs were first introduced in [64] to provide an affinely adjustable RO to solve linear optimization problems with uncertain parameters. The method was later expanded to solve multi-period inventory problems [65], control [66], and power systems operation problems [39–41].

The AP approach can be explained based on the following deterministic problem [65]:

$$\min_{u,y} \ \{c_1^T u + c_2^T y\} \tag{2.29}$$

$$\text{s.t. } \underline{y_n} u_n \leq y_n \leq \overline{y_n} u_n \quad \forall n \tag{2.30}$$

$$\sum_{n=1}^{N} y_n \geq d \tag{2.31}$$

where in (2.29), the cost function is minimized in terms of u and y, which are binary and continuous variables, respectively, while c_1^T and c_2^T are associated cost parameters. The upper and lower limits of y are given by (2.30), and a minimum demand d must be met, as per (2.31).

Considering uncertainties in demand d, its affine form is given as follows:

$$\hat{d} = d_0 + \Delta d \tag{2.32}$$

$$-\overline{\Delta d} \leq \Delta d \leq \overline{\Delta d} \tag{2.33}$$

where d_0 represents the center, and most likely value for $\hat{d}$, while Δd is the mismatch of the demand. The continuous variables y are represented in their affine form as follows:

$$\hat{y}_n = y_{n,0} + \beta_n \Delta d \quad \forall n \tag{2.34}$$

$$\sum_{n=1}^{N} \beta_n = 1 \tag{2.35}$$

where $y_{n,0}$ is the center of $\hat{y}_n$ and β_n is the adjustment with respect to Δd. Note that in AP, the affine variables share the mismatch terms Δd, which are constrained by (2.33), while for AA they share the noise terms ε which are within $[-1, 1]$.

Substituting (2.32) and (2.34) in (2.29)-(2.31), the problem can be reformulated as follows:

$$\min_{u} \left\{ c_1^T u + \max_{\Delta d} \min_{\hat{y}} c_2^T \hat{y} \right\} \tag{2.36}$$

$$\text{s.t. } \underline{y_n} u_n \leq y_{n,0} + \beta_n \Delta d \leq \overline{y_n} u_n \quad \forall n \tag{2.37}$$

$$\sum_{n=1}^{N} (y_{n,0} + \beta_n \Delta d) \geq (d_0 + \Delta d) \tag{2.38}$$

$$\frac{|\Delta d|}{\overline{\Delta d}} \leq \Gamma \tag{2.39}$$

where (2.36) presents a min-max-min structure in which the objective function is first minimized in terms of the binary decisions u, then maximized in terms of the demand uncertainty Δd, and finally, minimized in terms of the recourse actions $\hat{y}$. Constraints (2.37) and (2.38) ensure that no limits are violated and that the minimum demand is satisfied, respectively. Finally, in (2.39) the budget of uncertainty is introduced to control the conservatism of the model, where $\Gamma \in [0, 1]$.

An optimization problem with min-max-min structure cannot be solved in a straightforward manner. Several methods in the literature have been proposed to solve this problem, one of them is a two-stage approach, which can be stated as follows [40]:

$$\min_{u,\eta} \left\{ c_1^T u + \eta \right\} \tag{2.40}$$

$$\text{s.t. } \eta \geq Q(u) \tag{2.41}$$

$$Q(u) = \max_{\Delta d} \min_{\hat{y}} c_2^T \hat{y} \tag{2.42}$$

which can be solved through an iterative process by reformulating it as follows:

$$\min_{u,\eta} \left\{ c_1^T u + \eta \right\} \tag{2.43}$$

$$\text{s.t. } \eta \geq c_2^T \hat{y}_l \quad \forall l \tag{2.44}$$

where l denotes a set of extreme points and y_l is a vector associated with second stage decisions from l. Thus, the iterative algorithm to solve this problem consists of minimizing the gap between the lower boundary (LB) and upper boundary (UB), for an established tolerance ϵ, as follows:

1. Set $LB = -\infty$, $UB = \infty$ and $k = 0$.
2. Solve (2.43) with $l \leq k$, update optimal u^* and η^*, and set $LB \leftarrow c_1^T u^* + \eta^*$.
3. Evaluate $Q(u^*)$ in (2.42), store y_{k+1}, and set $UB \leftarrow min\{UB, c_1^T u^* + Q(u^*)\}$.
4. Check if $UB - LB \leq \epsilon$, in which case the algorithm converged. Else, set $l = k+1$, add y_l to (2.44), set $k = k+1$, go back to step 2, and repeat the process until convergence is achieved.

The execution of this process yields a solution where the variables present a center and adjustable terms, to better adapt with real-time uncertainties based on the budget of uncertainty defined in (2.39).

2.4 Mathematical Tools

2.4.1 Principal Components Analysis (PCA)

Optimization problems with large quantities of data may present a high computational cost. To address this issue, dimension reduction methods such as PCA can be employed to extract knowledge from the data set and transform a large set of variables into a smaller one. The reduction in the number of variables naturally decreases the model accuracy; hence, the main purpose of PCA is to reduce the number of variables while maintaining as much information as possible.

The step-by-step procedure to execute the PCA is as follows [67]:

- Standardization: To avoid dominance of variables with greater magnitudes, the original data D is standardized using the $\mathcal{Z}$-score:

$$\mathcal{Z} = \frac{1}{\sigma}(D - D_{av}\mathbf{1}) \tag{2.45}$$

  where D_{av} is the average and σ is the standard deviation of D, and $\mathbf{1}$ a vector of ones.

- Covariance: Compute the covariance matrix to determine how much the variables vary with respect to each other, thus capturing their inter-relationships.

- Eigen-analysis: The eigenvectors $\mathbf{V}$ of the covariance matrix are the Principal Component (PC) directions and the corresponding eigenvalues $\mathbf{\Lambda}$ yield their variances, as follows:

$$\mathbf{Z} = \text{cov}(\mathcal{Z}) \tag{2.46}$$
$$[\mathbf{V},\ \mathbf{\Lambda}] = \text{eig}(\mathbf{Z}) \tag{2.47}$$
$$\lambda = \text{diag}(\mathbf{\Lambda}) \tag{2.48}$$
$$\lambda_{inf} = \frac{\lambda}{\sum_i \lambda_i} \tag{2.49}$$

  where λ_{inf} represents the information level, in terms of percentage, for each eigenvector.

- Feature Vector: Discarding the PCs with lesser information, from $\mathbf{V}$, the remaining ones form a matrix known as Feature Vector $\mathbf{F}$, with the PCs being calculated as follows:

$$PC = \mathbf{F}^T D \tag{2.50}$$

where the quantity of PCs is determined by sorting λ_{inf} in descending order and aggregating them until a minimum amount of information is achieved.

2.4.2 Box Cox Transformation

Normality is an important assumption for statistical techniques. However, real world data may not always adhere to a normal shape behavior; thus, the Box Cox transformation can be employed to transform the non-normal data into a normal shape [68]. The Box Cox transformation W of non-normal data w can be defined as follows:

$$W = \begin{cases} \frac{w^\gamma - 1}{\gamma}, & \text{if } \gamma \neq 0 \\ log(w), & \text{if } \gamma = 0 \end{cases} \quad \gamma \in [-5, 5] \tag{2.51}$$

where γ is a parameter estimated to minimize the standard deviation of the transformed data. For example, if w represents the daily average energy price, obtained from the HOEP data for the months of May in the years from 2015 to 2019, Figure 2.2a depicts the histogram of w. Observe the non-normal shape of the data with some extreme points. Thus, W can be calculated using equation (2.51), where the data is normalized for $\gamma = 0.0249$, and its histogram is presented in Figure 2.2b.

Given the transformation W, the extreme points are filtered from the normal distribution using the concept of Confidence Interval (CI). For example, sorting the values of W in ascending order W^*, and assuming that the total number of samples is S, a CI of $p\%$ is given by [69]:

$$CI_{p\%} = \left[\overline{W} - \left(W^*_{(1+p)/2} - \overline{W}\right), \overline{W} - \left(W^*_{(1-p)/2} - \overline{W}\right)\right] \tag{2.52}$$

where $\overline{W}$ is the average of W, $W^*_{(1-p)/2}$ is the $(1-p)/2$ floor denoted by $W^*_{\lfloor S(1-p)/2 \rfloor}$ of the S samples, and $W^*_{(1+p)/2}$ is the $(1+p)/2$ ceiling denoted by $W^*_{\lceil S(1+p)/2 \rceil}$ of the S samples. Hence, the remaining data represents the majority of occurrences in the original data.

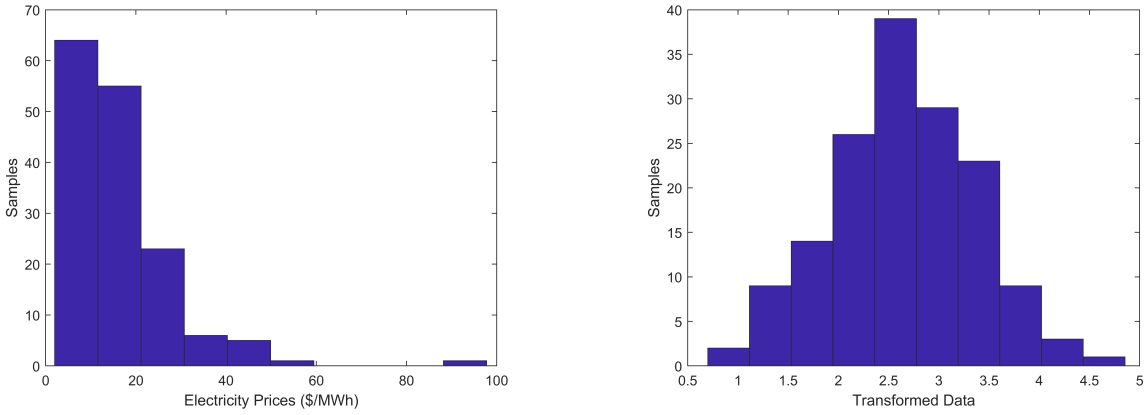

(a) (b)

Figure 2.2: Histogram of (a) w, and (b) W.

2.5 Summary

In this Chapter, the main background topics related to this thesis were covered. A general overview on ESS technologies and the services they may provide to the grid were first presented. A detailed description of CAES systems was provided, presenting its general configuration, operation modes, possible role in energy, reserve and frequency regulation markets, thermodynamic configurations, and storage vessels under development. The limitations of SO were discussed, and the alternative to represent uncertainties using range arithmetic based techniques such as RO, AA, and AP were presented. Finally, an introduction to PCA to reduce the dimension of a problem, and the Box Cox Transformation to remove outliers in historical data were presented.

Chapter 3

Deterministic Self-Scheduling Models of CAES Systems

This Chapter presents the mathematical model of a self-scheduling, price-taker CAES facility participating in day-ahead electricity markets, taking into account its detailed thermodynamic characteristics. Two different representations for the thermodynamics are presented: a step function model, as proposed in [19], and a linearized model.

3.1 CAES System Model

3.1.1 Self-Scheduling Model of CAES Facility

The CAES facility is assumed to be a price-taker, i.e., it cannot affect the electricity market prices by its actions. Hence, while participating in the day-ahead market, providing energy, spinning and idle reserves, its objective is to maximize the daily profit of the facility, given by:

$$\max_{P_t^X} \mathcal{F} = \sum_{t}^{T} \left[f(P_t^X) - OC_t \right] \tag{3.1}$$

where:

$$f(P_t^X) = A_t\pi_t^E + B_t\pi_t^{SR} + P_t^{ID}\pi_t^{ID} \qquad \forall t \qquad (3.2)$$

$$A_t = P_t^D - P_t^C \qquad \forall t \qquad (3.3)$$

$$B_t = P_t^{SRD} + P_t^{SRC} \qquad \forall t \qquad (3.4)$$

$$OC_t = CO_t^{NG} + P_t^D VOM^e + P_t^C VOM^c \qquad \forall t \qquad (3.5)$$

$$CO_t^{NG} = HR(P_t^D)P_t^D\pi^{NG} \qquad \forall t \qquad (3.6)$$

where all variables, parameters, indices and functions are defined in the Nomenclature section. The revenue from participation in the energy market is given by the first term of (3.2), where the CAES facility pays for charging and receives a payment for discharging as given in (3.3); the facility is paid for spinning reserve services during charge/discharge operation as denoted by the second term of (3.2) and (3.4); and payment for the idle reserve service is given by the third term of (3.2). The operations cost of the facility is given by (3.5), where its first term denotes the cost of natural gas usage during discharging (3.6), and the second and third terms denote the Variable Operational and Maintenance (VOM) costs for the expander and compressor, respectively.

The operational constraints are defined as follows:

$$x_t^C + x_t^D \leq 1 \qquad \forall t \qquad (3.7)$$

$$x_t^C + x_t^{ID} \leq 1 \qquad \forall t \qquad (3.8)$$

$$x_t^D + x_t^{ID} \leq 1 \qquad \forall t \qquad (3.9)$$

$$P_t^C \leq \overline{P}^C x_t^C \qquad \forall t \qquad (3.10)$$

$$P_t^D \geq \underline{P}^D x_t^D \qquad \forall t \qquad (3.11)$$

$$0 \leq P_t^{ID} \leq QSC x_t^{ID} \qquad \forall t \qquad (3.12)$$

$$P_t^{SRC} \leq P_t^C - \underline{P}^C x_t^C \qquad \forall t \qquad (3.13)$$

$$P_t^{SRD} \leq \overline{P}^D x_t^D - P_t^D \qquad \forall t \qquad (3.14)$$

The constraints (3.7), (3.8), and (3.9) ensure that the CAES facility operates in either charging, discharging, or idle modes; removing (3.7) would allow the CAES facility to charge and discharge simultaneously. Equations (3.10) to (3.12) denote the maximum power capacity during charging, minimum discharging capacity, and the range of idle operation, respectively. The lower and upper limits of the compressor charging power must be between 40%-100% of the rated power, where its efficiency is approximately constant, and for the turbine the lower and upper limits must be between 30%-100% of its rated

power, where its efficiency is not compromised [29]. In (3.13), P^{SRC} denotes the spinning reserve power made available to the system during charging operation, where the facility ramps down its charging in order to reduce the system load and hence provide a spinning reserve. Similarly, in (3.14), P^{SRD} denotes the spinning reserve during discharging operation, where the facility ramps up its discharging power to provide more energy to the grid. Up-charging or down-discharging to provide downward spinning reserve is not considered in this work.

The inter-temporal variation of the SOC is given by:

$$SOC_{t+1} = SOC_t + \frac{air_t^C 3,600}{\overline{CA}} - \frac{air_t^D 3,600}{\overline{CA}} \qquad \forall t \qquad (3.15)$$

$$air_t^C = AFR^C(SOC_t)P_t^C \qquad \forall t \qquad (3.16)$$

$$air_t^D = AFR^D(P_t^D)P_t^D \qquad \forall t \qquad (3.17)$$

$$\underline{SOC} \leq SOC_t \leq \overline{SOC} \qquad \forall t \qquad (3.18)$$

$$SOC_t \geq SOC^f \qquad \forall t = T \qquad (3.19)$$

The SOC at time $t+1$ is calculated in (3.15). The amount of air charged/discharged is determined by the Air Flow Rate (AFR) of the facility multiplied by the charging/discharging power, as in (3.16) and (3.17), respectively. Constraint (3.18) ensures the SOC is maintained within limits. Since the facility participates in the day-ahead market, it requires to maintain a specified minimum SOC at the end of the day, in order to be better prepared for the next day; thus, in (3.19) a minimum limit SOC^f is set.

The cost of natural gas (3.6), air charged (3.16) and air discharged (3.17) are variables dependent on the thermodynamic characteristics of the facility. As the SOC of the facility increases, so does the pressure inside the cavern; thus, it becomes difficult to store more air inside the cavern and the charging AFR decreases. The efficiency of a high pressure turbine reduces when operating below its rated power; thus, a greater discharging AFR is required to generate one unit of electricity. Hence, a higher AFR requires larger amount of natural gas, which increases the Heat Rate (HR) of the facility.

3.1.2 Thermodynamic Models

The thermodynamic characteristics of the CAES facilities were extracted from dynamic studies presented in [70]. When charging the facility from its minimum SOC to its maximum at full power, as the pressure inside the cavern increase it becomes harder to store

more air inside; thus, the charging AFR decreases as illustrated in Figure 3.1a. As previously discussed, the high pressure turbine efficiency decreases when operating below its rated power, resulting in a greater AFR is required to generate one unit of power along with a greater quantity of natural gas. Hence, the discharging AFR and HR increase for low discharging power, as depicted in Figure 3.1b and Figure 3.1c, respectively.

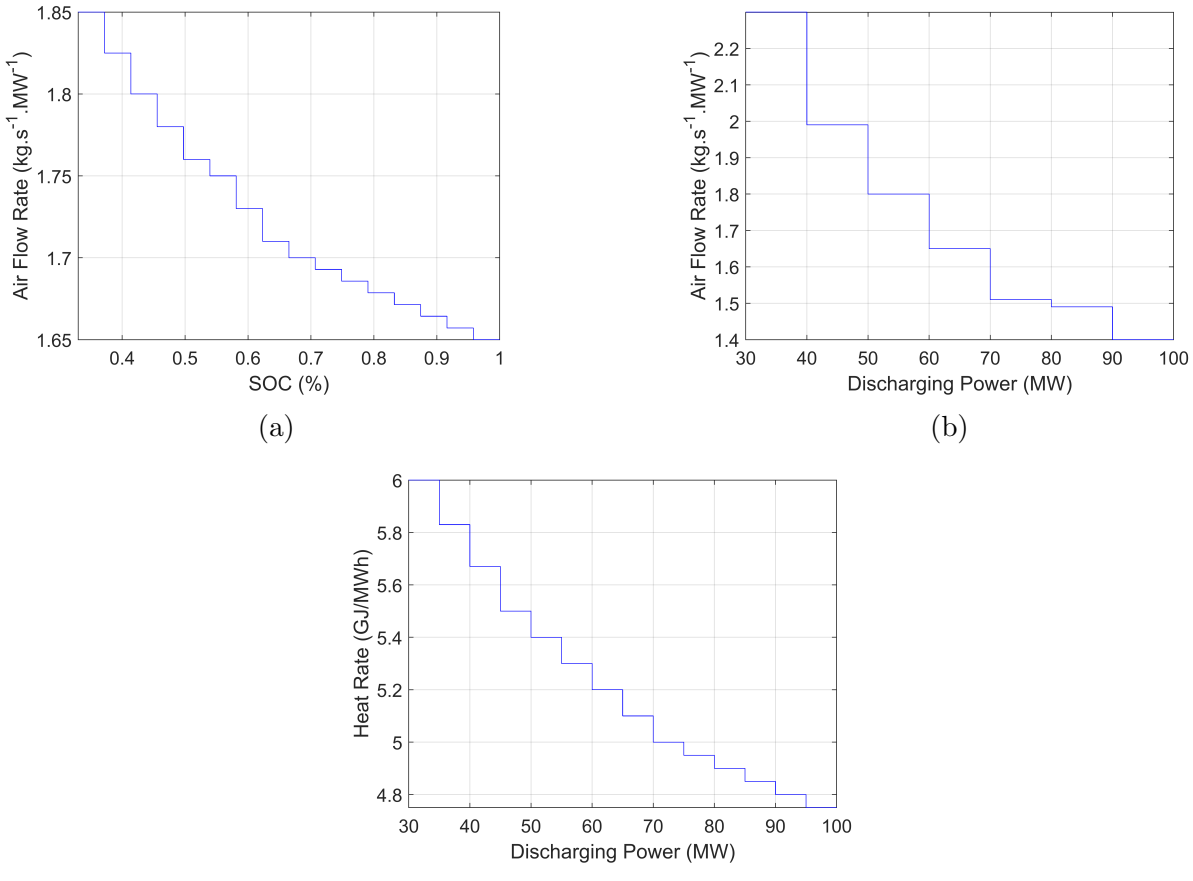

Figure 3.1: Original CAES thermodynamic characteristics: (a) AFR^C vs SOC, (b) AFR^D vs discharging power, and (c) HR vs discharging power [19].

Step Function Model

As proposed in [19], the thermodynamic characteristics of the CAES facility can be represented as step functions, as illustrated in Figure 3.2, assuming a 100 MW turbine. The charging/discharging AFR and HR of the facility are determined by identifying the operating point of the facility, i.e., the SOC and discharging power. For this purpose, a set of parameters, auxiliary and binary variables are introduced. The charging AFR based on the SOC of the cavern and mass of air charged are determined as follows:

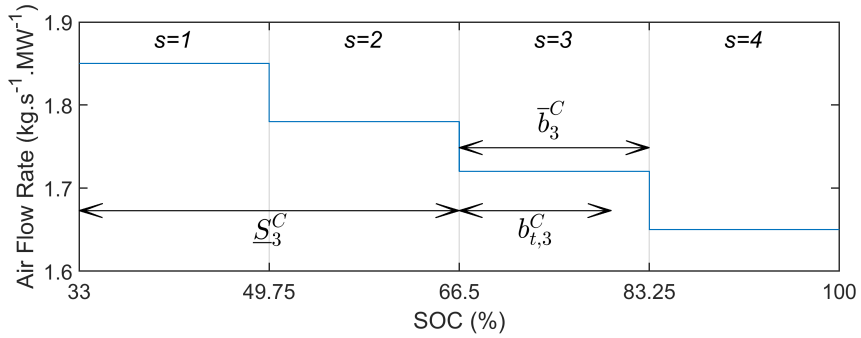

(a)

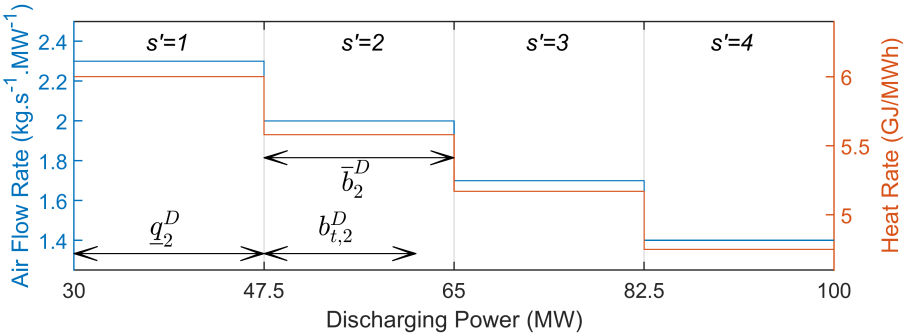

(b)

Figure 3.2: Step-function thermodynamic model: (a) charging AFR vs SOC, and (b) discharging AFR and HR vs discharging power.

$$SOC_t = \sum_{s=1}^{nc} (b^c_{t,s} + u^c_{t,s} \underline{S}^C_s) \qquad \forall t \qquad (3.20)$$

$$0 \leq b^C_{t,s} \leq u^C_{t,s} \bar{b}^C_s \qquad \forall t, s \qquad (3.21)$$

$$\sum_{s=1}^{nc} u^C_{t,s} = 1 \qquad \forall t \qquad (3.22)$$

$$air^C_t + M \geq AFR^C_s P^C_t + u^C_{t,s} M \qquad \forall t, s \qquad (3.23)$$

$$air^C_t - M \leq AFR^C_s P^C_t - u^C_{t,s} M \qquad \forall t, s \qquad (3.24)$$

where equations (3.20)-(3.22) identify the segment of operation, i.e., the charging AFR, and (3.23)-(3.24) calculates the mass of air charged.

The following equations determine the discharging AFR and HR based on the power discharged, and calculates the mass of air discharged and cost of natural gas:

$$P^D_t = \sum_{s'=1}^{nd} (b^D_{t,s'} + u^D_{t,s'} \underline{q}^D_{s'}) \qquad \forall t \qquad (3.25)$$

$$0 \leq b^D_{t,s'} \leq u^D_{t,s'} \bar{b}^D_{s'} \qquad \forall t, s' \qquad (3.26)$$

$$\sum_{s'=1}^{nd} u^D_{t,s'} = x^D_t \qquad \forall t \qquad (3.27)$$

$$air^D_t = \sum_{s'=1}^{nd} AFR^D_{s'} (b^D_{t,s'} + u^D_{t,s'} \underline{q}^D_{s'}) \qquad \forall t \qquad (3.28)$$

$$CO^{NG}_t = \sum_{s'=1}^{nd} HR_{s'} (b^D_{t,s'} + u^D_{t,s'} \underline{q}^D_{s'}) \pi^{NG} \qquad \forall t \qquad (3.29)$$

where equations (3.25)-(3.27) identify the segment of operation, i.e., the discharging AFR and HR, and (3.28)-(3.29) calculates the mass of air discharged and cost of natural gas, respectively.

Linear Thermodynamic Model

The previous step-function model, despite yielding a reasonable approximation of the thermodynamic characteristics, introduces several binary variables in the model, hence increasing the computational burden; furthermore, discontinuities make it difficult to implement

methods that track correlated uncertainties, such as AA and AP. Thus, a novel thermodynamic model of the CAES facility is proposed here using linear functions, based on the Huntorf project in Germany [12], as shown in Figure 3.3. This avoids introducing new binary and auxiliary variables to model the discontinuities, while also yielding a reasonable approximation to the original functions as illustrated in Figure 3.1. Therefore, the charging/discharging AFR and HR equations are obtained using linear interpolation as follows:

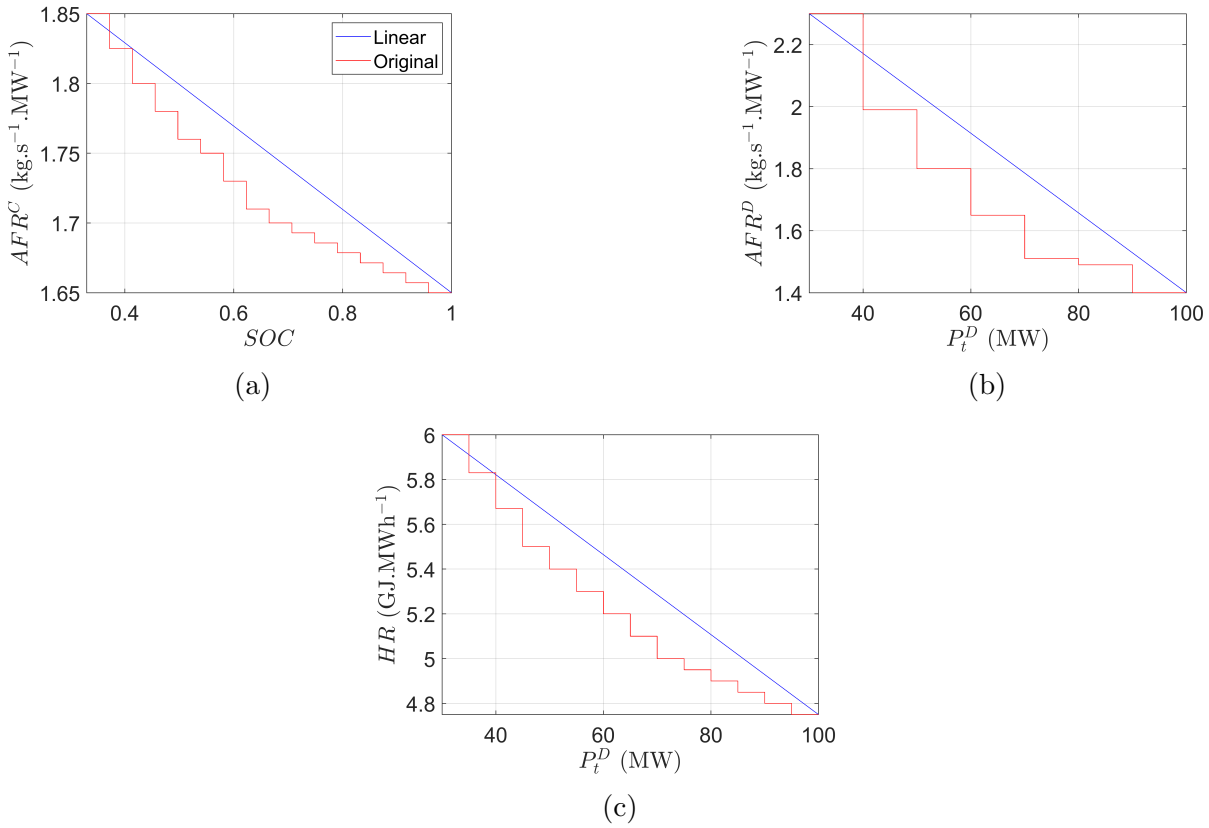

Figure 3.3: CAES thermodynamic characteristics: (a) AFR^C vs SOC, (b) AFR^D vs Discharging power, and (c) HR vs Discharging power.

$$AFR^C(SOC_t) = -0.3SOC_t + 1.95 \qquad \forall t \qquad (3.30)$$

$$AFR^D(P_t^D) = -\frac{0.9}{70}P_t^D + \frac{18.8}{7} \qquad \forall t \qquad (3.31)$$

$$HR(P_t^D) = -\frac{1.25}{70}P_t^D + \frac{457.5}{70} \qquad \forall t \qquad (3.32)$$

Replacing (3.30) in (3.16), the mass of air charged at time t is given by:

$$air_t^C = -0.3 \underbrace{SOC_t P_t^C}_{\text{Bi-linear term}} + 1.95 P_t^C \qquad \forall t \qquad (3.33)$$

where the bi-linear term in (3.33) can be linearized to transform the self-scheduling model of the CAES facility, discussed earlier, into an MILP problem. Thus, given the interval of the variables SOC_t and P_t^C, the bi-linear term can be relaxed into a set of linear constraints using McCormick Envelopes as follows [71]:

$$w_t = SOC_t P_t^C \qquad \forall t \qquad (3.34)$$

$$w_t \geq \underline{SOC}\, P_t^C + SOC_t \underline{P}^C - \underline{SOC}\, \underline{P}^C \qquad \forall t \qquad (3.35)$$

$$w_t \geq \overline{SOC}\, P_t^C + SOC_t \overline{P}^C - \overline{SOC}\, \overline{P}^C \qquad \forall t \qquad (3.36)$$

$$w_t \leq \underline{SOC} P_t^C + SOC_t \overline{P}^C - \underline{SOC} \overline{P}^C \qquad \forall t \qquad (3.37)$$

$$w_t \leq \overline{SOC} P_t^C + SOC_t \underline{P}^C - \overline{SOC} \underline{P}^C \qquad \forall t \qquad (3.38)$$

Accordingly, (3.33) can be reformulated as:

$$air_t^C = -0.3 w_t + 1.95 P_t^C \qquad \forall t \qquad (3.39)$$

Constraints (3.35)-(3.38) are valid when the CAES facility is charging, i.e., for P_t^C within its lower and upper limits. However, when the facility is not charging ($P_t^C = 0$) the problem becomes numerically infeasible, since (3.35) and (3.38) would force w_t to be positive and negative, respectively. Thus, the big M approach is used in the model to avoid numerical infeasibility, as follows:

$$w_t \leq M x_t^C \qquad \forall t \qquad (3.40)$$

$$w_t \geq \underline{SOC} P_t^C + SOC_t \underline{P}^C - \underline{SOC}\, \underline{P}^C - M(1 - x_t^C) \qquad \forall t \qquad (3.41)$$

$$w_t \geq \overline{SOC} P_t^C + SOC_t \overline{P}^C - \overline{SOC}\, \overline{P}^C - M(1 - x_t^C) \qquad \forall t \qquad (3.42)$$

$$w_t \leq \underline{SOC} P_t^C + SOC_t \overline{P}^C - \underline{SOC} \overline{P}^C + M(1 - x_t^C) \qquad \forall t \qquad (3.43)$$

$$w_t \leq \overline{SOC} P_t^C + SOC_t \underline{P}^C - \overline{SOC} \underline{P}^C + M(1 - x_t^C) \qquad \forall t \qquad (3.44)$$

The above set of constraints ensure that when the CAES facility is not in charging mode, i.e., $w_t = 0$, no numerical infeasilibility arises from the constraints.

The relationships for the mass of air discharged and the cost of natural gas are obtained from replacing (3.31) and (3.32) in (3.17) and (3.6), respectively, as follows:

$$air_t^D = -\frac{0.9}{70}\left(P_t^D\right)^2 + \frac{18.8}{7}P_t^D \qquad \forall t \tag{3.45}$$

$$\frac{CO_t^{NG}}{\pi^{NG}} = -\frac{1.25}{70}\left(P_t^D\right)^2 + \frac{457.5}{70}P_t^D \qquad \forall t \tag{3.46}$$

Taking the derivative of each equation in terms of P_t^D and equating to zero, yields the point of maxima, which are 104.4 MW and 183 MW, respectively. Since the CAES facility operates between 30-100 MW, the air discharged would be in the curvature of (3.45), and the cost of natural gas would be in the linear region of (3.46); thus, these equations can be approximated using piecewise linearization and a straight line, respectively, as shown in Figure 3.4. Their equations can then be approximated by:

$$P_t^D = \sum_{s=1}^{2}\left(b_{t,s}^D + \underline{q}_s u_{t,s}^D\right) \qquad \forall t \tag{3.47}$$

$$\sum_{s=1}^{2} u_{t,s}^D = x_t^D \qquad \forall t \tag{3.48}$$

$$0 \le b_{t,s}^D \le \bar{b}^D u_{t,s}^D \qquad \forall t, s \tag{3.49}$$

$$air_t^D = \sum_{s=1}^{2}\left(ang_s^D b_{t,s}^D + \underline{D}_s u_{t,s}^D\right) \qquad \forall t \tag{3.50}$$

$$CO_t^{NG} = \left(53.57x_t^D + 4.215P_t^D\right)\pi^{NG} \qquad \forall t \tag{3.51}$$

In (3.47) to (3.49), the power discharged by the CAES facility is decomposed in terms of variables and parameters that identify the point of operation of the facility and used to determine the mass of air discharged (3.50). In (3.51), the cost of natural gas is determined from the state of operation and discharged power. Hence, the model can be solved as an MILP problem, avoiding the complexities introduced by the discontinuities of step functions.

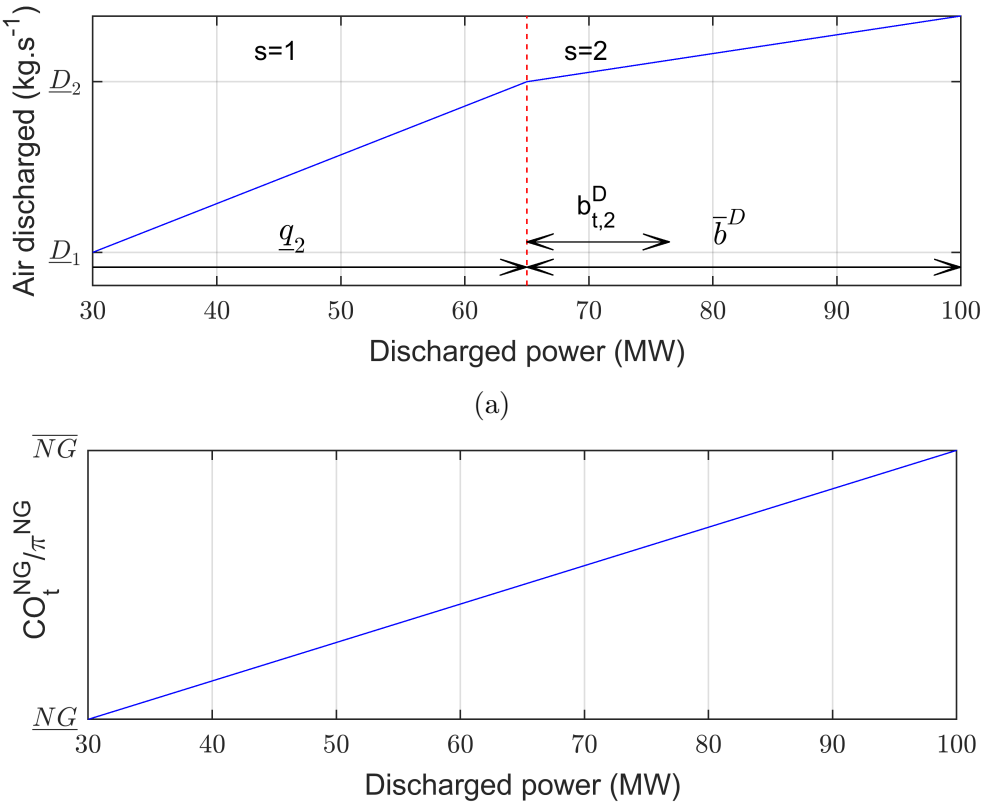

Figure 3.4: Linear approximations of (a) (3.45) and (b) (3.46).

3.2 Summary

In this Chapter, the deterministic self-scheduling model for a price-taker CAES facility that partakes in the day-ahead energy and reserve markets was presented. The operational constraints of the facility were presented, considering its thermodynamic characteristics for more realistic modeling. For this purpose, two mathematical models were presented: the first through step functions and the second using a linearization approach that significantly improves the solution convergence of the model, and also allows implementing techniques that keep track of correlated uncertainties, such as AA and AP methodologies.

Chapter 4

Modeling of CAES Systems Considering Uncertainties

This Chapter presents an extension of the mathematical model of the self-scheduling CAES price-taker facility participating in day-ahead electricity markets presented in Chapter 3, taking into account uncertainties in the electricity market prices. Three different approaches are used to represent the uncertainties, namely, RO, AA and PCA-AP. The detailed uncertainty model formulations for each of the approaches are presented next.

4.1 Robust Optimization (RO)

In the RO model, the objective is to maximize the daily profit of a price-taker CAES facility under worst case scenario. To this effect, electricity prices are expressed in terms of their center values (forecast price) and the deviation from it, as follows:

$$\pi_t^Y = \pi_{0,t}^Y(1 + \Delta\pi_t^Y) \qquad \forall t, Y \tag{4.1}$$

where $\Delta\pi^Y \in [-\overline{\Delta\pi}, \overline{\Delta\pi}]$. Substituting (4.1) in (3.2), one can write:

$$f(P_t^X) = A_t\pi_{0,t}^E(1 + \Delta\pi_t^E) + B_t\pi_{0,t}^{SR}(1 + \Delta\pi_t^{SR}) + P_t^{ID}\pi_{0,t}^{ID}(1 + \Delta\pi_t^{ID}) \qquad \forall t \tag{4.2}$$

which can be written as follows:

$$f(P_t^X) = \underbrace{A_t\pi_{0,t}^E + B_t\pi_{0,t}^{SR} + P_t^{ID}\pi_{0,t}^{ID}}_{f_0(P_t^X)} + \Delta\pi_t^E A_t\pi_t^E + \Delta\pi_t^{SR}B_t\pi_t^{SR} + \Delta\pi_t^{ID}P_t^{ID}\pi_t^{ID} \quad \forall t \tag{4.3}$$

Thus, substituting (4.3) in (3.1), and reformulating the objective function to maximize the profit under worst-case scenario, the objective function and additional constraints of the optimization problem can be stated as follows:

$$\max_{P_t^X} \min_{\Delta\pi_t^Y} \mathcal{F} = \sum_t^T [f_0(P_t^X) - OC_t + \underbrace{\Delta\pi_t^E A_t}_{\text{Bi-linear term}} \ \pi_{0,t}^E + \underbrace{\Delta\pi_t^{SR} B_t}_{\text{Bi-linear term}} \ \pi_{0,t}^{SR} + \underbrace{\Delta\pi_t^{ID} P_t^{ID}}_{\text{Bi-linear term}} \pi_{0,t}^{ID}] \tag{4.4}$$

where:

$$\Delta\pi_t^Y = \Delta\pi_t^{Y+} - \Delta\pi_t^{Y-} \qquad \forall t, Y \in [E, SR, ID] \tag{4.5}$$

$$\Delta\pi_t^{Y+} - \overline{\Delta\pi} \leq 0 \qquad \forall t, Y \tag{4.6}$$

$$\Delta\pi_t^{Y-} - \overline{\Delta\pi} \leq 0 \qquad \forall t, Y \tag{4.7}$$

$$\sum_t^T \frac{\Delta\pi_t^{Y+} + \Delta\pi_t^{Y-}}{\overline{\Delta\pi}} - \Gamma \leq 0 \qquad \forall Y \tag{4.8}$$

$$\Delta\pi_t^{Y+}, \Delta\pi_t^{Y-} \geq 0 \qquad \forall t, Y \tag{4.9}$$

The modified objective function (4.4) represents a max-min problem, where the profit is maximized in terms of power arbitrage variables and minimized in terms of price deviation variables. Equation (4.5) calculates the energy, spinning and idle reserve price deviations, and (4.6) and (4.7) limit the upward and downward price deviations to their maximum allowed levels, respectively. Finally, (4.8) controls the flexibility of conservatism in the model through the budget of uncertainty Γ, which limits the number of times the prices deviate from their forecast values. Choosing a higher $\overline{\Delta\pi}$ provides more financial protection against larger price mismatches.

The max-min structure in (4.4) is a saddle node problem, usually non-convex [31], with a set of bi-linear terms, which cannot be solved as an MILP optimization. To address this issue, the dual of the minimization problem (4.4)-(4.9) can be written as follows:

$$\max_{P_t^X, \alpha_{1,t}^Y - \alpha_{3,t}^Y, \alpha_4^Y} \mathcal{F} = \sum_t^T \Big[f_0(P_t^X) - OC_t + \overline{\Delta\pi}(\alpha_{2,t}^E + \alpha_{3,t}^E + \alpha_{2,t}^{SR} + \alpha_{3,t}^{SR} + \alpha_{2,t}^{ID} + \alpha_{3,t}^{ID}) \Big] + \big(\alpha_4^E + \alpha_4^{SR} + \alpha_4^{ID}\big)\Gamma \tag{4.10}$$

where:

$$\alpha_{2,t}^{Y},\ \alpha_{3,t}^{Y},\ \alpha_{4}^{Y} \leq 0 \qquad \forall t, Y \tag{4.11}$$

$$\alpha_{1,t}^{E} = A_t \pi_{0,t}^{E} \qquad \forall t \tag{4.12}$$

$$\alpha_{1,t}^{SR} = B_t \pi_{0,t}^{SR} \qquad \forall t \tag{4.13}$$

$$\alpha_{1,t}^{ID} = P_t^{ID} \pi_{0,t}^{ID} \qquad \forall t \tag{4.14}$$

$$-\alpha_{1,t}^{Y} + \alpha_{2,t}^{Y} + \frac{\alpha_{4}^{Y}}{\overline{\Delta\pi}} \leq 0 \qquad \forall t, Y \tag{4.15}$$

$$\alpha_{1,t}^{Y} + \alpha_{3,t}^{Y} + \frac{\alpha_{4}^{Y}}{\overline{\Delta\pi}} \leq 0 \qquad \forall t, Y \tag{4.16}$$

Thus, in (4.10), the objective function beams a maximization problem without bi-linear terms, and hence the problem can be solved as an MILP problem.

In RO, a constraint with n uncertain parameters has a probability $\mathcal{P}$ of being violated, which can be determined for a given value of Γ as follows [22]:

$$\mathcal{P} = 1 - \Phi\left(\frac{\Gamma - 1}{\sqrt{n}}\right) \tag{4.17}$$

where Φ is the cumulative distribution of a standard normal function. Thus, based on the results obtained and the probability of violation corresponding to Γ, the CAES facility operator can choose a schedule that ensures profit maximization while protecting it from a given level of uncertainty.

4.2 Affine Arithmetic (AA)

As stated earlier, the main sources of uncertainties for a price-taker CAES facility are the electricity market prices. These can be expressed in their affine forms, as follows:

$$\hat{\pi}_t^{Y} = \pi_{0,t}^{Y}(1 + \varepsilon_t^{Y}\overline{\Delta\pi}) \qquad \forall t, Y \tag{4.18}$$

In this case, a fixed interval of uncertainty is assumed for all hours of the day. However, intervals of uncertainty can be estimated based on historical data, as discussed in Section 4.3. The power dispatch variables can be expressed as:

$$\hat{P}_t^{X} = P_{0,t}^{X} + P_{1,t}^{X}\varepsilon_t^{E} + P_{2,t}^{X}\varepsilon_t^{SR} + P_{3,t}^{X}\varepsilon_t^{ID} \qquad \forall t, X \tag{4.19}$$

$$P_{h,t}^{X} \geq 0 \qquad \forall t, h \in [1, 2, 3] \tag{4.20}$$

where $P^X_{0,t}$ denotes the center terms of the power dispatch X, and $P^X_{1,t}$, $P^X_{2,t}$ and $P^X_{3,t}$ denotes the adjustments in power dispatch, given the mismatch in prices Y, i.e., energy, spinning and idle reserve prices, respectively. Substituting (4.18) and (4.19) in (3.1), yields:

$$\max_{\hat{P}^X_t} \mathcal{F} = \sum_t^T \left[\hat{f}(\hat{P}^X_t) - \widehat{OC}_t\right] \tag{4.21}$$

where the affine forms of the CAES facility's revenue and operating costs can be expressed as follows:

$$\hat{f}(\hat{P}^x_t) = (\hat{P}^D_t - \hat{P}^C_t)\hat{\pi}^E_t + (\hat{P}^{SRD}_t + \hat{P}^{SRC}_t)\hat{\pi}^{SR}_t + \hat{P}^{ID}_t\hat{\pi}^{ID}_t \qquad \forall t \tag{4.22}$$

$$\widehat{OC}_t = \widehat{CO}^{NG}_t + \hat{P}^D_t VOM^e + \hat{P}^C_t VOM^c \qquad \forall t \tag{4.23}$$

The affine form of the CAES facility's revenue in (4.22), can be expanded as follows:

$$\begin{aligned}\hat{f}(\hat{P}^x_t) =& \big(P^D_{0,t} + P^D_{1,t}\varepsilon^E_t + P^D_{2,t}\varepsilon^{SR}_t + P^D_{3,t}\varepsilon^{ID}_t \\ &- P^C_{0,t} - P^C_{1,t}\varepsilon^E_t - P^C_{2,t}\varepsilon^{SR}_t - P^C_{3,t}\varepsilon^{ID}_t\big)\pi^E_{0,t}(1 + \overline{\Delta\pi}\varepsilon^E_t) + \\ &\big(P^{SRD}_{0,t} + P^{SRD}_{1,t}\varepsilon^E_t + P^{SRD}_{2,t}\varepsilon^{SR}_t + P^{SRD}_{3,t}\varepsilon^{ID}_t \\ &+ P^{SRC}_{0,t} + P^{SRC}_{1,t}\varepsilon^E_t + P^{SRC}_{2,t}\varepsilon^{SR}_t + P^{SRC}_{3,t}\varepsilon^{ID}_t\big)\pi^{SR}_{0,t}(1 + \overline{\Delta\pi}\varepsilon^{SR}_t) \\ &+ \big(P^{ID}_{0,t} + P^{ID}_{1,t}\varepsilon^E_t + P^{ID}_{2,t}\varepsilon^{SR}_t + P^{ID}_{3,t}\varepsilon^{ID}_t\big)\pi^{ID}_{0,t}(1 + \overline{\Delta\pi}\varepsilon^{ID}_t) \qquad \forall t\end{aligned} \tag{4.24}$$

Executing the affine and non-affine operations, the resulting terms can be grouped as follows:

$$\begin{aligned}\hat{f}(\hat{P}^x_t) =& \underbrace{(P^D_{0,t} - P^C_{0,t})\pi^E_{0,t} + (P^{SRD}_{0,t} + P^{SRC}_{0,t})\pi^{SR}_{0,t} + P^{ID}_{0,t}\pi^{ID}_{0,t}}_{\text{Center terms}} + \\ &\underbrace{\Big(\big((P^D_{0,t} - P^C_{0,t})\overline{\Delta\pi} + P^D_{1,t} - P^C_{1,t}\big)\pi^E_{0,t} + (P^{SRD}_{1,t} + P^{SRC}_{1,t})\pi^{SR}_{0,t} + P^{ID}_{1,t}\pi^{ID}_{0,t}\Big)\varepsilon^E_t}_{\text{Affine energy terms}} + \\ &\underbrace{\Big((P^D_{2,t} - P^C_{2,t})\pi^E_{0,t} + \big((P^{SRD}_{0,t} - P^{SRC}_{0,t})\overline{\Delta\pi} + P^{SRD}_{2,t} + P^{SRC}_{2,t}\big)\pi^{SR}_{0,t} + P^{ID}_{2,t}\pi^{ID}_{0,t}\Big)\varepsilon^{SR}_t}_{\text{Affine spinning reserve terms}} + \\ &\underbrace{\Big((P^D_{3,t} - P^C_{3,t})\pi^E_{0,t} + (P^{SRD}_{3,t} + P^{SRC}_{3,t})\pi^{SR}_{0,t} + \big(P^{ID}_{0,t}\overline{\Delta\pi} + P^{ID}_{3,t}\big)\pi^{ID}_{0,t}\Big)\varepsilon^{ID}_t}_{\text{Affine idle reserve terms}} + \\ &\underbrace{\sum_{h=1}^{3}\Big((P^D_{h,t} - P^C_{h,t})\pi^E_{0,t} + (P^{SRD}_{h,t} - P^{SRC}_{h,t})\pi^{SR}_{0,t} + P^{ID}_{h,t}\pi^{ID}_{0,t}\Big)\overline{\Delta\pi}}_{\text{Non-affine terms}} \qquad \forall t\end{aligned} \tag{4.25}$$

Note that the noise associated with non-affine terms, i.e., the product of two noise terms, are assumed to be equal to 1, which is a conservative approach, but it provides more protection against internal sources of errors.

Substituting (3.51) in (4.23), the affine form representation of the CAES facility's operating cost can be expanded and written as follows:

$$\begin{aligned}\widehat{OC}_t =& 53.57\pi^{NG}x_t^D + (P_{0,t}^D + P_{1,t}^D\varepsilon_t^E + P_{2,t}^D\varepsilon_t^{SR} + P_{3,t}^D\varepsilon_t^{ID})4.215\pi^{NG} + \\ & (P_{0,t}^D + P_{1,t}^D\varepsilon_t^E + P_{2,t}^D\varepsilon_t^{SR} + P_{3,t}^D\varepsilon_t^{ID})VOM^e + \\ & (P_{0,t}^C + P_{1,t}^C\varepsilon_t^E + P_{2,t}^C\varepsilon_t^{SR} + P_{3,t}^C\varepsilon_t^{ID})VOM^c \qquad \forall t \end{aligned} \tag{4.26}$$

Executing the affine operations, the terms can be grouped like before, as follows:

$$\begin{aligned}\widehat{OC}_t =& \underbrace{53.57\pi^{NG}x_t^D + P_{0,t}^D(4.215\pi^{NG} + VOM^e) + P_{0,t}^C VOM^c}_{\text{Center terms}} + \\ & \underbrace{\big(P_{1,t}^D(4.215\pi^{NG} + VOM^e) + P_{1,t}^C VOM^c\big)\varepsilon_t^E}_{\text{Affine energy terms}} + \underbrace{\big(P_{2,t}^D(4.215\pi^{NG} + VOM^e) + P_{2,t}^C VOM^c\big)\varepsilon_t^{SR}}_{\text{Affine spinning reserve terms}} \\ & + \underbrace{\big(P_{3,t}^D(4.215\pi^{NG} + VOM^e) + P_{3,t}^C VOM^c\big)\varepsilon_t^{ID}}_{\text{Affine idle reserve terms}} \quad \forall t \end{aligned} \tag{4.27}$$

Subtracting (4.27) from (4.25) and re-organizing terms, one can write:

$$\begin{aligned}\mathcal{F}_{0,t} =& (P_{0,t}^D - P_{0,t}^C)\pi_{0,t}^E + (P_{0,t}^{SRD} + P_{0,t}^{SRC})\pi_{0,t}^{SR} + P_{0,t}^{ID}\pi_{0,t}^{ID} - 53.57\pi^{NG}x_t^D \\ & - P_{0,t}^D(4.215\pi^{NG} + VOM^e) - P_{0,t}^C VOM^c \qquad \forall t \end{aligned} \tag{4.28}$$

$$\begin{aligned}\mathcal{F}_{1,t} =& \Big(\big((P_{0,t}^D - P_{0,t}^C)\overline{\Delta\pi} + P_{1,t}^D - P_{1,t}^C\big)\pi_{0,t}^E + (P_{1,t}^{SRD} + P_{1,t}^{SRC})\pi_{0,t}^{SR} \\ & + P_{1,t}^{ID}\pi_{0,t}^{ID} - P_{1,t}^D(4.215\pi^{NG} + VOM^e) - P_{1,t}^C VOM^c\Big)\varepsilon_t^E \qquad \forall t \end{aligned} \tag{4.29}$$

$$\begin{aligned}\mathcal{F}_{2,t} =& \Big((P_{2,t}^D - P_{2,t}^C)\pi_{0,t}^E + \big((P_{0,t}^{SRD} - P_{0,t}^{SRC})\overline{\Delta\pi} + P_{2,t}^{SRD} + P_{2,t}^{SRC}\big)\pi_{0,t}^{SR} \\ & + P_{2,t}^{ID}\pi_{0,t}^{ID} - P_{2,t}^D(4.215\pi^{NG} + VOM^e) - P_{2,t}^C VOM^c\Big)\varepsilon_t^{SR} \qquad \forall t \end{aligned} \tag{4.30}$$

$$\begin{aligned}\mathcal{F}_{3,t} =& \Big((P_{3,t}^D - P_{3,t}^C)\pi_{0,t}^E + (P_{3,t}^{SRD} + P_{3,t}^{SRC})\pi_{0,t}^{SR} + \big(P_{0,t}^{ID}\overline{\Delta\pi} + P_{3,t}^{ID}\big)\pi_{0,t}^{ID} \\ & - P_{3,t}^D(4.215\pi^{NG} + VOM^e) - P_{3,t}^C VOM^c\Big)\varepsilon_t^{ID} \qquad \forall t \end{aligned} \tag{4.31}$$

$$\mathcal{F}_{4,t} = \sum_{h=1}^{3}\Big((P_{h,t}^D - P_{h,t}^C)\pi_{0,t}^E + (P_{h,t}^{SRD} - P_{h,t}^{SRC})\pi_{0,t}^{SR} + P_{h,t}^{ID}\pi_{0,t}^{ID}\Big)\overline{\Delta\pi} \qquad \forall t \tag{4.32}$$

where $\mathcal{F}_{0,t}$ denotes the center, $\mathcal{F}_{1,t}$ to $\mathcal{F}_{3,t}$ represent the affine terms for energy, spinning and idle reserve, respectively, and $\mathcal{F}_{4,t}$ corresponds to the non-affine terms of the objective function.

Since the CAES facility's self-scheduling model in affine form includes binary and inter-temporal variables, it cannot be solved using the decoupled approach of maximizing the center and radius of the objective function separately, as the solution of one problem may be infeasible for the other. Therefore, the objective function in affine form is formulated as follows:

$$\max_{\hat{P}_t^X} \sum_{t=1}^{T} \left(\mathcal{F}_{0,t} + \left| \sum_{h=1}^{3} \mathcal{F}_{h,t} - \mathcal{F}_{4,t} \right| \right) \tag{4.33}$$

Note that the center and modulus of the radius are maximized simultaneously, yielding a single and reasonably conservative day-ahead schedule for the CAES facility. Observe also that maximization of the radius takes place by maximizing the affine terms and minimizing the non-affine terms, thus avoiding a large and conservative radius, which may lead to significantly lower profits or even losses.

The AA approach is not applied to the step function thermodynamic model due to the large discontinuities present in it, which would require the introduction of new binary and auxiliary variables; hence, increasing significantly the computational costs of solving the problem. The proposed piecewise linear thermodynamic model, which presents a smoother profile, makes the AA approach more feasible.

The operational constraints presented in (3.7)-(3.12) can be formulated according to

(2.24), yielding:

$$P_{0,t}^{C} + \sum_{h=1}^{3} P_{h,t}^{C} \leq \overline{P}^{C} x_t^{C} \qquad \forall t \qquad (4.34)$$

$$P_{0,t}^{SRC} + \sum_{h=1}^{3} P_{h,t}^{SRC} \leq P_{0,t}^{C} - \sum_{h=1}^{3} P_{h,t}^{C} - \underline{P}^{C} x_t^{C} \qquad \forall t \qquad (4.35)$$

$$P_{0,t}^{SRD} + \sum_{h=1}^{3} P_{h,t}^{SRD} \leq \overline{P}^{D} x_t^{D} - P_{0,t}^{D} - \sum_{h=1}^{3} P_{h,t}^{D} \qquad \forall t \qquad (4.36)$$

$$P_{0,t}^{D} - \sum_{h=1}^{3} P_{h,t}^{D} \geq \underline{P}^{D} x_t^{D} \qquad \forall t \qquad (4.37)$$

$$0 \leq P_{0,t}^{ID} \pm \sum_{h=1}^{3} P_{h,t}^{ID} \leq QSC x_t^{ID} \qquad \forall t \qquad (4.38)$$

Note that binary variables cannot be represented in affine form, since they are not continuous, thus coordination constraints (3.7)-(3.9) remain unchanged.

The inter-temporal constraint (3.15) can be formulated according to (2.23), as follows:

$$SOC_{0,t+1} = SOC_{0,t} + \frac{(air_{0,t}^{C} - air_{0,t}^{D})3,600}{\overline{CA}} \qquad \forall t \qquad (4.39)$$

$$\sum_{h=1}^{p} SOC_{h,t+1} = \sum_{h=1}^{p} SOC_{h,t} + \sum_{h=1}^{p} \left[\frac{(air_{h,t}^{C} - air_{h,t}^{D})3,600}{\overline{CA}} \right] \qquad \forall t \qquad (4.40)$$

$$SOC_{0,t+1} + \sum_{h=1}^{p} |SOC_{h,t+1}| \leq \overline{SOC} \qquad \forall t \qquad (4.41)$$

$$SOC_{0,t+1} - \sum_{h=1}^{p} |SOC_{h,t+1}| \geq \underline{SOC} \qquad \forall t \qquad (4.42)$$

$$SOC_{0,t} - \sum_{h=1}^{p} |SOC_{h,t}| \geq SOC^{f} \qquad \forall t = T \qquad (4.43)$$

Note that $SOC_{h,t}$ are unrestricted-sign variables, and constraint (4.40) does not ensure equality among the h terms as per (2.23), but guarantees that no limits are violated.

Equations (3.39)-(3.44) can be represented in their affine forms as follows:

$$air^C_{0,t} = -0.3w_{0,t} + 1.95P^C_{0,t} \qquad \forall t \qquad (4.44)$$

$$\sum_{h=1}^{3} air^C_{h,t} = \sum_{h=1}^{3} \left[-0.3w_{h,t} + 1.95P^C_{h,t}\right] \qquad \forall t \qquad (4.45)$$

$$\begin{aligned} w_{0,t} - \sum_{h=1}^{3} w_{h,t} \geq\ & \underline{SOC} P^C_{0,t} + SOC_{0,t}\underline{P}^C - \underline{SOC}\,\underline{P}^C - M(1 - x^C_t) \\ & + \sum_{h=1}^{3} \left[\underline{SOC}\, P^C_{h,t} + |SOC_{h,t}|\underline{P}^C\right] \qquad \forall t \end{aligned} \qquad (4.46)$$

$$\begin{aligned} w_{0,t} - \sum_{h=1}^{3} w_{h,t} \geq\ & \overline{SOC} P^C_{0,t} + SOC_{0,t}\overline{P}^C - \overline{SOC}\,\overline{P}^C - M(1 - x^C_t) \\ & + \sum_{h=1}^{3} \left[\overline{SOC}\, P^C_{h,t} + |SOC_{h,t}|\overline{P}^C\right] \qquad \forall t \end{aligned} \qquad (4.47)$$

$$\begin{aligned} w_{0,t} + \sum_{h=1}^{3} w_{h,t} \leq\ & \underline{SOC} P^C_{0,t} + SOC_{0,t}\overline{P}^C - \underline{SOC}\,\overline{P}^C - M(1 - x^C_t) \\ & - \sum_{h=1}^{3} \left[\underline{SOC}\, P^C_{h,t} + |SOC_{h,t}|\overline{P}^C\right] \qquad \forall t \end{aligned} \qquad (4.48)$$

$$\begin{aligned} w_{0,t} + \sum_{h=1}^{3} w_{h,t} \leq\ & \overline{SOC} P^C_{0,t} + SOC_{0,t}\underline{P}^C - \overline{SOC}\,\underline{P}^C - M(1 - x^C_t) \\ & - \sum_{h=1}^{3} \left[\overline{SOC}\, P^C_{h,t} + |SOC_{h,t}|\underline{P}^C\right] \qquad \forall t \end{aligned} \qquad (4.49)$$

$$w_{0,t},\ w_{h,t} \geq 0 \qquad \forall t, h \qquad (4.50)$$

Note that (4.45) does not ensure equality among the h terms as per (2.23), but guarantees that the intervals are not violated.

Finally, the air discharged and the cost of natural gas can be represented in their affine

forms as follows:

$$P^D_{0,t} = \sum_{s=1}^{2} \left(b^D_{t,s} + \underline{q}_s u^D_{t,s}\right) \qquad \forall t \qquad (4.51)$$

$$P^D_{0,t} - \sum_{h=1}^{3} P^D_{h,t} = \sum_{s'=1}^{2} \left(b^D_{t,s'} + \underline{q}_{s'} u^D_{t,s'}\right) \qquad \forall t \qquad (4.52)$$

$$\sum_{s=1}^{2} u^D_{t,s} = x^D_t \qquad \forall t \qquad (4.53)$$

$$\sum_{s'=1}^{2} u^D_{t,s'} = x^D_t \qquad \forall t \qquad (4.54)$$

$$0 \le b^D_{t,s} \le \bar{b}^D u^D_{t,s} \qquad \forall t, s \qquad (4.55)$$

$$0 \le b^D_{t,s'} \le \bar{b}^D u^D_{t,s'} \qquad \forall t, s' \qquad (4.56)$$

$$air^D_{0,t} = \sum_{s=1}^{2} \left(ang^D_s b^D_{t,s} + \underline{D}_s u^D_{t,s}\right) \qquad \forall t \qquad (4.57)$$

$$\underline{air}^D_t = \sum_{s'=1}^{2} \left(ang^D_{s'} b^D_{t,s'} + \underline{D}_{s'} u^D_{t,s'}\right) \qquad \forall t \qquad (4.58)$$

$$\sum_{h=1}^{3} air^D_{h,t} = air^D_{0,t} - \underline{air}^D_t \qquad \forall t \qquad (4.59)$$

$$CO^{NG}_{0,t} = \left(53.57 x^D_t + 4.215 P^D_{0,t}\right)\pi^{NG} \qquad \forall t \qquad (4.60)$$

$$CO^{NG}_{h,t} = 4.215 P^D_{h,t}\pi^{NG} \qquad \forall t, h \qquad (4.61)$$

where the set s', parameters $\underline{q}_{s'}$ and $\underline{D}_{s'}$, and variables $b^D_{t,s'}$ and $u^D_{t,s'}$ play a similar role as s, $\underline{q}_s$, $\underline{D}_s$, $b^D_{t,s}$ and $u^D_{t,s}$, respectively, to determine the lower bound for the air discharged in (4.58). Thus, the interval of the air discharged is determined by subtracting the lower bound from the center value, as in (4.59) and illustrated in Figure 4.1. Since the cost of natural gas is a linear function as shown in Figure (3.4b), its uncertainty terms can be determined directly, as in (4.60) and (4.61).

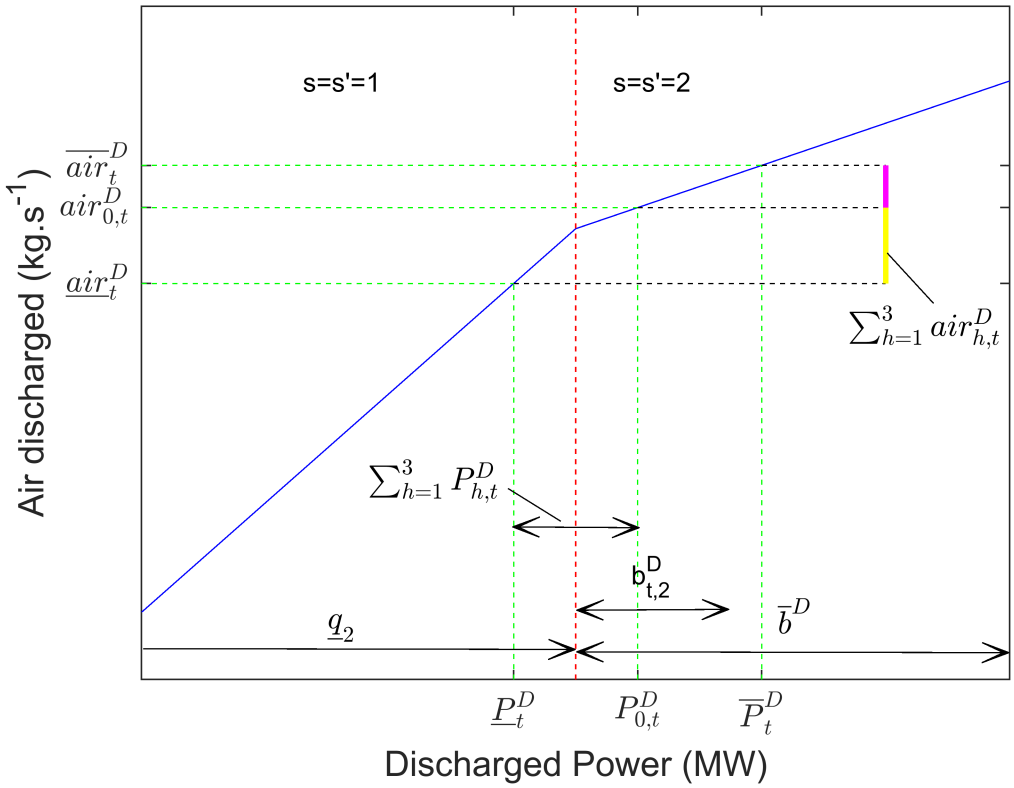

Figure 4.1: Typical air discharge characteristic of CAES facility denoting various intervals.

4.3 Principal Components Analysis (PCA)-Affine Policies (AP)

The first step in the PCA-AP model is to determine the matrix of eigenvectors $\mathbf{V}$ associated with the price matrices. Motivated by the use of PCA to forecast electricity prices and study their fluctuations [72, 73], it is assumed here that PCA price matrices can be formed using the hourly electricity prices for energy, spinning, and idle reserves for $\mathcal{D}$ days, which can be expressed as follows:

$$\mathbf{\Pi^Y} = \begin{bmatrix} \pi_{1,1}^Y & \cdots & \pi_{1,24}^Y \\ \vdots & \ddots & \vdots \\ \pi_{\mathcal{D},1}^Y & \cdots & \pi_{\mathcal{D},24}^Y \end{bmatrix} \qquad \forall Y \tag{4.62}$$

where the rows represent the day and the columns the hour. Executing the aforementioned PCA steps, based on the eigenvectors $\mathbf{V^Y}$ and eigenvalues $\mathbf{\Lambda^Y}$ of $\mathbf{\Pi^Y}$, the PC can be determined as follows [67]:

$$PC^Y_{24\times 1} = \left(\mathbf{V^Y}\right)^T_{24\times 24}\pi^Y_{24\times 1} \qquad \forall Y \tag{4.63}$$

Electricity prices have a forecast value and a range of uncertainty, which can be represented using APs as follows:

$$\hat{\pi}^Y_t = \pi^Y_{0,t}(1+\Delta\pi^Y_t) \qquad \forall t, Y \tag{4.64}$$

$$-\overline{\Delta\pi}^Y_t \leq \Delta\pi^Y_t \leq \overline{\Delta\pi}^Y_t \qquad \forall t, Y \tag{4.65}$$

where $\Delta\pi^Y_t$ represents the mismatches in prices of Y, which can be included in the representation of power dispatch variables in AP form to adjust the dispatch according to the mismatches in actual prices with respect to the forecast, as explained next.

Replacing (4.64) in (4.63), the AP form of PC^Y can be obtained as follows:

$$\widehat{PC}^Y = \underbrace{\left(\mathbf{V^Y}\right)^T\pi^Y_0}_{PC^Y_0} + \underbrace{\left(\mathbf{V^Y}\right)^T\pi^Y_0 \odot \Delta\pi^Y}_{\Delta PC^Y} \qquad \forall Y \tag{4.66}$$

where $\pi^Y_0 = [\pi^Y_{0,1}\,\pi^Y_{0,2}\ldots\pi^Y_{0,24}]^T$ and $\pi^Y_0 \odot \Delta\pi^Y = [\pi^Y_{0,1}\Delta\pi^Y_1\,\pi^Y_{0,2}\Delta\pi^Y_2\ldots\pi^Y_{0,24}\Delta\pi^Y_{24}]^T$. From (4.66), the following limits can be defined, based on (4.65):

$$\overline{\Delta PC}^Y = \left(\mathbf{V^Y}\right)^T\pi^Y_0\overline{\Delta\pi}^Y \qquad \forall Y \tag{4.67}$$

$$-\overline{\Delta PC}^Y \leq \Delta PC^Y \leq \overline{\Delta PC}^Y \qquad \forall Y \tag{4.68}$$

From (4.63), electricity prices can be represented as a function of PCs. In order to do so, the matrix $\mathbf{L^Y}$ can be defined as follows:

$$\mathbf{L^Y} = \begin{bmatrix} l^Y_{1,1} & \cdots & l^Y_{1,24} \\ \vdots & \ddots & \vdots \\ l^Y_{24,1} & \cdots & l^Y_{24,24} \end{bmatrix} = \left(\left(\mathbf{V^Y}\right)^T\right)^{-1} \qquad \forall Y \tag{4.69}$$

Discarding the columns associated with the PCs with low information, the AP form of prices can be expressed as follows:

$$\hat{\pi}^Y_{24\times 1} = \mathbf{L^Y}_{24\times NPC}\widehat{PC}^Y_{NPC\times 1} \qquad \forall Y \tag{4.70}$$

$$\hat{\pi}^Y_t = \underbrace{\sum_{n=1}^{NPC} l^Y_{t,n}PC^Y_{0,n}}_{\pi^Y_{0,t}} + \underbrace{\sum_{n=1}^{NPC} l^Y_{t,n}\Delta PC^Y_n}_{\Delta\pi^Y_t} \qquad \forall t, Y \tag{4.71}$$

And the power dispatch variables in their AP forms can be represented as follows:

$$\hat{P}_t^X = P_{0,t}^X + \sum_Y \sum_{n=1}^{NPC} p_{n,t}^{X,Y} \Delta PC_n^Y \qquad \forall t, X \tag{4.72}$$

where $p_{n,t}^{X,Y}$ are the adjustment terms of power dispatch X with respect to the mismatch of PC n of electricity price Y at time t, which are unrestricted sign variables. Hence:

$$P_{0,t}^X + \sum_Y \sum_{n=1}^{NPC} \left|p_{n,t}^{X,Y}\right| \overline{\Delta PC}_n^Y \leq \overline{P}^X \qquad \forall t, X \tag{4.73}$$

$$P_{0,t}^X - \sum_Y \sum_{n=1}^{NPC} \left|p_{n,t}^{X,Y}\right| \overline{\Delta PC}_n^Y \geq \underline{P}^X \qquad \forall t, X \tag{4.74}$$

Since there are modulus in the above formulation, and in order to avoid non-linearities, auxiliary variables and binary variables can be introduced as follows [74]:

$$p_{n,t}^{X,Y} = p_{n,t}^{X,Y+} - p_{n,t}^{X,Y-} \qquad \forall t, n, X, Y \tag{4.75}$$

$$p_{n,t}^{X,Y+} \leq M x p_{n,t}^{X,Y} \qquad \forall t, n, X, Y \tag{4.76}$$

$$p_{n,t}^{X,Y-} \leq M(1 - x p_{n,t}^{X,Y}) \qquad \forall t, n, X, Y \tag{4.77}$$

$$\left|p_{n,t}^{X,Y}\right| = p_{n,t}^{X,Y+} + p_{n,t}^{X,Y-} \qquad \forall t, n, X, Y \tag{4.78}$$

$$p_{n,t}^{X,Y+}; p_{n,t}^{X,Y-} \geq 0 \qquad \forall t, n, X, Y \tag{4.79}$$

where M is a large number. Thus, as the number of PCs NPC increase, so does the variables and constraints in the model.

For better presentation, (4.72) can be rewritten as:

$$\hat{P}_t^X = P_{0,t}^X + \Delta P_t^X \qquad \forall t, X \tag{4.80}$$

where:

$$\Delta P_t^X = \sum_Y \sum_{n=1}^{NPC} p_{n,t}^{X,Y} \Delta PC_n^Y \qquad \forall t, X \tag{4.81}$$

Then, substituting (4.71) and (4.80) in (3.1) yields:

$$\max_{\hat{P}_t^X} \mathcal{F} = \sum_t^T \left[\hat{f}(\hat{P}_t^X) - \widehat{OC}_t\right] \tag{4.82}$$

where:

$$\hat{f}(\hat{P}_t^x) = (\hat{P}_t^D - \hat{P}_t^C)\hat{\pi}_t^E + (\hat{P}_t^{SRD} + \hat{P}_t^{SRC})\hat{\pi}_t^{SR} + \hat{P}_t^{ID}\hat{\pi}_t^{ID} \qquad \forall t \qquad (4.83)$$

$$\widehat{OC}_t = \widehat{CO}_t^{NG} + \hat{P}_t^D VOM^e + \hat{P}_t^C VOM^c \qquad \forall t \qquad (4.84)$$

Expanding the AP form representation of the CAES facility's revenue in (4.83), one has:

$$\begin{aligned}\hat{f}(\hat{P}_t^X) =& (P_{0,t}^D + \Delta P_t^D - P_{0,t}^C - \Delta P_t^C)(\pi_{0,t}^E + \Delta\pi_t^E) + \\ & (P_{0,t}^{SRD} + \Delta P_t^{SRD} + P_{0,t}^{SRC} + \Delta P_t^{SRC})(\pi_{0,t}^{SR} + \Delta\pi_t^{SR}) + \\ & (P_{0,t}^{ID} + \Delta P_t^{ID})(\pi_{0,t}^{ID} + \Delta\pi_t^{ID}) \qquad \forall t \end{aligned} \qquad (4.85)$$

which, re-arranging and grouping terms, results in:

$$\begin{aligned}\hat{f}(\hat{P}_t^X) =& \underbrace{(P_{0,t}^D - P_{0,t}^C)\pi_{0,t}^E + (P_{0,t}^{SRD} + P_{0,t}^{SRC})\pi_{0,t}^{SR} + P_{0,t}^{ID}\pi_{0,t}^{ID}}_{\text{Center terms}} + \\ & \underbrace{(P_{0,t}^D - P_{0,t}^C)\Delta\pi_t^E + (\Delta P_t^D - \Delta P_t^C)\pi_t^E}_{\text{Energy linear uncertainty terms}} + \\ & \underbrace{(P_{0,t}^{SRD} + P_{0,t}^{SRC})\Delta\pi_t^{SR} + (\Delta P_t^{SRD} + \Delta P_t^{SRC})\pi_t^{SR}}_{\text{Spinning reserve linear uncertainty terms}} + \\ & \underbrace{P_{0,t}^{ID}\Delta\pi_t^{ID} + \Delta P_t^{ID}\pi_t^{ID}}_{\text{Idle reserve linear uncertainty terms}} + \\ & \underbrace{(\Delta P_t^D - \Delta P_t^C)\Delta\pi_t^E + (\Delta P_t^{SRD} + \Delta P_t^{SRC})\Delta\pi_t^{SR} + \Delta P_t^{ID}\Delta\pi_t^{ID}}_{\text{Non-linear uncertainty terms}} \qquad \forall t \end{aligned} \qquad (4.86)$$

Expanding the operations cost of the CAES facility expressed in AP form in (4.84), one obtains:

$$\begin{aligned}\widehat{OC}_t =& \underbrace{53.57\pi^{NG}x_t^D + P_{0,t}^D(4.215\pi^{NG} + VOM^e) + P_{0,t}^C VOM^c}_{\text{Center terms}} + \\ & \underbrace{\Delta P_t^D(4.215\pi^{NG} + VOM^e) + \Delta P_t^C VOM^c}_{\text{Linear uncertainty terms}} \qquad \forall t \end{aligned} \qquad (4.87)$$

Subtracting (4.87) from (4.86), the result can then be split into the following terms:

$$\begin{aligned}
\mathcal{F}_{0,t} =&(P^D_{0,t} - P^C_{0,t})\pi^E_{0,t} + (P^{SRD}_{0,t} + P^{SRC}_{0,t})\pi^{SR}_{0,t} + P^{ID}_{0,t}\pi^{ID}_{0,t} - 53.57\pi^{NG}x^D_t \\
&- P^D_{0,t}(4.215\pi^{NG} + VOM^e) - P^C_{0,t}VOM^c && \forall t \quad (4.88)\\
\mathcal{F}_{l,t} =&(P^D_{0,t} - P^C_{0,t})\Delta\pi^E_t + (\Delta P^D_t - \Delta P^C_t)\pi^E_t + \\
&(P^{SRD}_{0,t} + P^{SRC}_{0,t})\Delta\pi^{SR}_t + (\Delta P^{SRD}_t + \Delta P^{SRC}_t)\pi^{SR}_t + \\
&P^{ID}_{0,t}\Delta\pi^{ID}_t + \Delta P^{ID}_t\pi^{ID}_t - \Delta P^D_t(4.215\pi^{NG} + VOM^e) - \Delta P^C_t VOM^c && \forall t \quad (4.89)\\
\mathcal{F}_{nl,t} =&(\Delta P^D_t - \Delta P^C_t)\Delta\pi^E_t + (\Delta P^{SRD}_t + \Delta P^{SRC}_t)\Delta\pi^{SR}_t + \Delta P^{ID}_t\Delta\pi^{ID}_t && \forall t \quad (4.90)
\end{aligned}$$

where $\mathcal{F}_{0,t}$ denotes the center, $\mathcal{F}_{l,t}$ the linear uncertainty terms, and $\mathcal{F}_{nl,t}$ the non-linear uncertainty terms. To secure protection from the worst uncertainties, the self-scheduling model of the CAES facility is be optimized for the widest intervals of uncertainty, i.e., for $\Delta PC^Y = \overline{\Delta PC}^Y$, which linearizes the bi-linear terms in (4.90).

The objective function can be summarized as follows:

$$\max_{\hat{P}^X_t} \sum_{t=1}^{T} \Big(\mathcal{F}_{0,t} + \mathcal{F}_{l,t} - \mathcal{F}_{nl,t} \Big) \tag{4.91}$$

where the center $\mathcal{F}_{0,t}$ and radius $\mathcal{F}_{l,t}$ and $\mathcal{F}_{nl,t}$ of the profit are maximized simultaneously; to avoid a conservative result, the radius is maximized in terms of $\mathcal{F}_{l,t}$ and minimized in terms of $\mathcal{F}_{nl,t}$. Similar to AA, the PCA-AP approach is not applied to the step model due to its discontinuities, which make the tracking of correlated uncertainties highly complex. Thus, the proposed approach is applied in the proposed piecewise linear thermodynamic model, where the discontinuities present a smoother profile. The operational constraints of this optimization problem representing the CAES facility (3.7)-(3.12) can then be reformulated using (4.73) and (4.74), which are given by:

$$\begin{aligned}
&\big|\Delta P^X_t\big| = \sum_{Y} \sum_{n=1}^{NPC} \Big| p^{X,Y}_{n,t} \Big| \, \overline{\Delta PC}^Y_n && \forall t, X \quad (4.92)\\
&P^C_{0,t} + \big|\Delta P^C_t\big| \le \overline{P}^C x^C_t && \forall t \quad (4.93)\\
&P^{SRC}_{0,t} + \big|\Delta P^{SRC}_t\big| \le P^C_{0,t} - \big|\Delta P^C_t\big| - \underline{P}^C x^C_t && \forall t \quad (4.94)\\
&P^{SRD}_{0,t} + \big|\Delta P^{SRD}_t\big| \le \overline{P}^D x^D_t - P^D_{0,t} - \big|\Delta P^D_t\big| && \forall t \quad (4.95)\\
&P^D_{0,t} - \big|\Delta P^D_t\big| \ge \underline{P}^D x^D_t && \forall t \quad (4.96)\\
&0 \le P^{ID}_{0,t} \pm \big|\Delta P^{ID}_t\big| \le QSC x^{ID}_t && \forall t \quad (4.97)
\end{aligned}$$

The inter-temporal constraints (3.15) can be represented using the following set of relations:

$$SOC_{0,t+1} = SOC_{0,t} + \frac{(air^C_{0,t} - air^C_{0,t})3,600}{\overline{CA}} \qquad \forall t \qquad (4.98)$$

$$\Delta SOC_{t+1} = \Delta SOC_t + \frac{(\Delta air^C_t - \Delta air^C_t)3,600}{\overline{CA}} \qquad \forall t \qquad (4.99)$$

$$SOC_{0,t+1} + |\Delta SOC_t| \leq \overline{SOC} \qquad \forall t \qquad (4.100)$$

$$SOC_{0,t+1} - |\Delta SOC_t| \geq \underline{SOC} \qquad \forall t \qquad (4.101)$$

$$SOC_{0,t+1} - |\Delta SOC_t| \geq SOC^f \qquad \forall t = T \qquad (4.102)$$

Equations (3.39)-(3.44) can be represented using the following relations:

$$air^C_{0,t} = -0.3w_{0,t} + 1.95P^C_{0,t} \qquad \forall t \qquad (4.103)$$

$$\Delta air^C_t = -\Delta w_t + 1.95\left|\Delta P^C_t\right| \qquad \forall t \qquad (4.104)$$

$$\begin{aligned} w_{0,t} - \Delta w_t \geq\ & \underline{SOC} P^C_{0,t} + SOC_{0,t}\underline{P}^C - \underline{SOC}\,\underline{P}^C - M(1 - x^C_t) \\ & + \left[\underline{SOC}\,\left|\Delta P^C_t\right| + |\Delta SOC_t|\,\underline{P}^C\right] \end{aligned} \qquad \forall t \qquad (4.105)$$

$$\begin{aligned} w_{0,t} - \Delta w_t \geq\ & \overline{SOC} P^C_{0,t} + SOC_{0,t}\overline{P}^C - \overline{SOC}\,\overline{P}^C - M(1 - x^C_t) \\ & + \left[\overline{SOC}\,\left|\Delta P^C_t\right| + |\Delta SOC_t|\,\overline{P}^C\right] \end{aligned} \qquad \forall t \qquad (4.106)$$

$$\begin{aligned} w_{0,t} + \Delta w_t \leq\ & \underline{SOC} P^C_{0,t} + SOC_{0,t}\overline{P}^C - \underline{SOC}\,\overline{P}^C - M(1 - x^C_t) \\ & - \left[\underline{SOC}\,\left|\Delta P^C_t\right| + |\Delta SOC_t|\,\overline{P}^C\right] \end{aligned} \qquad \forall t \qquad (4.107)$$

$$\begin{aligned} w_{0,t} + \Delta w_t \leq\ & \overline{SOC} P^C_{0,t} + SOC_{0,t}\underline{P}^C - \overline{SOC}\,\underline{P}^C - M(1 - x^C_t) \\ & - \left[\overline{SOC}\,\left|\Delta P^C_t\right| + |\Delta SOC_t|\,\underline{P}^C\right] \end{aligned} \qquad \forall t \qquad (4.108)$$

$$w_{0,t},\ \Delta w_t \geq 0 \qquad \forall t, h \qquad (4.109)$$

Finally, the relations pertaining to the air discharged and cost of natural gas are represented

as follows:

$$P_{0,t}^{D} = \sum_{s=1}^{2} \left(b_{t,s}^{D} + \underline{q}_{s} u_{t,s}^{D} \right) \qquad \forall t \qquad (4.110)$$

$$P_{0,t}^{D} - \left| \Delta P_{t}^{D} \right| = \sum_{s'=1}^{2} \left(b_{t,s'}^{D} + \underline{q}_{s'} u_{t,s'}^{D} \right) \qquad \forall t \qquad (4.111)$$

$$\sum_{s=1}^{2} u_{t,s}^{D} = x_{t}^{D} \qquad \forall t \qquad (4.112)$$

$$\sum_{s'=1}^{2} u_{t,s'}^{D} = x_{t}^{D} \qquad \forall t \qquad (4.113)$$

$$0 \leq b_{t,s}^{D} \leq \overline{b}^{D} u_{t,s}^{D} \qquad \forall t, s \qquad (4.114)$$

$$0 \leq b_{t,s'}^{D} \leq \overline{b}^{D} u_{t,s'}^{D} \qquad \forall t, s' \qquad (4.115)$$

$$air_{0,t}^{D} = \sum_{s=1}^{2} \left(ang_{s}^{D} b_{t,s}^{D} + \underline{D}_{s} u_{t,s}^{D} \right) \qquad \forall t \qquad (4.116)$$

$$\underline{air}_{t}^{D} = \sum_{s'=1}^{2} \left(ang_{s'}^{D} b_{t,s'}^{D} + \underline{D}_{s'} u_{t,s'}^{D} \right) \qquad \forall t \qquad (4.117)$$

$$\Delta air_{t}^{D} = air_{0,t}^{D} - \underline{air}_{t}^{D} \qquad \forall t \qquad (4.118)$$

$$CO_{0,t}^{NG} = \left(53.57 x_{t}^{D} + 4.215 P_{0,t}^{D} \right) \pi^{NG} \qquad \forall t \qquad (4.119)$$

$$\Delta CO_{t}^{NG} = 4.215 \Delta P_{t}^{D} \pi^{NG} \qquad \forall t, h \qquad (4.120)$$

Note that the main difference between the objective functions in AP, given by (4.91), with that of the AA approach, given by (4.33), is that in the AP model the radius is not maximized in terms of the modulus, since the adjustment variables $p_{n,t}^{X,Y}$ are unrestricted sign variables, while in AA the adjustment variables $P_{h,t}^{X}$ are positive (4.20).

4.4 Summary

The self-scheduling model of a price-taker CAES facility presented in Chapter 3 was further extended in this Chapter to consider uncertainties in prices of various electricity market services such as energy, spinning and idle reserves, based on range arithmetic techniques.

For this purpose, novel representations of electricity price uncertainties and the corresponding mathematical models using RO, AA, and PCA-AP approaches were presented. The challenges of implementing each technique were discussed, and the mathematical approach to transform each of them into an MILP problem was presented.

Chapter 5

Numerical Studies and Comparisons

This Chapter presents detailed numerical studies and comparisons by simulating the CAES self-scheduling models under deterministic and price uncertainty scenarios. First, results are presented considering the step function representation of the CAES thermodynamic model using RO to represent uncertainties, comparing them with MCS. Thereafter, results are presented considering the proposed novel linear thermodynamic model for given intervals of uncertainty. A comparison between the step-function-based model and the proposed linear model is carried out for the deterministic case, followed by uncertainty model comparisons for the RO, AA, and MCS techniques. Finally, studies and comparisons for the proposed linear thermodynamic model, using uncertainty intervals based on historical data, are carried out for the AA, PCA-AP, and MCS approaches.

5.1 Step Function Representation of CAES Thermodynamics

The deterministic self-scheduling model of the CAES facility considering step-function representation of its thermodynamic characteristics includes the objective function (3.1) and constraints (3.2)-(3.5), (3.7)-(3.15), and (3.18)-(3.29). For all simulations, the maximum charging and discharging capacities of the CAES facility are considered to be 60 MW and 100 MW, respectively, while the minimum charging and discharging capacities are 25 MW and 30 MW, respectively, with a quick-start capacity of 40 MW, based on the facility studied in [19]. The SOC is maintained between 33% and 100%, the initial SOC is 60%,

and the final SOC is set to be at least 60%, since the facility has to be prepared for the following day's market. All simulations were executed in GAMS interfaced with MATLAB.

5.1.1 Robust Optimization (RO)

In order to use RO to represent the uncertainties, the deterministic objective function (3.1) is replaced by (4.10) and associated constraints (4.11)-(4.16), as discussed in the previous chapter. The RO simulations were carried out for the following different combinations of ($\overline{\Delta\pi}$, Γ) to examine their impact on CAES facility profit and its optimum schedule: $\overline{\Delta\pi} \in$ [8%, 15%, 20%], and $\Gamma \in$ [0, 5, 10, 15, 20, 24], which yield 18 possible scenarios for different combinations of the above parameters.

The hourly electricity prices were taken from the HOEP historical data of January 19, 2019 [75], depicted in Figure 5.1. Table 5.1 presents the profit of the CAES facility for the next day, and the corresponding violation probability for each value of Γ. Note that the probability of a constraint being violated, calculated using (4.17), drops significantly as the budget of uncertainty increases, being lower than 5% for $\Gamma = 10$. Observe that for $\Gamma = 0$, i.e., the deterministic scenario, all profits are the same, and as the budget of uncertainty increases, the number of times that the price deviates from the forecast values increases, which leads to a decrease in profits. As the budget of uncertainty approximates to the most conservative scenario $\Gamma = 24$, the profit sensitivity decreases. Greater values of $\overline{\Delta\pi}$ yield lower profits, as expected.

Table 5.1: CAES profit in ($) for ($\overline{\Delta\pi}, \Gamma$).

Γ	Violation Probability [%]	CAES profit for $\overline{\Delta\pi}$		
		8%	15%	20%
0 (Deterministic)	58.09	25,592	25,592	25,592
5	20.71	22,367	19,661	17,926
10	3.31	21,117	17,412	14,874
15	0.21	20,403	16,582	13,895
20	5.258e-3	20,360	16,297	13,895
24	1.334e-4	20,360	16,297	13,895

The optimum daily schedule of the CAES facility is sensitive to changes to Γ and $\overline{\Delta\pi}$. Thus, the SOC for the deterministic case $\Gamma = 0$, and for the cases considering ($\overline{\Delta\pi} = 8\%, \Gamma = 15$), ($\overline{\Delta\pi} = 15\%, \Gamma = 10$), and ($\overline{\Delta\pi} = 20\%, \Gamma = 20$) are presented in Figure 5.2. Note that in the deterministic schedule, the CAES facility operates with higher

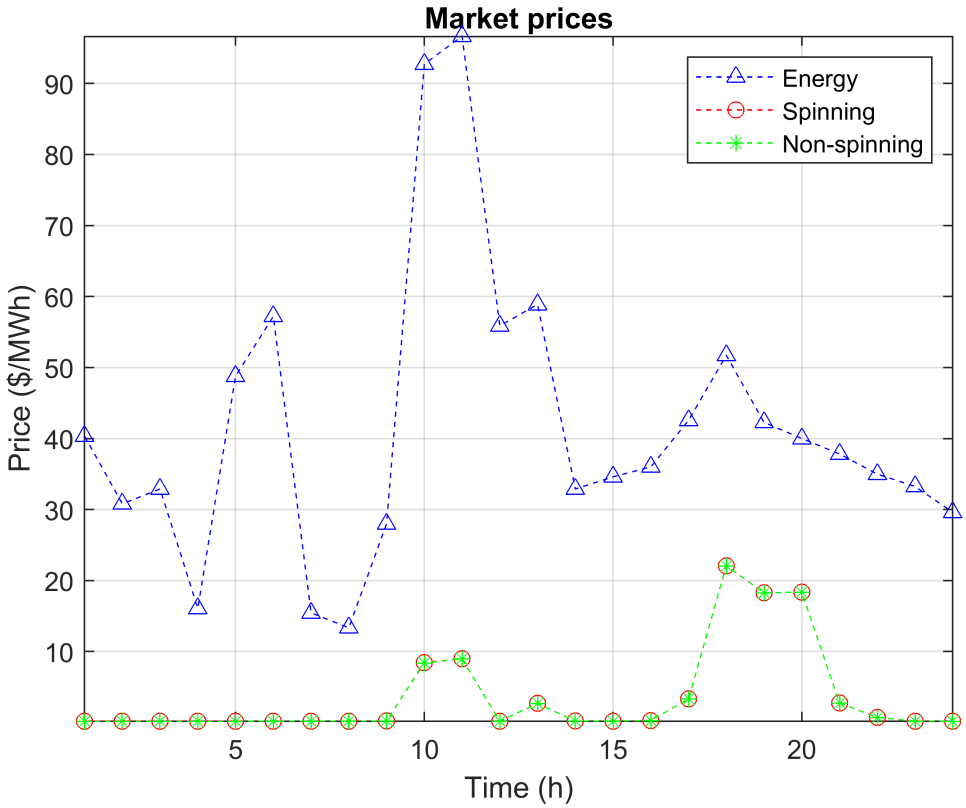

Figure 5.1: Electricity price on January 19, 2019.

Depth of Discharge (DoD), while in scenarios where uncertainties are taken into consideration, it operates in the idle mode for more hours, as expected. Observe also that different ranges of price uncertainty and the number of times the prices deviate from their forecast values affect the optimal schedule of the CAES facility. Based on the results obtained, the facility operator can choose a schedule that provides a certain level of protection against uncertainties in each scenario. Note that the operator does not need to choose a conservative schedule to achieve a high degree of financial protection, since for $\Gamma = 10$, the probability of violation is lower than 5%.

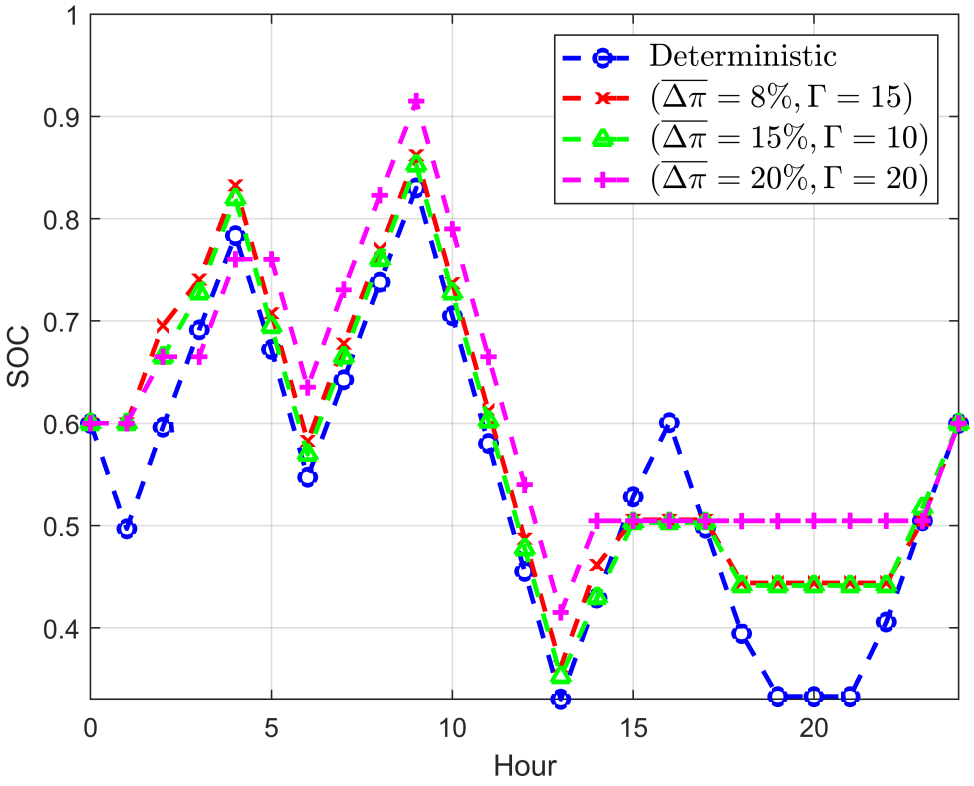

Figure 5.2: SOC for different $(\overline{\Delta\pi}, \Gamma)$.

5.1.2 Monte Carlo Simulations (MCS)

To validate the results obtained from the RO approach, a comparison is made with MCS, which are formulated as deterministic problems with prices varying randomly based on a uniform distribution. Three uniform random PDF ranges, i.e., [0.92, 1], [0.85, 1], and [0.8, 1], each with thousand data points that yield MCS convergence, were simulated, representing three $\overline{\Delta\pi}$ scenarios of 8%, 15%, and 20%. In Figure 5.3 it can be observed that the MCS and the RO results present a similar pattern, i.e., as the range of uncertainty increases, their respective profits decrease.

Computationally, the RO approach is much faster than the MCS method, guaranteeing that the CAES facility's profit is maximized for the worst-case scenario. In the worst-case, when the CAES facility is discharging, i.e., selling energy, and the price of electricity suddenly falls, it sells power at cheaper rates, whereas when it is charging, i.e., buying

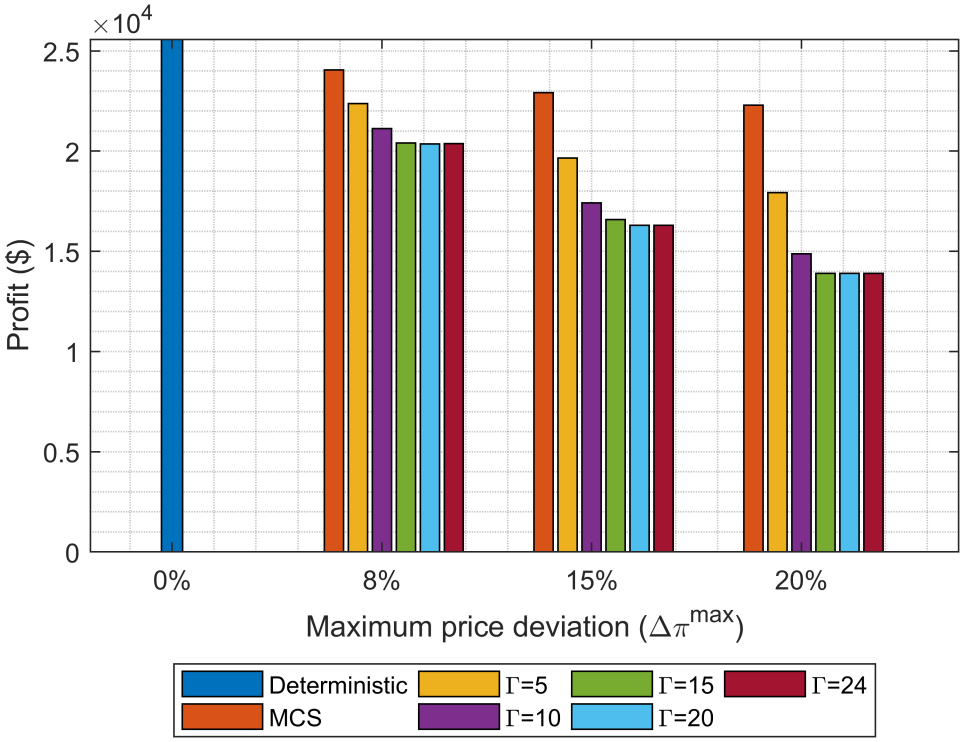

Figure 5.3: Comparison of CAES profit with RO and MCS approaches for the step model of the CAES facility.

energy, if the prices suddenly increase, it purchases power at a higher price.

The simulations carried out for the step-function thermodynamic model considering uncertainties were only done for the RO approach. This is due to, as previously explained, the significant discontinuities present in the model, which make the implementation of methods that keep track of correlated uncertainties such as AA and AP infeasible in practice because of the need to add multiple binary and auxiliary variables to the mathematical models.

5.2 Proposed CAES Linear Model With Fixed Intervals

The deterministic self-scheduling model of the CAES facility considering the proposed linear representation of the thermodynamic behaviour, comprises the objective function (3.1) and constraints (3.2)-(3.5), (3.7)-(3.15), (3.18)-(3.19), (3.39)-(3.44), and (3.47)-(3.51). The simulation studies presented next are for two different days with volatile price profiles denoted as Day 1 (February 6, 2019) and Day 2 (January 19, 2019), depicted in Figure 5.4.

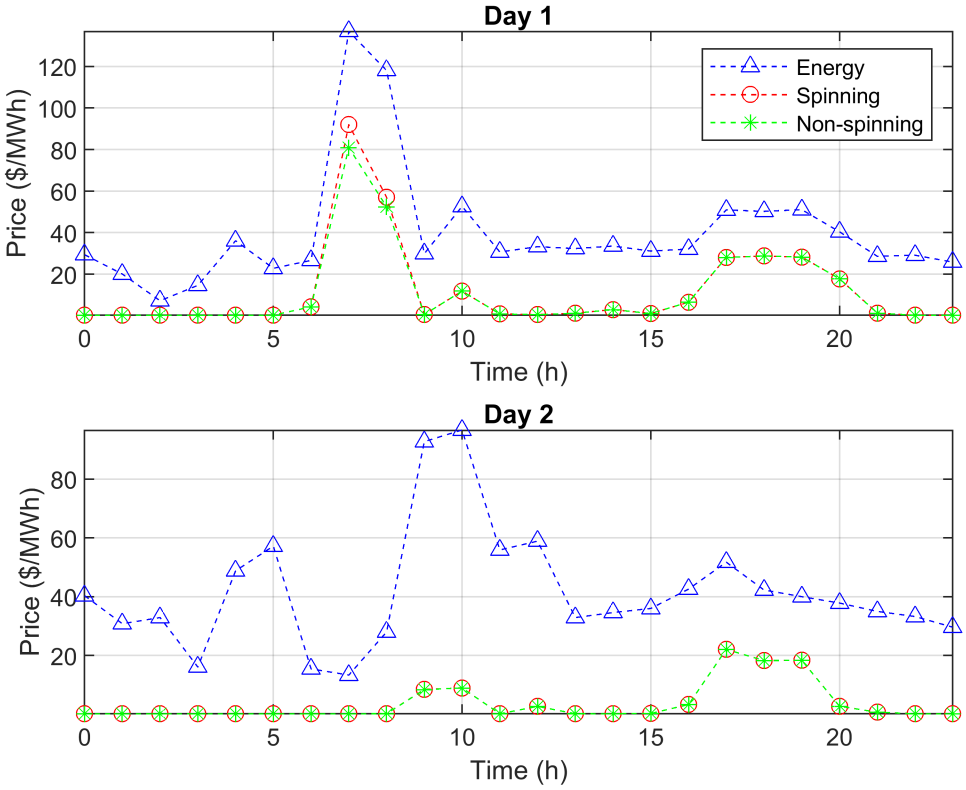

Figure 5.4: Prices profile for Days 1 and 2.

5.2.1 Deterministic Proposed Model versus Step Model

To validate and evaluate the performance of the proposed linear thermodynamic model of the CAES facility, the results obtained for a deterministic case are compared with those obtained with the step-function-based thermodynamic model of the facility. Table 5.2 presents a comparison of the profit and computation cost of the linear model and the step-function model. Note that both methods yield similar profits, with a maximum mismatch of 1%, but the linear model is computationally much faster. Thus, the linear model converges in seconds, while the step function model takes much longer, with significant solution time differences between Day 1 to Day 2, which suggests that the step-function model's computational performance is sensitive to market prices.

Table 5.2: Comparison between Linear and Step models.

		Linear Model	Step Model
Day 1	Profit ($)	30,919	30,932
	Computing Time	1.23s	28min42s
Day 2	Profit ($)	25,349	25,617
	Computing Time	1.17s	2min58s

Observe in Figure 5.5 that the optimum schedules for both days and the different thermodynamic models are very similar and match closely. Therefore, the linear model can be considered to be equivalent to the step-function model but with significantly lower computational burden.

5.2.2 Robust Optimization (RO)

Using RO to represent price uncertainties, the objective function (3.1) is replaced by (4.10) and the constraints (4.11)-(4.16) are added to the model. Similar to Section 5.1.1, simulation studies for different combinations of $(\overline{\Delta\pi}, \Gamma)$ are carried out, where $\overline{\Delta\pi} \in [8\%, 15\%, 20\%]$ and $\Gamma \in [0, 5, 10, 15, 20, 24]$. All possible $(\overline{\Delta\pi}, \Gamma)$ combinations were considered for each day, obtaining the profit of the CAES facility presented in Table 5.3. Note that in the deterministic case ($\Gamma = 0$), the profit does not change for different values of $\overline{\Delta\pi}$. As Γ increases, the number of times the prices deviate from their forecast increases, resulting in decreasing profits. Also, the sensitivity of profit reduces as Γ tends to the most conservative scenario, i.e., $\Gamma = 24$. As expected, higher values of $\overline{\Delta\pi}$ lead to lower profits. Observe also that the facility's profit on Day 1 is generally higher than on Day 2,

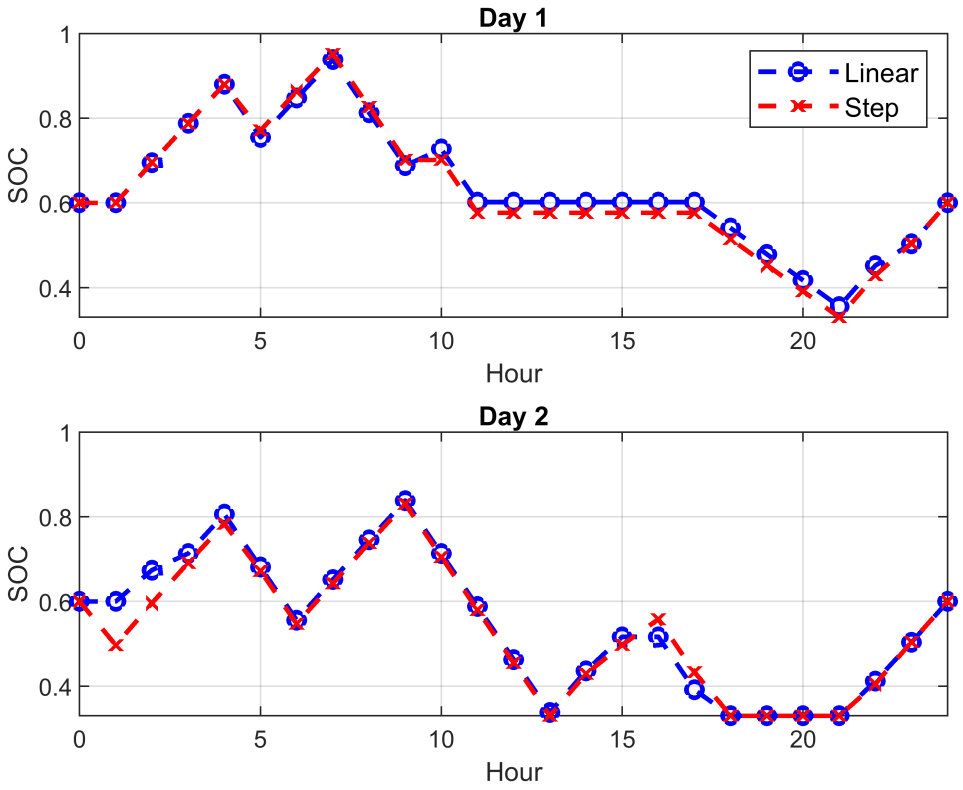

Figure 5.5: SOC comparison of the Linear and Step models.

which can be attributed to the overall higher market price profile on Day 1, as shown in Figure 5.4.

Table 5.3: Profit of CAES Facility with RO Approach ($).

Γ	Day 1			Day 2		
	8%	15%	20%	8%	15%	20%
0	30,919	30,919	30,919	25,349	25,349	25,349
5	27,484	24,566	22,482	22,236	19,592	17,704
10	26,908	23,481	21,057	21,028	17,436	14,927
15	26,649	23,159	20,677	20,505	16,566	13,876
20	26,649	23,159	20,677	20,374	16,317	13,876
24	26,649	23,159	20,677	20,374	16,317	13,876

As prices deviate from their actual values, the optimum daily schedule is susceptible to changes. Thus, in Figure 5.6 and Figure 5.7, the SOC for different combinations of $\overline{\Delta\pi}$ and Γ for Day 1 and Day 2 are presented. The power dispatch for Day 2 for the deterministic and RO with $(\overline{\Delta\pi} = 20\%, \Gamma = 20)$ scenarios are presented in Figure 5.8, note that in the deterministic scenario with the actual prices, i.e., assuming a perfect forecast, the facility charges and discharges more, whereas in case of uncertainties, it is more conservative and operates in idle mode for more hours, as expected.

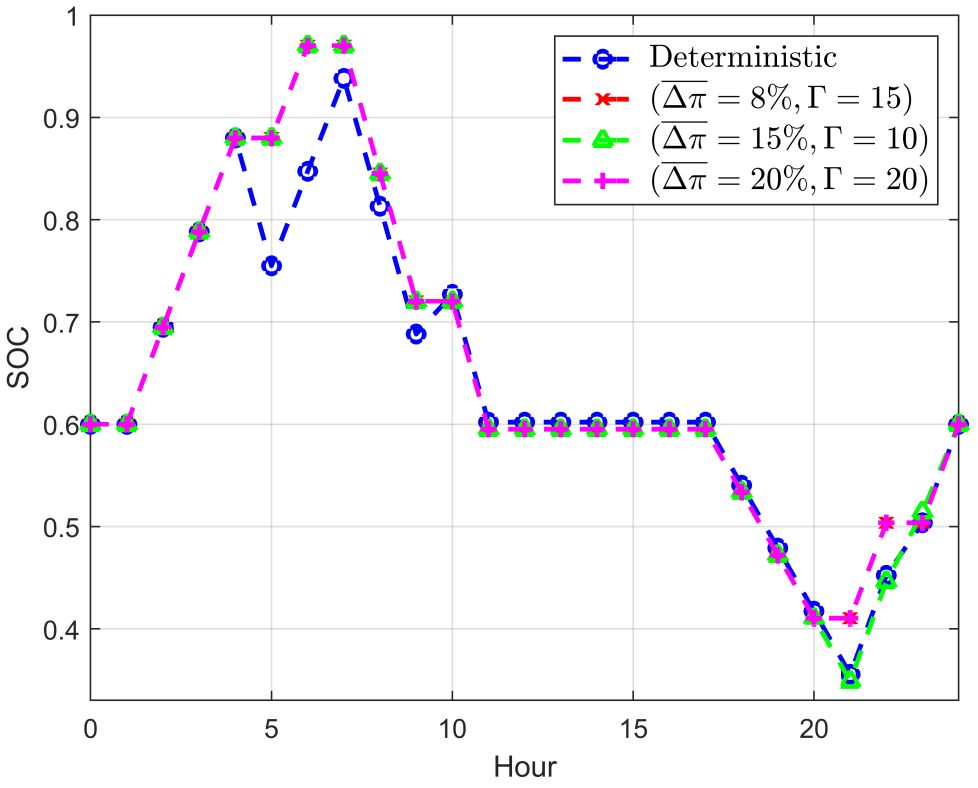

Figure 5.6: Day 1 SOC for different $\overline{\Delta\pi}$ and Γ.

The purpose of RO is to optimize for the worst-case scenario for a given Γ. Therefore, for self-scheduling models of a price-taker CAES facility the worst-case realization is the facility charging when the prices increase, and discharging when the prices decrease, i.e., it pays more and gets paid less. Figure 5.4 depicts the actual electricity prices for Day 2, which are used to compute the actual profits presented in Table 5.4 from the dispatches

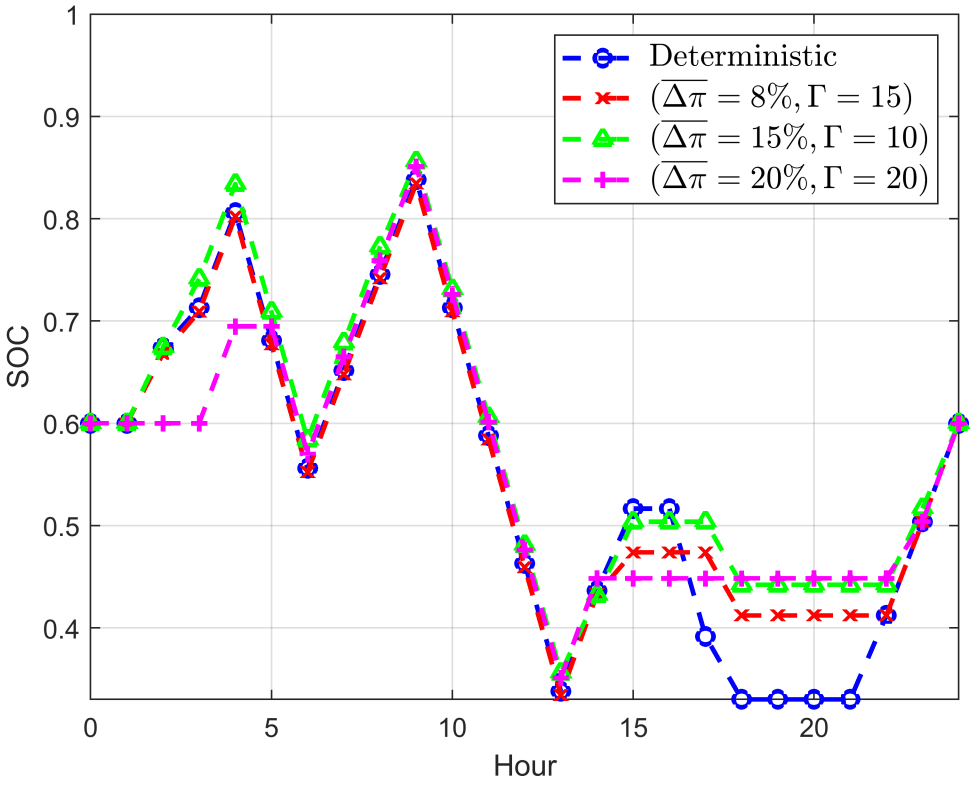

Figure 5.7: Day 2 SOC for different $\overline{\Delta\pi}$ and Γ.

depicted in Figure 5.8 for the deterministic and RO techniques with $(\overline{\Delta\pi} = 20\%, \Gamma = 20)$. Note that the deterministic dispatch yields higher profits than the RO, as expected.

Table 5.4: Actual Day 2 profit for different schedules ($).

Schedule	Profit
Deterministic	25,349
$(\overline{\Delta\pi} = 20\%, \Gamma = 20)$	23,488

Given the set of schedules obtained from RO, the operator may choose the interval of uncertainty $\overline{\Delta\pi}$ and the desired level of conservatism Γ. Similar results can be obtained in this case as those presented in Table 5.1, where it can be observed that low probability of violation can be achieved without having to resort to high values of Γ, while ensuring

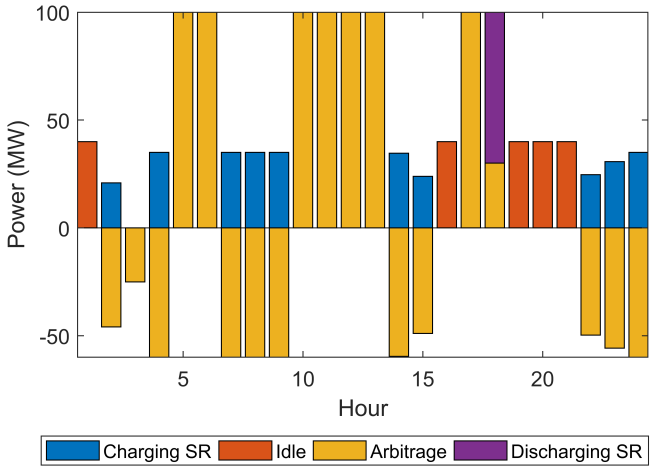

(a)

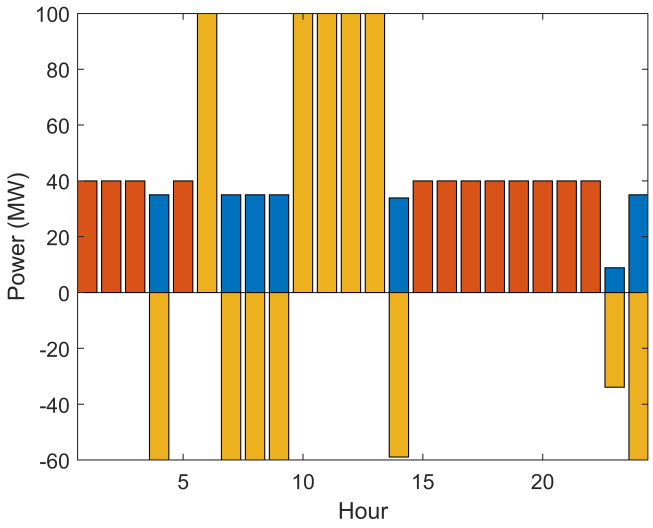

(b)

Figure 5.8: Day 2 schedule for (a) deterministic approach with perfect forecast, and (b) RO approach with ($\overline{\Delta\pi} = 20\%, \Gamma = 20$).

greater profits.

5.2.3 Affine Arithmetic (AA)

In the AA approach, the uncertain parameters and variables are represented in their affine forms, as per (4.18) and (4.19). In this case, the CAES facility's day-ahead self-scheduling model comprises the objective function (4.33) and constraints (3.7)-(3.9), and (4.34)-(4.61). In this case, simulations were carried out to maximize the center and radius of the profit, simultaneously. Since there are no parameters to control the level of conservatism, AA yields a single optimum interval schedule for each $\overline{\Delta\pi}$.

Table 5.5 presents the center, upper and lower bounds of the CAES facility's profit for each day. Observe that as $\overline{\Delta\pi}$ increases, the center and radius of the profit increases, i.e., a larger difference can be seen between the upper and lower bounds with respect to the center value, as expected.

Table 5.5: Profit of CAES Facility with AA approach ($).

$\overline{\Delta\pi}$	Day 1			Day 2		
	Lower	Center	Upper	Lower	Center	Upper
8%	17,065	27,000	36,936	8,961	20,555	32,149
15%	15,409	28,416	41,422	8,996	22,697	36,397
20%	12,604	28,704	44,877	6,538	23,235	39,932

The optimum daily schedules of the CAES facility are sensitive to changes in $\overline{\Delta\pi}$, as illustrated in Figure 5.9 and Figure 5.10, which considers the two most extreme intervals of price deviation. Note that the SOC interval depends on the magnitude of the power dispatch adjustment terms $P^C_{h,t}/P^D_{h,t}$, which determines whether the SOC has tighter or larger intervals. As in the case of the deterministic schedule, the dispatch decisions obtained from AA are similar most of the time, but with different DoD.

When operating the CAES facility in real-time, the actual power dispatch variables can be obtained from the intervals computed using the AA model. Thus, when the actual price mismatch with respect to the forecasted center value ε^Y_t is known, the power dispatch of the facility can be obtained. For example, assuming that the optimum schedule of the CAES facility is within the intervals obtained for $\overline{\Delta\pi} = 8\%$ on Day 1, and if at $t = 1$ the facility is discharging, for an energy price mismatch of -5% but no mismatches in the other prices, the noise values can be determined to be $\varepsilon^E_1 = -\frac{5\%}{8\%} = -0.625$, $\varepsilon^{SR}_1 = 0$ and $\varepsilon^{ID}_1 = 0$; the SOC at $t = 2$ can then be computed to be $SOC_2 = 0.464$. If the mismatch is lower than -8% or greater than 8%, ε^E_t can be set to -1 or 1, respectively.

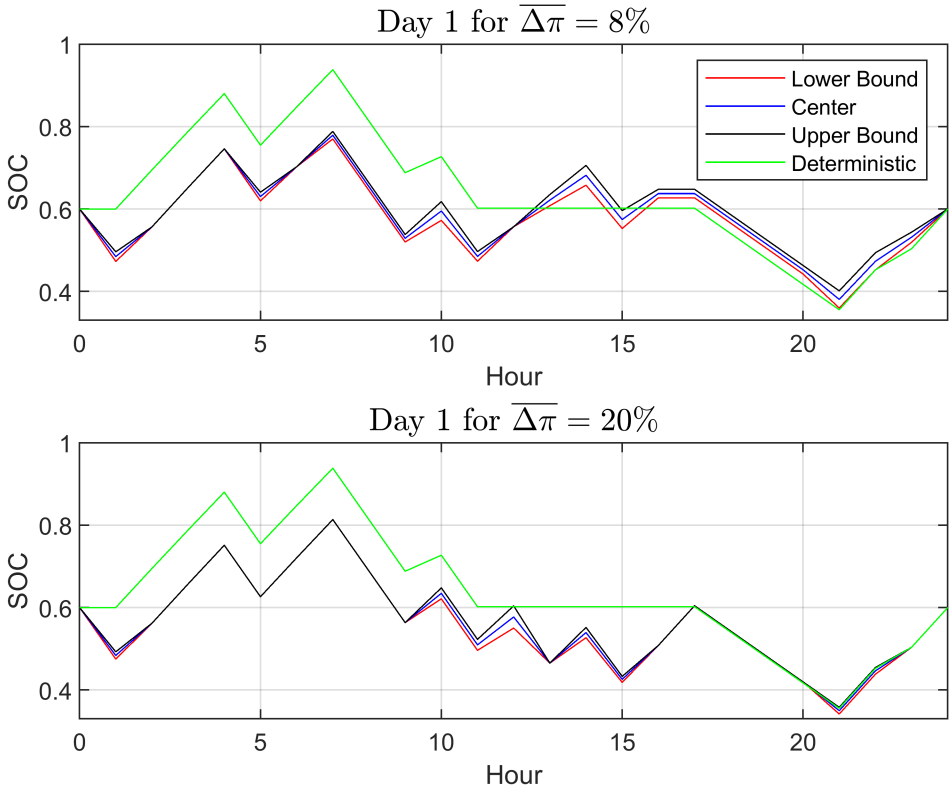

Figure 5.9: Day 1 SOC for different $\overline{\Delta\pi}$.

The AA center power dispatch for Day 2, corresponding to the actual electricity prices illustrated in Figure 5.4, is presented in Figure 5.11, which yields a daily center profit of \$20,555. Note that, compared with the "perfect" deterministic and RO schedules presented in Figure 5.8, the CAES facility operates in idle mode for fewer hours in the AA dispatch and presents a lower profit, due to its riskier behavior.

Note that the PCA-AP approach is not applied in this case, due to the fact that the price intervals extracted from the HOEP are fixed for specific days. Thus, there is no need to extract information from the data.

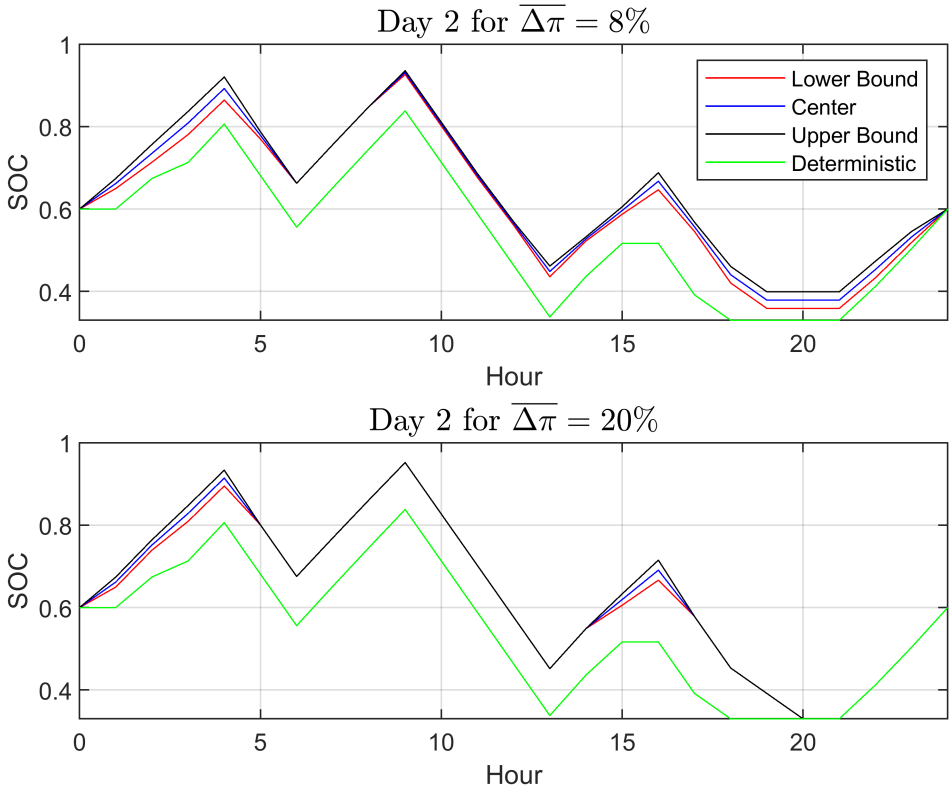

Figure 5.10: Day 2 SOC for different $\overline{\Delta\pi}$.

5.2.4 Monte Carlo Simulations (MCS)

To validate the results obtained from RO and AA approaches, these are compared with the MCS approach where the random prices are generated using a uniform PDF. Three uniform distributions are generated, each with 1,000 data points, so that MCS converges, for the ranges [0.92, 1.08], [0.85, 1.15], and [0.8, 1.2], corresponding to the three cases of market price deviations $\overline{\Delta\pi}$ of 8%, 15%, and 20%.

Figure 5.12 presents a comparison between the MCS, AA, and RO approaches for both days, depicting the upper and lower bounds of the solution, in each approach, denoted by MCS-UB and MCS-LB, AA-UB and AA-LB and RO-UB and RO-LB. For RO, the upper and lower bounds corresponds to the results of the deterministic case and the most conservative scenario, i.e., $\Gamma = 0$ and $\Gamma = 24$, respectively. Observe for both days and all values of $\overline{\Delta\pi}$ that the AA solution profile envelops both the MCS and RO solutions. Since

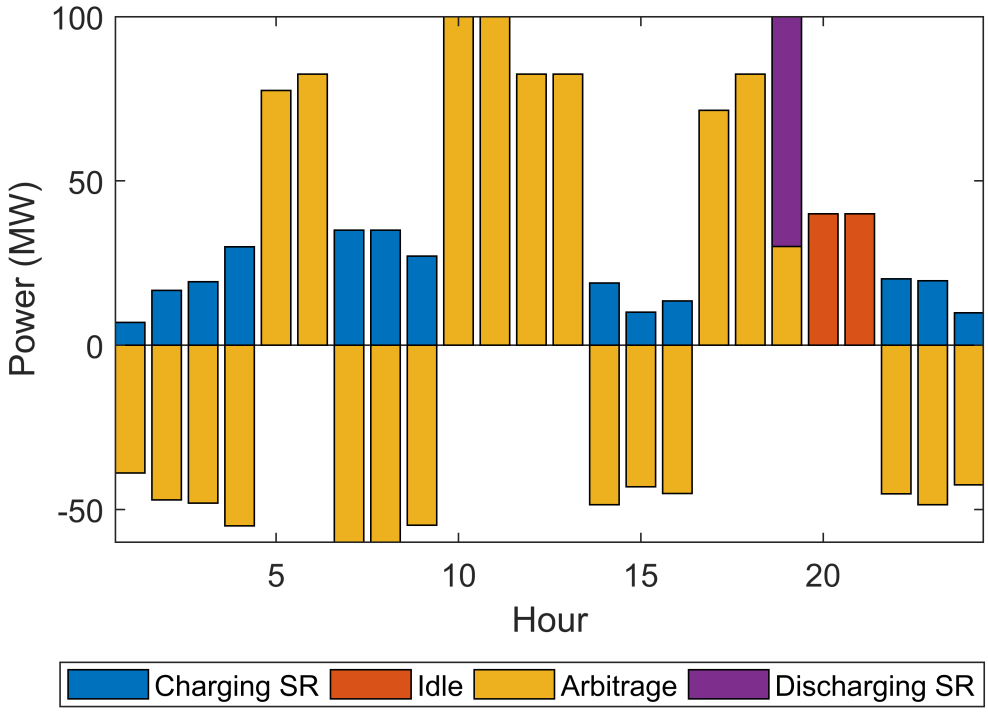

Figure 5.11: Day 2 AA center dispatch for $\overline{\Delta\pi} = 8\%$ and actual prices, i.e., $\varepsilon_t^Y = 0\,\forall t, Y$.

the RO objective is to optimize the profit for the worst-case scenario, its profits are higher in the lower bound, as compared to AA.

The MCS approach has the highest computational cost, while RO has the least, converging in a few seconds, as presented in Table 5.6. Since a large number of variables are used to keep track of the correlated uncertainties, the AA approach has a larger computational burden than RO; however, it still converges within a few seconds. Therefore, given a $\overline{\Delta\pi}$ which the CAES facility seeks to be protected from, the plant operator may determine the optimum schedule using either RO or AA. If RO is employed, given the probabilities of violation, the operator may choose a schedule with the desired protection level. However, if AA is used, a unique optimum schedule is determined, given the real-time mismatch in prices.

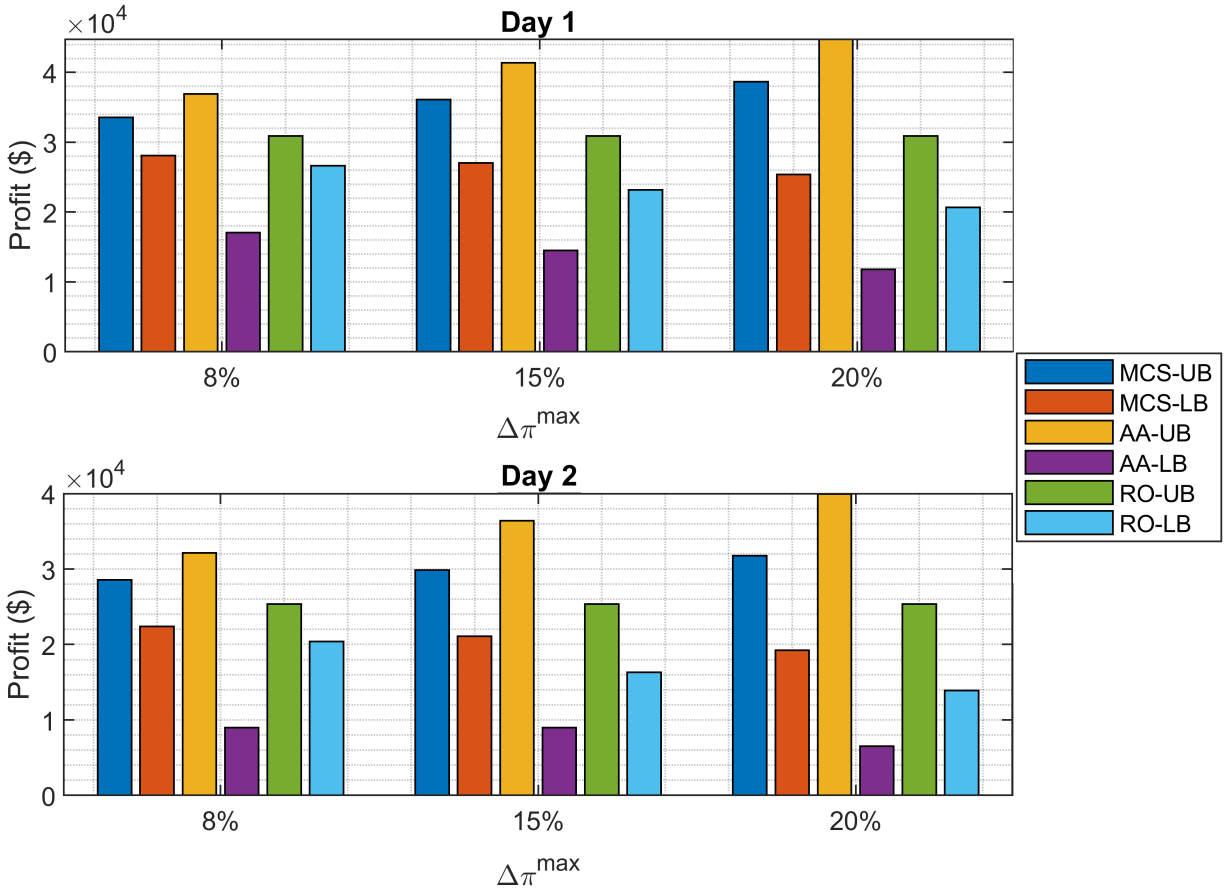

Figure 5.12: Comparison of MCS, AA, and RO approaches for the linear model of the CAES facility.

5.2.5 Effects of Different SOC Levels

In this section, the impact of initial and final values of the SOC, SOC_0 and SOC^f, for the optimum operation of the CAES facility are analyzed. Since electricity prices are usually low during the early hours of the day, the facility typically starts the day by charging and reaching a high value of SOC, and when prices increase it starts discharging. Thus, a high initial SOC would yield a conservative schedule wherein the range of operation will be constrained. If the final SOC is held at a relatively high value, then the facility would not have a high DoD, resulting in low profits. Therefore, different initial and final SOC levels are tested here using the price profile of Day 1, to demonstrate the impact of SOC_0 and

Table 5.6: MCS, AA and RO computational burden.

Method		Day 1 $\overline{\Delta\pi}$			Day 2 $\overline{\Delta\pi}$		
		8%	15%	20%	8%	15%	20%
RO $\Gamma =$	0	1.20s	1.33s	1.22s	1.29s	1.13s	1.13s
	5	1.22s	1.22s	1.22s	1.13s	1.22s	1.12s
	10	1.24s	1.23s	1.22s	1.24s	1.23s	1.13s
	15	1.24s	1.24s	1.12s	1.24s	1.13s	1.23s
	20	1.23s	1.24s	1.22s	1.23s	1.13s	1.23s
	24	1.24s	1.24s	1.23s	1.13s	1.23s	1.22s
AA		10s	7.90s	6.16s	17s	16s	11s
MCS		20min33s	20min25s	20min24s	17min50s	17min55s	18min13s

SOC^f on profits and optimum daily schedules.

Table 5.7 presents the profits of the CAES facility using the RO approach for SOC_0 and SOC^f set both at 0.7 (70% SOC) and 0.8 (80% SOC). When compared to Table 5.3, which uses SOC_0 and SOC^f values of 60% for both, it is noted that the profits decrease from the deterministic schedule ($\Gamma = 0$) to the most conservative case ($\Gamma = 24$) for higher SOC^f, and all price mismatch scenarios. Figure 5.13 illustrates the deterministic optimum schedule for the CAES facility for different values of SOC_0 and SOC^f. Observe that when $SOC_0 = SOC^f = 0.6$, the CAES facility operates with a larger DoD as compared to cases with both SOC_0 and SOC^f set to 70% and 80%.

Table 5.7: CAES Profit with RO for Day 1 with Different SOC_0 and SOC^f ($).

Γ	$SOC_0 = SOC^f = 0.7$			$SOC_0 = SOC^f = 0.8$		
	8%	15%	20%	8%	15%	20%
0	30,676	30,676	30,676	29,952	29,952	29,952
5	27,157	24,143	22,075	26,440	23,415	21,311
10	26,547	23,076	20,710	25,828	22,325	19,925
15	26,287	22,776	20,286	25,502	21,941	19,652
20	26,287	22,776	20,286	25,502	21,941	19,652
24	26,287	22,776	20,286	25,502	21,941	19,652

Table 5.8 depicts the CAES facility's profits using the AA approach for different values of both SOC_0 and SOC^f. Observe that the center, lower, and upper boundaries of the profit decreases for higher values of initial and final SOC, since the interval of operation

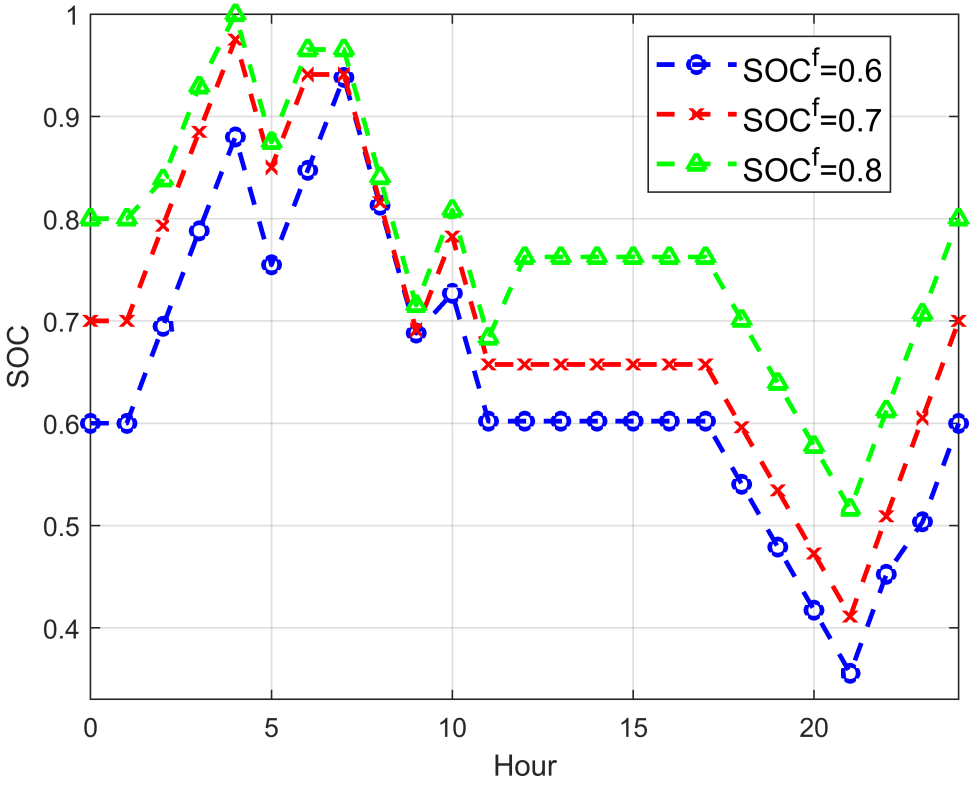

Figure 5.13: Deterministic schedule for Day 1.

is tighter, as shown in Figure 5.14. Note that compared to the deterministic schedule, the dispatch decisions remain similar but with different DoDs. Therefore, operating with high SOC^f values is not advantageous for the CAES facility, since it yields conservative schedules and profits to ensure that the desired final SOC value is met at the end of the day, thus missing opportunities to maximize the daily profit.

Table 5.8: CAES Profit with AA for Day 1 with Different SOC_0 and SOC^f ($).

$\overline{\Delta\pi}$	$SOC^f = 0.7$			$SOC^f = 0.8$		
	Lower	Center	Upper	Lower	Center	Upper
8%	17,083	26,840	36,597	16,946	26,463	35,979
15%	14,912	28,022	41,131	14,414	27,506	40,598
20%	12,467	28,533	44,599	12,410	28,260	44,111

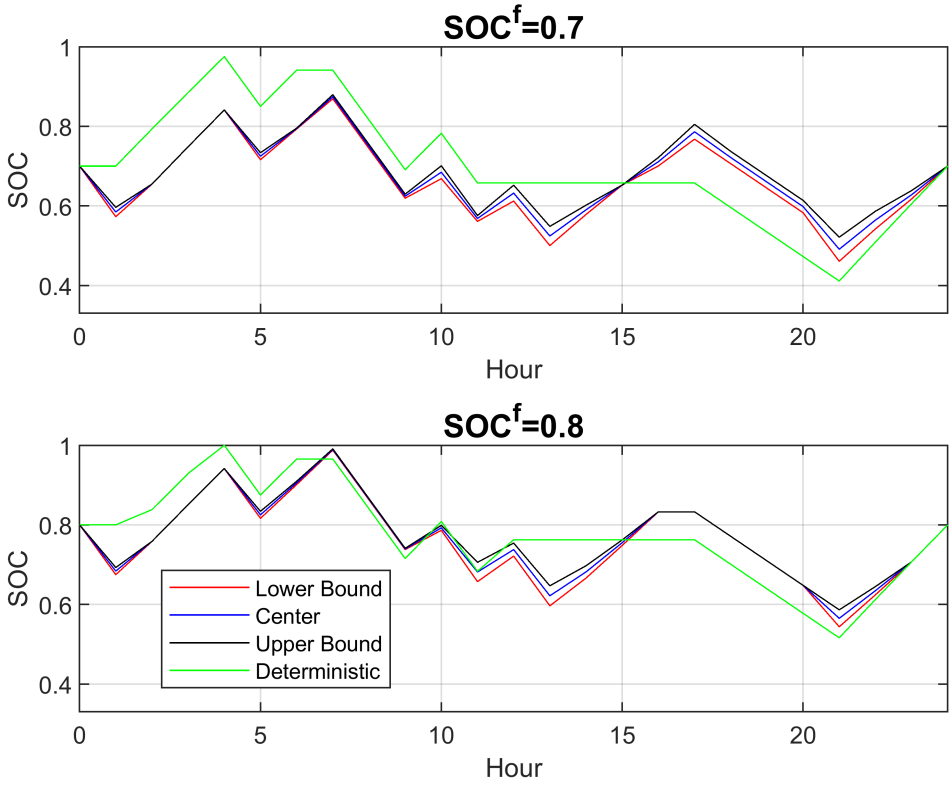

Figure 5.14: AA schedule for $\overline{\Delta\pi} = 8\%$ for Day 1.

5.3 CAES Linear Model Based on Historical Data

As presented in Section 5.2, the CAES facility's day-ahead self-scheduling model with piecewise linear thermodynamic relationships, comprises the objective function (3.1) and constraints (3.2)-(3.5), (3.7)-(3.15), (3.18)-(3.19), (3.39)-(3.44) and (3.47)-(3.51). The price intervals used in this section, are obtained from the HOEP data for 2015 to 2019 [75], with all prices adjusted to 2019 using the average inflation index of Canada for the 5 years [76]. The 5-year average energy price for each month is presented in Figure 5.15. The simulations are carried out for the specific months of February, May, August and November, which represent each season. Electricity market prices can be volatile, with price spikes occurring following unexpected system conditions such as demand fluctuations or contingencies, or can be negative if there is an excess of RES generation [77]. Therefore, the interval of

electricity prices can be too conservative if only the extremes of historical data are used to define the intervals, as done in Section 5.2. Thus, to obtain a more reasonable range of electricity prices, the following approach was used:

- The average daily electricity prices were transformed using the Box Cox Transformation (2.51). A CI of $p = 50\%$ was used to filter the significant price spikes.
- From the remaining data, the average and standard deviation of the hourly prices were determined, i.e., the center and interval of uncertainty, respectively.

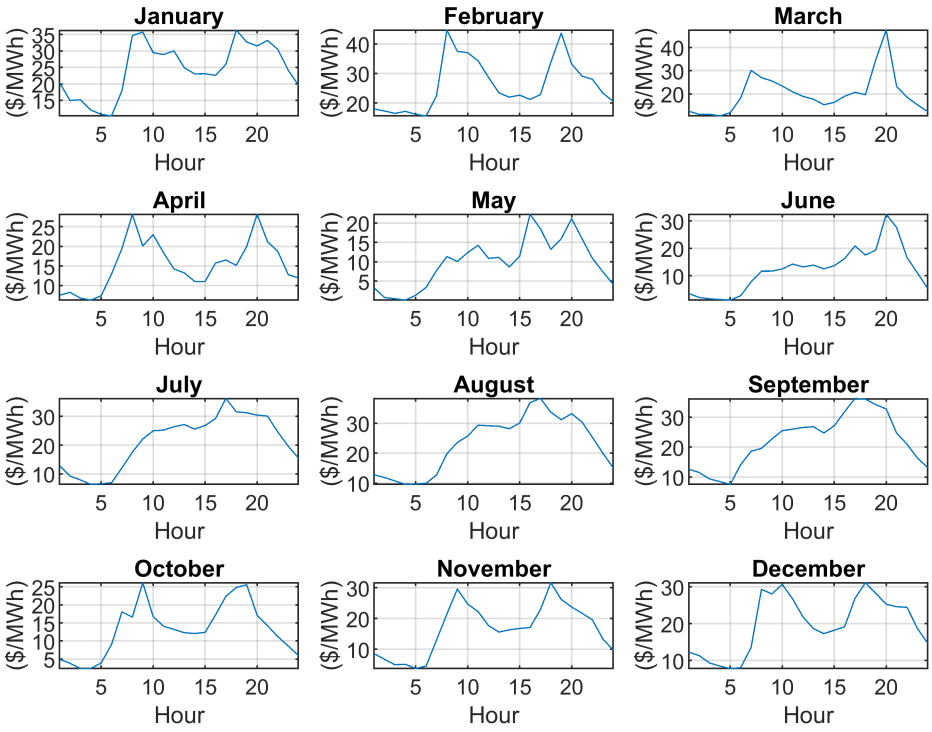

Figure 5.15: Average monthly energy price profiles for 2015-2019, adjusted for inflation to 2019.

To avoid a conservative interval of uncertainty, the upper limit on the price deviations was set to 15%, based on [78]. The filtered average price intervals obtained for August, which is the peak demand month, are presented in Figure 5.16.

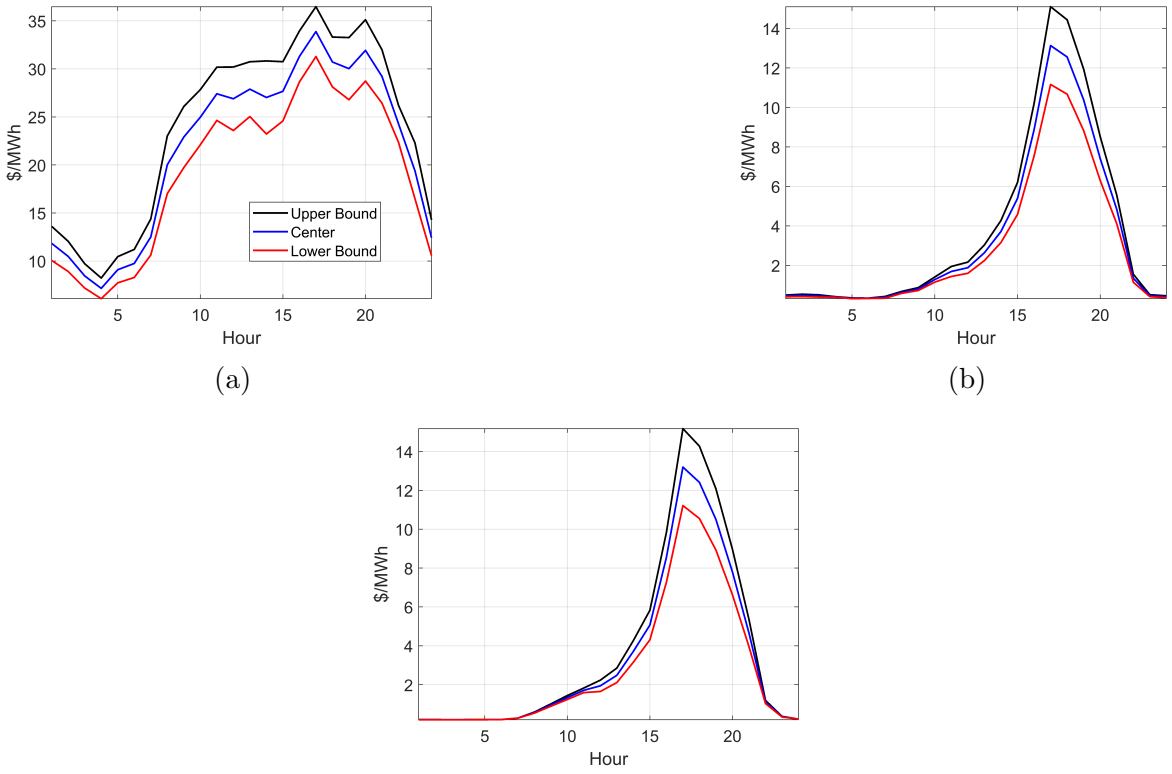

Figure 5.16: Filtered average price intervals for August: (a) energy, (b) spinning, and (c) idle reserve.

5.3.1 Principal Components Analysis (PCA)-Affine Policies (AP)

Based on the AP approach to represent uncertainties, the uncertain parameters and variables can be modeled in their affine forms, as per (4.71), (4.80) and (4.81). The CAES facility's day-ahead self-scheduling model used in this case comprises the objective function (4.91) and constraints (3.7)-(3.9), (4.92)-(4.120). Similar to the AA approach, the PCA-AP model does not use a parameter to control the level of conservatism, yielding a single optimum scheduling interval for a given interval of price uncertainties. However, the PCA-AP model is based on PCs, which are defined by the amount of information aggregated. Thus, simulations were carried out for information levels of 95%, 97.5%, 99%, and 100%, with the number of PCs and their values being determined based on (2.49) and (2.50), respectively.

Since electricity prices are represented as a function of PCs, discarding those that represent lesser information introduces an error associated with the representation of PCs with respect to the original data. For a specific information level, the Number of Principal Components (NPC) and the Mean Percentage Error (MPE) for each electricity price (energy, spinning and idle reserve), the center and radius of the profit, the computational burden, and optimum schedules can be computed.

Table 5.9 presents the NPC and MPE for the electricity prices of one of the four months considered in the studies (August); similar results were obtained for the other months. Note that for higher information levels, as the NPC increases, the MPE decreases, as expected. Note that a large number of PCs are required to properly represent the prices, which implies that these prices show significant volatility, thus yielding poor PCA performance. Due to its low values, the reserve prices presented a greater MPE, especially for the idle reserves. A comparison between the energy price representation obtained from PCA with the original data for August is presented in Figure 5.17. Note that for information levels of 95% and 97.5%, the energy prices differ to some extent from the original data, especially for the former.

Table 5.9: NPC and MPE of Electricity Prices for August.

PCA	π^{E}		π^{SR}		π^{ID}	
	NPC	MPE (%)	NPC	MPE (%)	NPC	MPE (%)
95%	16	1.3452	15	8.9349	15	19.2885
97.5%	19	1.1136	18	1.7703	18	7.3474
99%	21	0.8579	20	0.5356	21	5.1105
100%	24	0	24	0	24	0

Table 5.10 presents the center value and radius of the CAES facility's profit and computational burden for each month. Note that in all cases the center is greater than the radius; hence, there are no losses in the most pessimistic scenario. Since the 95% and 97.5% representations involve fewer variables and constraints as compared to the 99% and 100% cases, they would be expected to be computationally more efficient; however, that is not the case for all months. For example, for February, weak representation of input data at a 95% information level yielded a result that deviates significantly from the rest, while presenting a greater computational cost. The reason for this is that the computational burden depends on the CAES model and is thus sensible to the input data, thus impacting the solution convergence when weak representations are used. Even though the computational burden varies depending on the monthly price profile, all simulations converged in less than 5 minutes, which is reasonable for day-ahead operation planning.

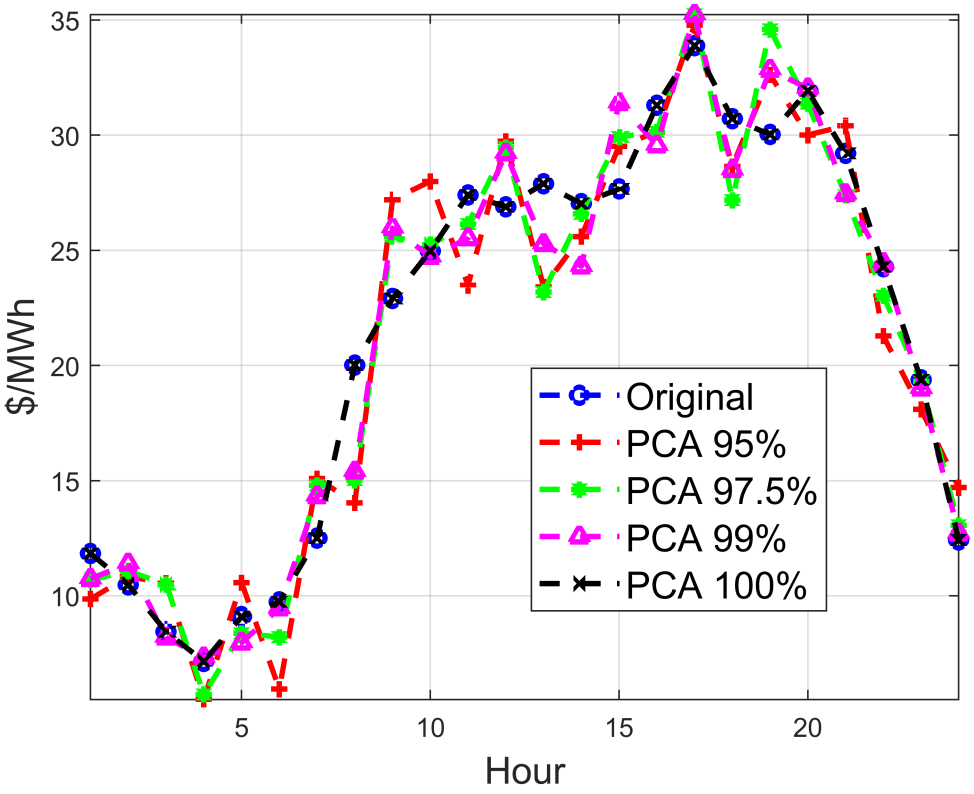

Figure 5.17: Energy prices from PCA as compared to original prices for August.

The optimum SOC profiles for the CAES facility for August are presented in Figure 5.18 for different levels of information. The depicted SOC results were obtained from the real-time price mismatch $\Delta\pi_t^Y$, with the deviation in the PCs ΔPC^Y being determined as per (4.66), and the dispatch being updated as per (4.72). Note that as the information level increases, so does the accuracy of the input data with respect to the original prices, as expected. The dispatch schedules of the CAES facility with low information can be observed to have more frequent changes from idle/discharge states and, as information level increases, the operation of the CAES becomes smoother.

Table 5.10: PCA-AP Profit and Computational Burden.

	February			May		
PCA	Profit ($)		Comp. Cost	Profit ($)		Comp. Cost
	Center	Radius		Center	Radius	
95%	7,603	4,651	1min11s	10,977	2,570	6.37s
97.5%	8,716	2,368	47s	10,583	2,494	7.47s
99%	7,848	2,695	56s	10,562	2,429	26s
100%	8,399	2,186	47s	10,505	2,419	41s
	August			November		
PCA	Profit ($)		Comp. Cost	Profit ($)		Comp. Cost
	Center	Radius		Center	Radius	
95%	5,921	2,341	3min25s	6,469	1,838	33s
97.5%	5,977	2,341	2min38s	6,374	2,299	29s
99%	6,210	2,151	3min38s	6,225	2,205	41s
100%	5,637	2,127	4min17s	6,383	1,984	46s

The power dispatch for the PCA-AP using 100% information for the month of August, with the center prices illustrated in Figure 5.16, is presented in Figure 5.19. Note that the facility charges during the early hours of the day, discharges during the peak hours and operates in idle mode for the remaining hours, yielding a daily profit of $5,637. Note that different prices were used in these simulations, and thus these results cannot be directly compared with the deterministic, RO, and AA results presented in Section 5.2.

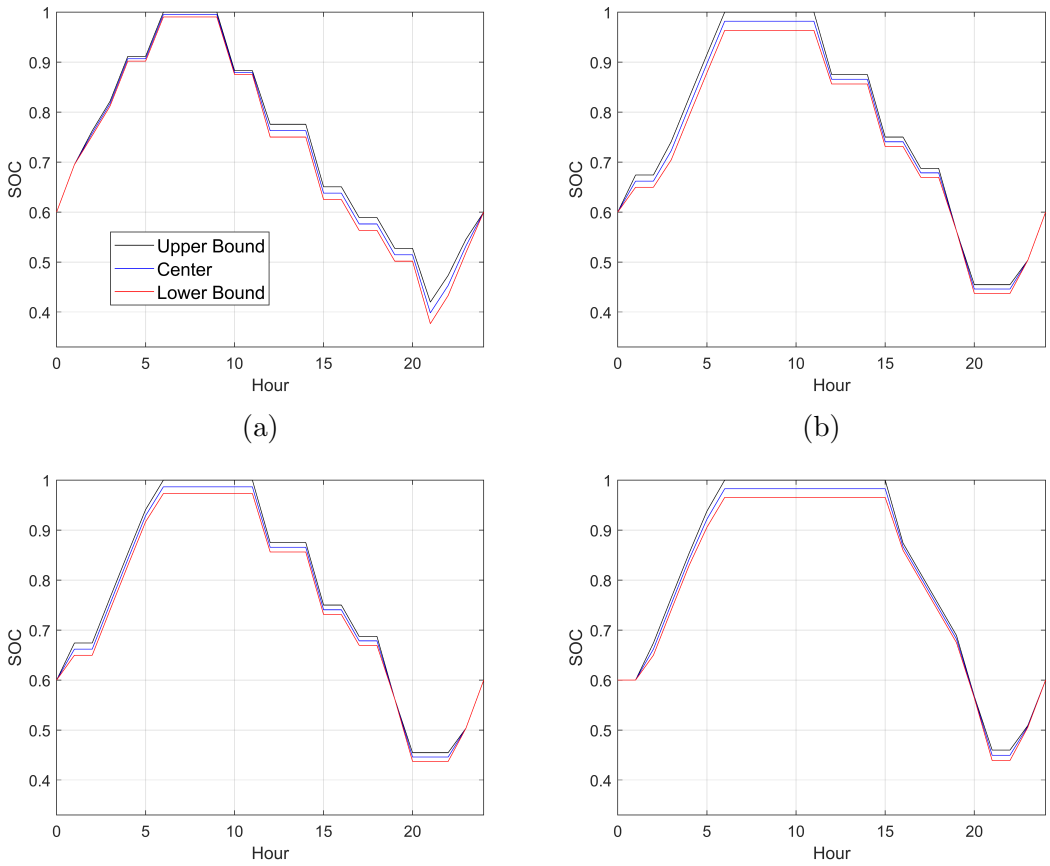

Figure 5.18: SOC profiles from PCA-AP for August: (a) 95%, (b) 97.5%, (c) 99%, and (d) 100% precision levels.

5.3.2 Affine Arithmetic (AA)

Using AA to represent uncertainties, the uncertain parameters and variables can be represented in their affine forms as per (4.18) and (4.19). In this case, the mathematical model is comprised of the objective function (4.33) and constraints (3.7)-(3.9), and (4.34)-(4.61).

As previously discussed, the AA model yields a single optimum schedule, for the price intervals presented in Figure 5.16. Table 5.11 illustrates the center and radius of the facility's profit and the computational costs for all AA simulations. Note that, in all cases, the center is greater then the radius; hence, in the most pessimistic scenario, there are no

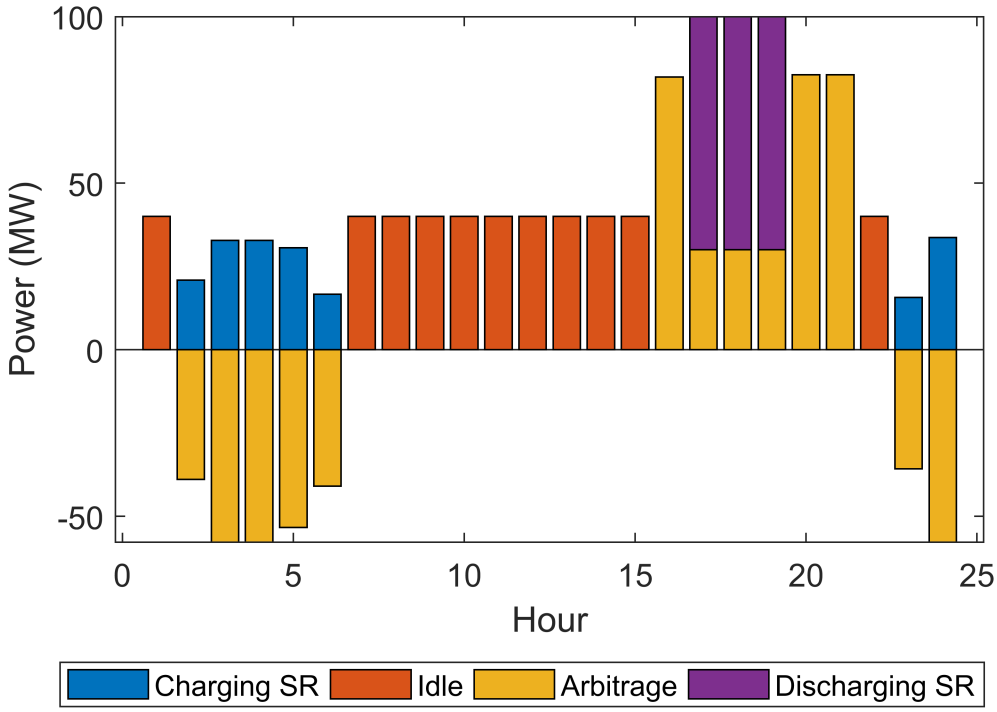

Figure 5.19: Center dispatch for PCA-AP using 100% information for the center values of the the month of August.

losses. Observe that all the cases present low computational burden, converging in less than a minute.

Table 5.11: AA Profit and Computational Burden.

Month	Profit ($)		Comp. Cost
	Center	Radius	
February	7,322	5,351	12s
May	10,237	2,616	2.40s
August	5,695	3,190	48s
November	6,186	3,048	3.84s

The optimum SOC profile for August obtained from the AA-based charging/discharging dispatch of the CAES facility is illustrated in Figure 5.20. Note that the dispatch decisions and intervals are similar to the schedules obtained using the PCA-AP presented in Figure 5.18d. Therefore, based on the real-time price mismatch $\Delta\pi_t^Y$, from which the noise terms can be defined as $\varepsilon_t^Y = \frac{\Delta\pi_t^Y}{\overline{\Delta\pi}_t}$, the dispatch can then be updated as per (4.19).

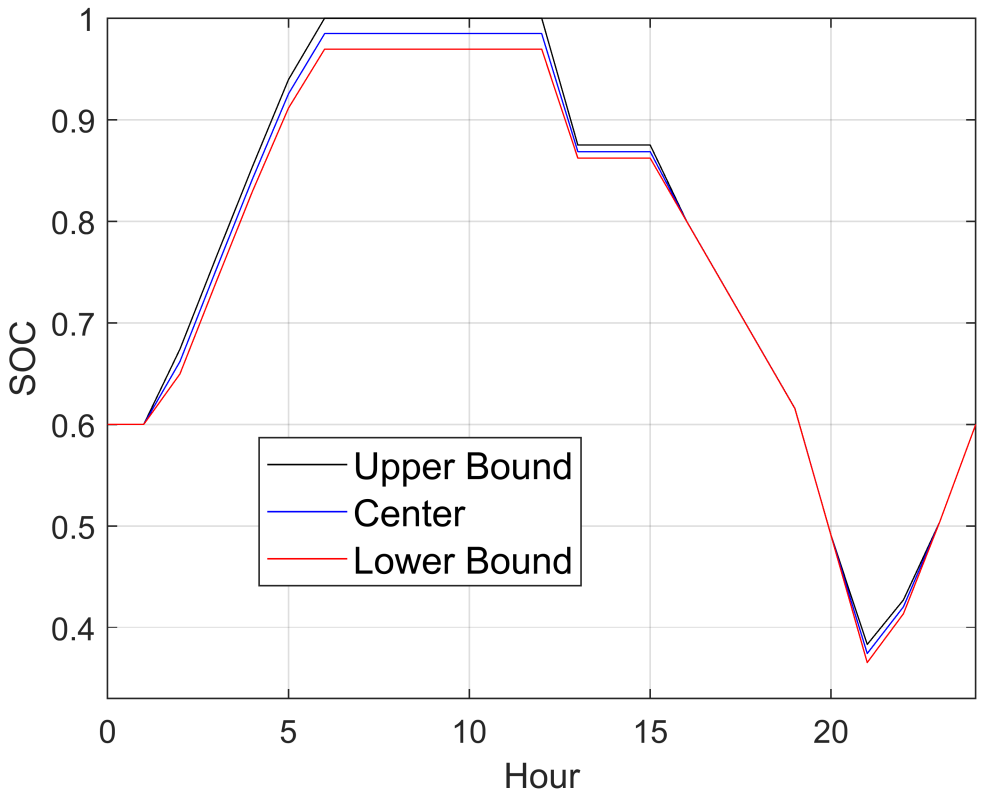

Figure 5.20: SOC Profiles from AA for August.

The AA center power dispatch for the month of August, using the center price values in Figure 5.16, is presented in Figure 5.21, accrues a daily profit of $5,695. Note that the AA dispatch is very similar with that obtained for the PCA-AP using 100% information shown in Figure 5.19, and the same applies for the profits, given its $5,637 profit value.

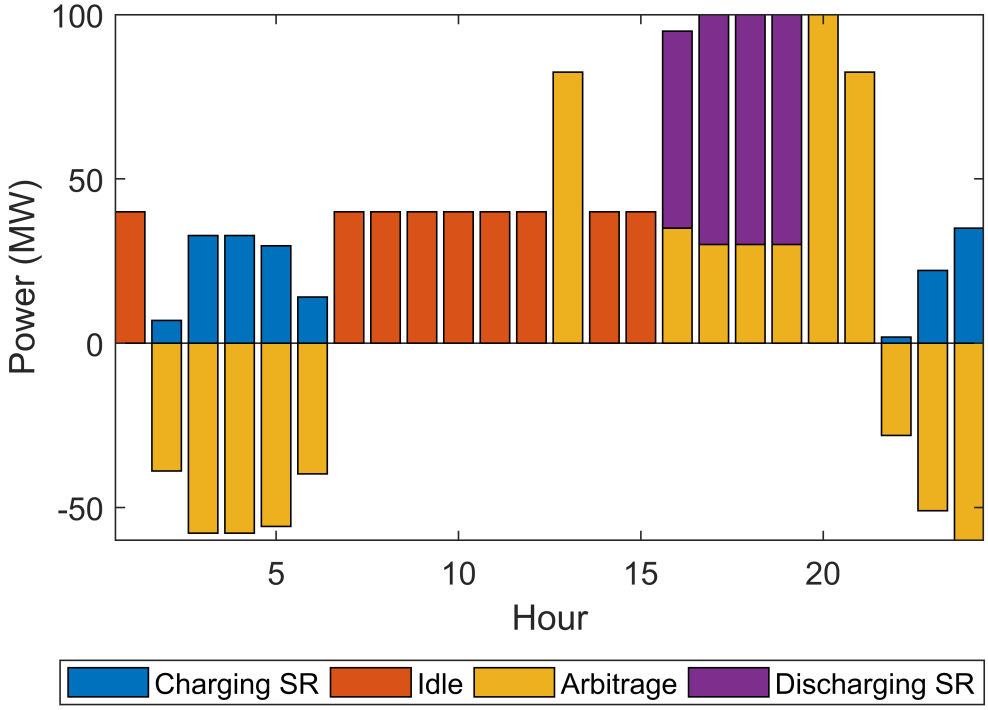

Figure 5.21: Center AA dispatch for the center values of the month of August.

5.3.3 Monte Carlo Simulations (MCS)

The results obtained from the PCA-AP and AA models are compared here with the MCS approach. For this purpose, three random uniform PDFs with 3,000 data points each were used to yield different combinations of electricity prices as input data. The convergence tolerance for the MCS was set to 0.1%.

Table 5.12 presents the lower boundary (LB) and upper boundary (UB) of the CAES facility's profits obtained from the PCA-AP, AA, and MCS approaches, along with their respective computational costs. Note that the AA approach presents the lowest computational burden, and the results envelop most of the results of the MCS and the PCA-AP approaches with 99% and 100% information. However, the AA approach also results in the widest radius and pessimistic scenarios, which yields significantly lower profits. The PCA-AP approach with 95% and 97.5% information show poor representation of the input

Table 5.12: Comparison of Profits and Computational Burden from PCA-AP, AA and MCS Approaches.

Method		February			May		
		LB ($)	UB ($)	Comp. Cost	LB ($)	UB ($)	Comp. Cost
PCA-AP	95%	2,952	12,255	1min11s	8,428	13,567	6.37s
	97.5%	6,349	11,084	47s	8,089	13,077	7.47s
	99%	5,154	10,543	56s	8,133	12,991	26s
	100%	6,213	10,585	47s	8,086	12,924	41s
AA		1,971	12,673	12s	7,621	12,852	2.40s
MCS		5,560	8,240	1h27min	10,837	13,284	1h05min
Method		August			November		
		LB ($)	UB ($)	Comp. Cost	LB ($)	UB ($)	Comp. Cost
PCA-AP	95%	3,580	8,261	3min25s	4,631	8,306	33s
	97.5%	3,637	8,318	2min38s	4,075	8,673	29s
	99%	4,059	8,361	3min38s	4,020	8,429	41s
	100%	3,511	7,764	4min17s	4,400	8,367	46s
AA		2,505	8,885	48s	3,138	9,233	3.84s
MCS		5,978	8,105	1h20min	5,548	8,071	1h06min

data, resulting in some cases in higher computational costs and profit intervals that differ significantly from rest of the results. The PCA-AP results with 99% and 100% information envelop most of the results of the MCS approach.

Despite the PCA-AP model presenting higher computational costs as compared to the AA in all cases, convergence was achieved in less than 5 minutes, rendering the proposed PCA-AP approach reasonable for day-ahead operations. The approach also presented less conservative results, i.e., tighter profit boundaries, yielding a more profitable margin of operation in pessimistic scenarios.

5.3.4 Concurrent Charging and Discharging

As stated earlier, removing the constraint (3.7) from the CAES operations model will enable the facility to charge and discharge concurrently. In order to assess the facility's performance in this operating mode, the PCA-AP simulations are repeated here for the

month of August.

Table 5.13 presents a comparison with the previous model, where the facility operates either in charging/discharging/idle mode at a given interval (non-concurrent operation), with the concurrent mode operation. The possibility of charging and discharging concurrently increases the number of available operational combinations; hence, higher profits can be achieved in the optimistic scenario. However, this also implies a greater computational cost and a wider profit interval in pessimistic scenarios, wherein lower profits are obtained, resulting in losses in some cases, as seen for the concurrent case for 95% information level in Table 5.13.

Table 5.13: Charging and/or discharging operation for August.

PCA	Non-concurrent			Concurrent		
	Profit ($)		Comp. Cost	Profit ($)		Comp. Cost
	LB	UB		LB	UB	
95%	3,580	8,261	3min25s	-1,328	8,836	12min59s
97.5%	3,637	8,318	2min38s	1,868	8,510	16min56s
99%	4,059	8,361	3min38s	1,010	8,540	15min11s
100%	3,511	7,621	4min17s	665	8,045	22min22s

The optimum SOC profiles for the CAES facility charging and discharging concurrently in August are presented in Figure 5.22. Compared with the SOC obtained from the non-concurrent model (Figure 5.18), it can be observed that the concurrent model presents a more flexible profile of the SOC over several hours of the day. This is due to the minimum charging (4.94) and discharging (4.96) power limits of the CAES facility. When operating non-concurrently, there is a minimum upward or downward variation in the SOC, whereas operating concurrently it presents more flexibility in the SOC variation.

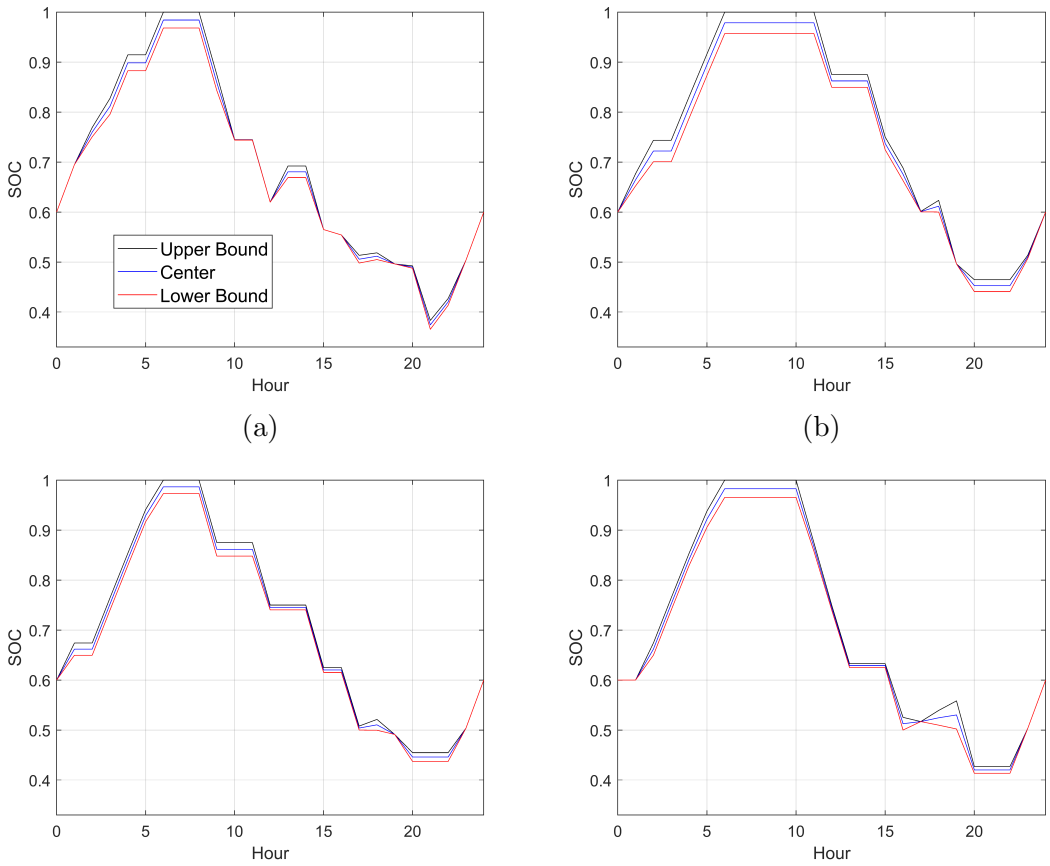

Figure 5.22: SOC profiles for concurrent CAES from PCA-AP for August: (a) 95%, (b) 97.5%, (c) 99%, and (d) 100% precision levels.

5.4 Summary

This Chapter presented the results obtained from the CAES models proposed in Chapter 3. First, the results obtained using the step-function thermodynamic model of the facility were presented. Using RO to represent uncertainties, the model yielded schedules protected against the worst-case scenario for a given budget of uncertainty, with a lower computational cost than the MCS.

Second, the operational results considering the proposed linear thermodynamic model of the facility, were presented. This model yielded similar results at significantly lower

computational burden, as compared to the step-function model. Next, for fixed intervals of uncertainty, the RO and AA approaches were simulated. Compared to RO, a greater computational burden and more conservative results were obtained with the AA approach.

Third, for uncertainty intervals obtained from historic electricity price data, the PCA-AP simulations provided schedules protected against uncertainty at a tighter range of profit compared to the AA approach. Finally, the concurrent charging/discharging aspects of the facility were assessed. The larger number of combinations of operations available, allowed the facility to achieve higher profits, but at increased computational costs.

Chapter 6

Conclusions

6.1 Summary and Conclusions

In this thesis, a novel linear thermodynamic model for a CAES facility was proposed, which considered the pressure inside the cavern and the efficiency of the high pressure turbine, based on the dynamic characteristics of the Huntorf CAES facility in Germany. These detailed thermodynamic models were included in a day-ahead self-scheduling operations model for a price-taker CAES facility participating in the day-ahead energy and reserve markets. Then, for a given day-ahead electricity price forecast, the optimum schedule of the facility was determined. However, electricity prices are subject to uncertainties; thus, methods based on range arithmetic, specifically RO, AA and AP, were developed to determine operation decisions for a price-taker CAES facility under price uncertainties.

In the first part of the thesis, a deterministic self-scheduling model for a CAES facility was presented. Three non-linear functions were used, representing the thermodynamic characteristics of the mass of air charged, mass of air discharged, and the cost of natural gas. This nonlinear representation was linearized using McCormick Envelopes and linear piecewise approximations, to avoid discontinuities, thus making it easier to implement methods that keep track of correlated uncertainties, reducing the number of binary variables in the model. This novel formulation was compared with the step-function model of the CAES facility reported in [19], which despite yielding a reasonable approximation of a real model, is highly complex due to the presence of discontinuities and significant large number of binary variables, making it difficult to employ methods that take uncertainties into account. Both models were executed for different days of the year with corresponding HOEPs, demonstrating that the proposed piecewise linear thermodynamic model yielded

similar results, at a significantly lower computational burden compared to the step-function model.

In the second part of the thesis, range arithmetic techniques to represent electricity price uncertainties were introduced in the model. First, an RO model was presented to optimize the CAES facility's day-ahead operations for the worst-case scenario for a given budget of uncertainty, which allowed to study a range of scenarios from the deterministic to the most conservative case. With this model, low probability of violation can be achieved without the need for a large budget of uncertainty, thus enabling the operator to choose schedules that yield greater profits. Next, an AA model was presented, where the uncertain parameters and variables were represented in affine forms, keeping track of correlated uncertainties. The model maximized the center and radius of the profit and yielded an optimum range with upper and lower bounds for the dispatch. In this case, for a real-time mismatch in electricity prices from their forecast, the actual dispatch can be updated accordingly. In order to avoid a conservative schedule that yields losses in pessimistic scenarios, the radius was maximized for the affine terms and minimized for the non-affine terms. For both RO and AA models, simulations were carried out for specific days of the year with their corresponding HOEPs, considering fixed intervals of uncertainty. Both methods were benchmarked with the MCS approach, obtaining intervals that enveloped the MCS results at significantly lower computational costs.

Finally, a PCA-AP model was presented, where unlike for the RO and AA models, five-year data of HOEPs were used to estimate the center and intervals of electricity prices for each month, based on their hourly averages and standard deviations. A PCA algorithm was implemented to extract information from each of the three electricity prices, energy, spinning reserves and idle reserves, to reduce the dimension of the problem. Depending on the information level, the number of variables and constraints in the model changed; however, lower levels of information did not necessarily resulted in lower computational costs, since the model resulted on a weaker representation in some cases. Similar to AA, in the proposed PCA-AP model, the uncertain parameters and variables were represented in their affine forms, and the center and radius of the profit were maximized simultaneously. Despite the greater computational cost, the PCA-AP model yielded tighter profit intervals as compared to AA, i.e., a more profitable margin of operation in pessimistic scenarios. The operation of a CAES facility charging and discharging concurrently was also assessed, resulting in an increased computational burden; however, higher profits and a smoother SOC profile was obtained. Finally, the PCA-AP was also benchmarked against the MCS approach, resulting in lower computational costs and similar profit intervals.

The following conclusions can be drawn from this work:

- The proposed piecewise linear thermodynamic representation of the CAES facility significantly reduced the computational burden of the self-scheduling model, without loss of accuracy, making it simpler to implement techniques that keep track of correlated uncertainties.

- The RO model yielded optimum schedules that were protected against the worst-case scenario, for a given budget of uncertainty. Through the latter, the model could be varied from deterministic to the most conservative, and low probability of violation could be achieved without resorting to a large budget of uncertainty. However, the optimum schedules obtained from the RO approach were fixed for the assumed budget of uncertainty, without allowing adjustment with respect to the actual price deviations from the forecast.

- The AA model, based on electricity price centers and intervals, yielded optimum ranges for the schedules, which allowed to determine the power dispatch for the actual prices based on their deviation with respect to the forecast. The profit was maximized for the center and affine terms and minimized for the non-affine terms, thus avoiding a conservative radius that could lead to losses in pessimistic scenarios.

- The PCA-AP model also yielded optimum schedules with power dispatch affine intervals, but at tighter profit intervals than the AA, thus resulting in a more profitable margin of operation. Unlike the RO and AA approaches, the input data used was not for a specific day, but was based on the monthly averages and standard deviations of prices from 2015 to 2019. This allowed to estimate the electricity price center and intervals using Box Cox technique to filter the outliers. A PCA method was used to extract data for each month and reduce the number of variables for a given level of information. However, low information levels could lead to weak representations, yielding greater computational costs and inaccurate results.

- The possibility of the CAES facility to charge and discharge concurrently, despite presenting a greater computational burden, allowed the facility to achieve higher profits with the more varied operational strategies. Furthermore, a smoother transition in the SOC profile was noted when compared with the non-concurrent operations. However, for pessimistic scenarios, it yielded worse values for the lower bounds.

6.2 Contributions

The main contributions of this thesis can be summarized as follows:

- A novel linear thermodynamic model of a CAES facility was proposed and validated, incorporating it into a day-ahead, self-scheduling operations model of a price-taker facility participating in energy and reserve electricity markets. The proposed comprehensive operations model of the CAES facility provides important insights into price-taker energy storage facility operations in electricity markets.
- The effectiveness of applying RO to model electricity price uncertainties is demonstrated for the operation of a CAES facility for the worst-case scenario at a given budget of uncertainty. It was shown that operators do not need to resort to conservative scenarios to obtain a low probability of violation, so that greater profits can be ensured.
- For the first time, a self-scheduling model based on AA was developed for a CAES facility to represent electricity price uncertainties, keeping track of correlated uncertainties. The proposed model allows the facility owner to determine an optimum operating range for a given interval of uncertainty.
- The application of Box Cox interval to remove outliers from historical electricity price data was demonstrated, enabling a more precise estimation of the center and intervals of electricity prices for affine interval modeling of uncertainties.
- A new PCA-AP-based self-scheduling model was proposed using PCA to extract information from the price data, and APs to keep track of correlated uncertainties. It was shown that the proposed method yields an optimum operating range, with tighter profit bounds compared to AA.
- The operation of a CAES facility charging and discharging concurrently was studied, demonstrating that the possible operational combinations allow greater profits to be achieved.

The proposed models, approaches, and results presented in the thesis were published in [79] and [80], and have been submitted for publication in [81].

6.3 Future Work

Based on the work presented in this thesis, the following issues could be addressed in the future:

- Enhance the self-scheduling model of concurrent CAES operation to consider real-time market participation, so that the facility may partake in frequency regulation market, expanding its opportunities to increase revenue.
- Implement the presented techniques to model uncertainties in both day-ahead and real-time markets.
- Consider the CAES facility participating as a price-maker in the market. For this purpose, a bi-level model could be developed to study the impact in electricity prices of such a facility.
- Apply the proposed techniques to model uncertainties in other system parameters such as demand and RES generation.

References

[1] G. T. Heydt, "Grand challenges in electric power engineering: extreme system reliability," *IEEE Power Engineering Society Summer Meeting*, vol. 3, pp. 1695–1697, July 2002.

[2] B. Mohandes, M. S. E. Moursi, N. Hatziargyriou, and S. E. Khatib, "A review of power system flexibility with high penetration of renewables," *IEEE Transactions on Power Systems*, vol. 34, no. 4, pp. 3140–3155, 2019.

[3] B. Zhou, T. Littler, and H. Wang, "The impact of vehicle-to-grid on electric power systems: A review," in *2nd IET Renewable Power Generation Conference (RPG 2013)*, 2013, pp. 1–4.

[4] J. Tamura, M. Rosyadi, R. Takahashi, A. Umemura, T. Fukushima, A. Kuwayama, K. Yoshioka, and T. Kaiso, "A new method for analyzing frequency and voltage fluctuations of power system with wind generators installed," *IECON 2013 - 39th Annual Conference of the IEEE Industrial Electronics Society*, pp. 1466–1471, Nov. 2013.

[5] W. Xian, W. Yuan, Y. Yan, and T. A. Coombs, "Minimize frequency fluctuations of isolated power system with wind farm by using superconducting magnetic energy storage," *2009 International Conference on Power Electronics and Drive Systems (PEDS)*, pp. 1329–1332, Nov. 2009.

[6] P. Ribeiro, B. Johnson, M. Crow, A. Arsoy, and Y. Liu, "Energy storage systems for advanced power applications," *Proceedings of the IEEE*, vol. 89, no. 12, pp. 1744–1756, 2001.

[7] P. D. Lund, J. Lindgren, J. Mikkola, and J. Salpakari, "Review of energy system flexibility measures to enable high levels of variable renewable electricity," *Renewable and Sustainable Energy Reviews*, vol. 45, pp. 785–807, 2015.

[8] H. Chen, T. N. Cong, W. Yang, C. Tan, Y. Li, and Y. Ding, "Progress in electrical energy storage system: A critical review," *Progress in Natural Science*, vol. 19, no. 3, pp. 291–312, 2009. [Online]. Available: http://www.sciencedirect.com/science/article/pii/S100200710800381X

[9] R. Carnegie, D. Gotham, D. Nderitu, and P. V. Preckel, "Utility scale energy storage systems: Benefits, applications, and technologies," State Utility Forecasting Group. [Online]. Available: https://www.purdue.edu/discoverypark/energy/assets/pdfs/SUFG/publications/SUFG%20Energy%20Storage%20Report.pdf

[10] A. F. Zobaa, *Energy storage - technologies and applications*. INTECH, 2014.

[11] S. Hameer and J. Van Niekerk, "A review of large-scale electrical energy storage," *International Journal of Energy Research*, vol. 39, pp. 1179–1195, Feb. 2015.

[12] B. J. Davidson, I. Glendenning, R. D. Harman, A. B. Hart, B. J. Maddock, R. D. Moffitt, V. G. Newman, T. F. Smith, P. J. Worthington, and J. K. Wright, "Large-scale electrical energy storage," *IEE Proceedings A - Physical Science, Measurement and Instrumentation, Management and Education - Reviews*, vol. 127, no. 6, pp. 345–385, 1980.

[13] T. V. Nguyen, "Integration of compressed air energy storage with wind turbine to provide energy source for combustion turbine generator," *IEEE PES Innovative Smart Grid Technologies, Europe*, pp. 1–5, 2014.

[14] B. Cleary, A. Duffy, A. OConnor, M. Conlon, and V. Fthenakis, "Assessing the economic benefits of compressed air energy storage for mitigating wind curtailment," *IEEE Transactions on Sustainable Energy*, vol. 6, no. 3, pp. 1021–1028, 2015.

[15] M. King, A. Jain, R. Bhakar, J. Mathur, and J. Wang, "Overview of current compressed air energy storage projects and analysis of the potential underground storage capacity in India and the UK," *Renewable and Sustainable Energy Reviews*, vol. 139, p. 110705, 2021. [Online]. Available: https://www.sciencedirect.com/science/article/pii/S1364032121000022

[16] "Goderich A-CAES facility," Hydrostor, 2021. [Online]. Available: https://www.hydrostor.ca/goderich-a-caes-facility/

[17] "Toronto A-CAES facility," Hydrostor, 2021. [Online]. Available: https://www.hydrostor.ca/toronto-a-caes-facility/

[18] J. Arteaga and H. Zareipour, "A price-maker/price-taker model for the operation of battery storage systems in electricity markets," *IEEE Transactions on Smart Grid*, vol. 10, no. 6, pp. 6912–6920, 2019.

[19] S. Shafiee, H. Zareipour, and A. M. Knight, "Considering thermodynamic characteristics of a CAES facility in self-scheduling in energy and reserve markets," *IEEE Transactions on Smart Grid*, vol. 9, no. 4, pp. 3476–3485, 2018.

[20] I. Calero, C. A. Cañizares, and K. Bhattacharya, "Compressed air energy storage system modeling for power system studies," *IEEE Transactions on Power Systems*, vol. 34, no. 5, pp. 3359–3371, 2019.

[21] X. Liu, Y. Liu, J. Liu, Y. Xiang, and X. Yuan, "Optimal planning of AC-DC hybrid transmission and distributed energy resource system: Review and prospects," *CSEE Journal of Power and Energy Systems*, vol. 5, no. 3, pp. 409–422, 2019.

[22] D. Bertsimas and M. Sim, "The price of robustness," *Operations Research*, vol. 52, no. 1, pp. 35–53, 2004.

[23] W. Kenton, "Monte carlo simulations," 2018. [Online]. Available: https://www.investopedia.com/terms/m/montecarlosimulation.asp

[24] L. A. Hannah, "Stochastic optimization," 2014. [Online]. Available: http://www.stat.columbia.edu/~liam/teaching/compstat-spr14/lauren-notes.pdf

[25] S. Shafiee, H. Zareipour, A. M. Knight, N. Amjady, and B. Mohammadi-Ivatloo, "Risk-constrained bidding and offering strategy for a merchant compressed air energy storage plant," *IEEE Transactions on Power Systems*, vol. 32, no. 2, pp. 946–957, 2017.

[26] S. Nojavan, A. Najafi-Ghalelou, M. Majidi, and K. Zare, "Optimal bidding and offering strategies of merchant compressed air energy storage in deregulated electricity market using robust optimization approach," *Energy*, vol. 142, pp. 250 – 257, 2018. [Online]. Available: http://www.sciencedirect.com/science/article/pii/S0360544217316973

[27] A. Attarha, N. Amjady, S. Dehghan, and B. Vatani, "Adaptive robust self-scheduling for a wind producer with compressed air energy storage," *IEEE Transactions on Sustainable Energy*, vol. 9, no. 4, pp. 1659–1671, 2018.

[28] R. Khatami, K. Oikonomou, and M. Parvania, "Look-ahead optimal participation of compressed air energy storage in day-ahead and real-time markets," *IEEE Transactions on Sustainable Energy*, vol. 11, no. 2, pp. 682–692, 2020.

[29] Y. Li, S. Miao, B. Yin, W. Yang, S. Zhang, X. Luo, and J. Wang, "A real-time dispatch model of CAES with considering the part-load characteristics and the power regulation uncertainty," *International Journal of Electrical Power & Energy Systems*, vol. 105, pp. 179 – 190, 2019.

[30] Z. Guo, W. Wei, L. Chen, Z. Wang, and S. Mei, "Operation of distribution network considering compressed air energy storage unit and its reactive power support capability," *IEEE Transactions on Smart Grid*, vol. 11, no. 4, pp. 2954–2965, 2020.

[31] J. D. Lara, D. E. Olivares, and C. A. Cañizares, "Robust energy management of isolated microgrids," *IEEE Systems Journal*, vol. 13, no. 1, pp. 680–691, March 2019.

[32] A. H. Hajimiragha, C. A. Canizares, M. W. Fowler, S. Moazeni, and A. Elkamel, "A robust optimization approach for planning the transition to plug-in hybrid electric vehicles," *IEEE Transactions on Power Systems*, vol. 26, no. 4, pp. 2264–2274, Nov. 2011.

[33] G. Liu, Y. Xu, and K. Tomsovic, "Bidding strategy for microgrid in day-ahead market based on hybrid stochastic/robust optimization," *IEEE Transactions on Smart Grid*, vol. 7, no. 1, pp. 227–237, Jan. 2016.

[34] J. Yi, P. F. Lyons, P. J. Davison, P. Wang, and P. C. Taylor, "Robust scheduling scheme for energy storage to facilitate high penetration of renewables," *IEEE Transactions on Sustainable Energy*, vol. 7, no. 2, pp. 797–807, 2016.

[35] M. Pirnia, C. A. Cañizares, K. Bhattacharya, and A. Vaccaro, "A novel affine arithmetic method to solve optimal power flow problems with uncertainties," *IEEE Transactions on Power Systems*, vol. 29, no. 6, pp. 2775–2783, 2014.

[36] A. Vaccaro and C. A. Cañizares, "An affine arithmetic-based framework for uncertain power flow and optimal power flow studies," *IEEE Transactions on Power Systems*, vol. 32, no. 1, pp. 274–288, 2017.

[37] D. Romero-Quete and C. A. Cañizares, "An affine arithmetic-based energy management system for isolated microgrids," *IEEE Transactions on Smart Grid*, vol. 10, no. 3, pp. 2989–2998, 2019.

[38] A. Vaccaro, M. Petrelli, and A. Berizzi, "Robust optimization and affine arithmetic for microgrid scheduling under uncertainty," *2019 IEEE International Conference on Environment and Electrical Engineering and 2019 IEEE Industrial and Commercial Power Systems Europe (EEEIC / I CPS Europe)*, pp. 1–6, 2019.

[39] R. A. Jabr, "Adjustable robust OPF with renewable energy sources," *IEEE Transactions on Power Systems*, vol. 28, no. 4, pp. 4742–4751, 2013.

[40] A. Lorca, X. A. Sun, E. Litvinov, and T. Zheng, "Multistage adaptive robust optimization for the unit commitment problem," *Operations Research*, vol. 64, no. 1, pp. 32–51, 2016.

[41] Álvaro Lorca and X. A. Sun, "Multistage robust unit commitment with dynamic uncertainty sets and energy storage," *IEEE Transactions on Power Systems*, vol. 32, no. 3, pp. 1678–1688, 2017.

[42] S. Rehman, L. M. Al-Hadhrami, and M. M. Alam, "Pumped hydro energy storage system: A technological review," *Renewable and Sustainable Energy Reviews*, vol. 44, pp. 586–598, 2015. [Online]. Available: https://www.sciencedirect.com/science/article/pii/S1364032115000106

[43] M. Amiryar and K. Pullen, "A review of flywheel energy storage system technologies and their applications," *Applied Sciences*, vol. 7, no. 3, p. 286, March 2017.

[44] G. L. Bullard, H. B. Sierra-Alcazar, H. L. Lee, and J. L. Morris, "Operating principles of the ultracapacitor," *IEEE Transactions on Magnetics*, vol. 25, no. 1, pp. 102–106, Jan. 1989.

[45] S. Vazquez, S. M. Lukic, E. Galvan, L. G. Franquelo, and J. M. Carrasco, "Energy storage systems for transport and grid applications," *IEEE Transactions on Industrial Electronics*, vol. 57, no. 12, pp. 3881–3895, Dec. 2010.

[46] P. Alotto, M. Guarnieri, and F. Moro, "Redox flow batteries for the storage of renewable energy: A review," *Renewable and Sustainable Energy Reviews*, vol. 29, pp. 325–335, 2014. [Online]. Available: http://www.sciencedirect.com/science/article/pii/S1364032113005418

[47] K. Kishimoto, K. Hasegawa, and T. Asano, "Development of generator of liquid air storage energy system," *Technical Review - Mitsubishi Heavy Industries*, vol. 35, no. 3, pp. 117–120, 1998.

[48] F. Salimijazi, E. Parra, and B. Barstow, "Electrical energy storage with engineered biological systems," *Journal of Biological Engineering*, vol. 13, no. 38, 2019.

[49] J. Simmons, A. Barnhart, S. Reynolds, and Y.-J. Son, "Study of compressed air energy storage with grid and photovoltaic energy generation," Technical Report, The Arizona Research Institute for Solar Energy (AzRISE), 2010. [Online]. Available: http://u.arizona.edu/~sreynold/caes.pdf

[50] R. B. Schainker and M. Nakhamkin, "Compressed air energy storage (CAES): Overview, performance and cost data for 25MW to 220MW plants," *IEEE Transactions on Power Apparatus and Systems*, vol. PAS-104, no. 4, pp. 790–795, July 1985.

[51] S. Succar and R. H. Williams, "Compressed air energy storage: Theory, resources, and applications for wind power," Technical Report, Princeton Environmental Institute, 2008. [Online]. Available: https://acee.princeton.edu/wp-content/uploads/2016/10/SuccarWilliams_PEI_CAES_2008April8.pdf

[52] "Bethel energy center," Apex, 2021. [Online]. Available: http://www.apexcaes.com/

[53] N. Hartmann, O. Vöhringer, C. Kruck, and L. Eltrop, "Simulation and analysis of different adiabatic compressed air energy storage plant configurations," *Applied Energy*, vol. 93, pp. 541–548, 2012. [Online]. Available: https://www.sciencedirect.com/science/article/pii/S0306261911008014

[54] G. Huff, N. Tong, R. Fioravanti, P. Gordon, L. Markel, P. Agrawal, and A. Nourai, "Characterization and assessment of novel bulk storage technologies: A study for the DOE energy storage systems program," Technical Report, Sandia National Laboratories, Albuquerque, New Mexico and Livermore, California, April 2011. [Online]. Available: http://prod.sandia.gov/techlib/access-control.cgi/2011/113700.pdf

[55] "Toronto Island energy storage facility," Hydrostor, 2021. [Online]. Available: https://www.hydrostor.ca/toronto-a-caes-facility/

[56] S. Sen and D. Kothari, "Optimal thermal generating unit commitment: a review," *International Journal of Electrical Power & Energy Systems*, vol. 20, no. 7, pp. 443–451, 1998. [Online]. Available: https://www.sciencedirect.com/science/article/pii/S0142061598000131

[57] A. R. Jordehi, "How to deal with uncertainties in electric power systems? A review," *Renewable and Sustainable Energy Reviews*, vol. 96, pp. 145–155, 2018. [Online]. Available: http://www.sciencedirect.com/science/article/pii/S1364032118305641

[58] A. Shapiro, D. Dentcheva, and A. Ruszczynski, *Lectures in Stochastic Programming: Modeling and Theory*. SIAM, 2009.

[59] D. E. Olivares, J. D. Lara, C. A. Canizares, and M. Kazerani, "Stochastic-predictive energy management system for isolated microgrids," *IEEE Transactions on Smart Grid*, vol. 6, no. 6, pp. 2681–2693, Nov. 2015.

[60] B. Fanzeres, A. Street, and L. A. Barroso, "Contracting strategies for renewable generators: A hybrid stochastic and robust optimization approach," *IEEE Transactions on Power Systems*, vol. 30, no. 4, pp. 1825–1837, 2015.

[61] A. L. Soyster, "Convex programming with set-inclusive constraints and applications to inexact linear programming," *Operations Research*, vol. 21, no. 5, pp. 1154–1157, 1973. [Online]. Available: http://www.jstor.org/stable/168933

[62] A. Ben-Tal and A. Nemirovski, "Robust solutions of uncertain linear programs," *Operations Research Letters*, vol. 25, no. 1, pp. 1–13, 1999. [Online]. Available: http://www.sciencedirect.com/science/article/pii/S0167637799000164

[63] J. Stolfi and L. H. D. Figueiredo, "Self-validated numerical methods and applications," *Trends in Applied Computational Mathematics*, vol. 4, no. 3, 2003.

[64] A. Ben-Tal, A. Goryashko, E. Guslitzer, and A. Nemirovski, "Adjustable robust solutions of uncertain linear programs," *Mathematical Programming, Ser. A.*, vol. 99, pp. 351–376, 2004.

[65] D. Bertsimas, D. A. Iancu, and P. A. Parrilo, "Optimality of affine policies in multistage robust optimization," *Mathematics of Operations Research*, vol. 35, no. 2, pp. 363–394, 2010.

[66] M. Hadjiyiannis, P. Goulart, and D. Kuhn, "An efficient method to estimate the suboptimality of affine controllers." *IEEE Transactions on Automatic Control*, vol. 56, pp. 2841–2853, 01 2011.

[67] I. T. Jolliffe and J. Cadima, "Principal component analysis: a review and recent developments," *Philosophical Transactions of the Royal Society A: Mathematical, Physical and Engineering Sciences*, vol. 374, no. 2065, 2016.

[68] R. Sakia, "The box-cox transformation technique: A review," *The Statistician*, vol. 41, 01 1992.

[69] L. Kogan, "Small-sample inference and bootstrap," 2010. [Online]. Available: https://ocw.mit.edu/courses/sloan-school-of-management/15-450-analytics-of-finance-fall-2010/lecture-notes/MIT15_450F10_lec09.pdf

[70] P. Zhao, L. Gao, J. Wang, and Y. Dai, "Energy efficiency analysis and off-design analysis of two different discharge modes for compressed air energy storage system using axial turbines," *Renewable Energy*, vol. 85, pp. 1164–1177, 2016. [Online]. Available: https://www.sciencedirect.com/science/article/pii/S0960148115301907

[71] A. Costa and L. Liberti, "Relaxations of multilinear convex envelopes: dual is better than primal," *International Symposium on Experimental Algorithms*, pp. 87–98, 2012.

[72] Y.-Y. Hong and C.-P. Wu, "Day-ahead electricity price forecasting using a hybrid principal component analysis network," *Energies*, vol. 5, 2012.

[73] K. Li, J. D. Cursio, and Y. Sun, "Principal component analysis of price fluctuation in the smart grid electricity market," *Sustainability, MDPI*, pp. 1–16, 2018.

[74] W. L. Winston and M. A. Venkataramanan, *Operations research*. Thomson, 2003.

[75] "Market prices," IESO. [Online]. Available: http://reports.ieso.ca/public/PriceHOEPPredispOR/

[76] "Canada inflation," Statista. [Online]. Available: https://www.statista.com/statistics/271247/inflation-rate-in-canada/

[77] R. Weron, "Electricity price forecasting: A review of the state-of-the-art with a look into the future," *International Journal of Forecasting*, vol. 30, no. 4, pp. 1030–1081, 2014.

[78] H. S. Sandhu, L. Fang, and L. Guan, "Forecasting day-ahead price spikes for the Ontario electricity market," *Electric Power Systems Research*, vol. 141, pp. 450–459, 2016.

[79] M. F. Z. de Souza, C. A. Canizares, and K. Bhattacharya, "Self-scheduling models of a CAES facility under uncertainties," *IEEE Transactions on Power Systems*, vol. 36, no. 4, pp. 3607–3617, 2021.

[80] ——, "Operation of a CAES facility under price uncertainties using robust optimization," *IEEE-PES General Meeting 2021*, pp. 1–5, July 2021.

[81] M. F. Z. de Souza, C. A. Canizares, K. Bhattacharya, and A. Lorca, "Affine policies and principal components analysis for self-scheduling in CAES facilities," *IEEE Transactions on Power Systems*, Submitted October 2021, 10 pages.